MEDRC Series of R&D Reports
MEDRC Project: 16-JS-040

THE SPATIAL AND TEMPORAL SIMULATION OF THE HYDROLOGICAL WATER BUDGET FOR YARMOUK RIVER BASIN UNDER CURRENT AND PROJECTED FUTURE CLIMATE

M. Sc. Thesis

Submitted By

Alham Walid Saud Al-Shurafat

Principal Investigator

Prof. Fayez A. Abdullah

Jordan University of Science and Technology

Middle East Desalination Research Center Muscat, Sultanate of Oman

2016

THE SPATIAL AND TEMPORAL SIMULATION OF THE HYDROLOGICAL WATER BUDGET FOR YARMOUK RIVER BASIN UNDER CURRENT AND PROJECTED FUTURE CLIMATE

THE SPATIAL AND TEMPORAL SIMULATION OF THE HYDROLOGICAL WATER BUDGET FOR YARMOUK RIVER BASIN UNDER CURRENT AND PROJECTED FUTURE CLIMATE

By

Alham Walid Saud Al-Shurafat

Advisor

Prof. Fayez A. Abdullah

Thesis submitted in partial fulfillment of the requirements for the degree of

M.Sc. in Civil Engineering

At

The Faculty of Graduate Studies

Jordan University of Science and Technology

December, 2016

THE SPATIAL AND TEMPORAL SIMULATION OF THE HYDROLOGICAL WATER BUDGET FOR YARMOUK RIVER BASIN UNDER CURRENT AND PROJECTED FUTURE CLIMATE

By

Alham Walid Saud Al-Shurafat

Signature of Author	……
Committee Member	Signature and Date
Prof. Fayez A. Abdulla (Chairman)	……
Prof. Wa'il Abu-El-Sha'r (Member)	……
Prof. Hani A. Abu Qdais (Member)	……
Prof. Nezar A. Al-Hammouri (External Examiner)	……

December, 2016

تفويض

نحن الموقعين أدناه، نتعهد بمنح جامعة العلوم والتكنولوجيا الأردنية حرية التصرف في نشر محتوى الرسالة الجامعية، بحيث تعود حقوق الملكية الفكرية لرسالة الماجستير الى الجامعة وفق القوانين والأنظمة والتعليمات المتعلقة بالملكية الفكرية وبراءة الاختراع.

المشرف الرئيس	الطالب
أ. د. فايز احمد عبدالله	**الهام وليد سعود الشرفات**
التوقيع والتاريخ	الرقم الجامعي والتوقيع **20133023018** .....

DEDICATION

To my precious Father Walid and to my Mother Mariam

ACKNOWLEDGMENT

At the outset, I thank God Almighty for giving me the confidence and strength to finish the master program which culminated in this thesis. During the two years I spent in the master's program, I have gained the knowledge and support of many people who will always have a special place in my memory.

No words enough to express my deepest gratitude for my supervisor Prof. Fayez Al Abdullah on his guidance and continuous support during this phase of my life as well as his believe in me when I didn't even believe in myself.

My deepest sincere thanks and appreciations to my professors are also not-expressible who I had the honor to be schooled under their hands. I would like to specifically thank the examining members of the Committee Prof. Wa'il Abu-El-Sha'r and Prof. Hani A. Abu Qdais from the Civil Engineering Department and Professor Nezar A. Al-Hammouri from the Hashemite University who I had the honor to have their presence in this important step in my life. I would like to thank the Civil Engineering Department staff at Jordan University of Science and Technology, especially Dr. Samer Talozi who has helped me a lot, and I greatly would like to thank my wonderful friends and colleagues for their help and support and to the special ones Mohammad Jamous, Mohammad Telfah, Nusaibah, Tassnem, Manal, We'am, Isra'a, Tamara, Amneh, and Rushdi.

Many grateful thanks to the Middle East Desalination Research Center (MEDRIC) for enhancing my educational experience and financing me while my working on the thesis letting me abler to focus more on my courses and thesis. I would love to thank gratefully the Ministry of Water and Irrigation (MWI) and Water Authority of Jordan (WAJ) for their cooperation and providing me with all the necessary data and feedback.

I want to express my gratitude and my love for my family members who have long halt beside me and supported me in every way, thanks to my precious mother Mariam, father Walid, grandmother Salma, wonderful sisters Salma, Nussaibah and Saba' and my brothers Saud and Abdul Rahman as well as my loving aunts.

TABLE OF CONTENTS

Title **Page**

LIST OF FIGURES

LIST OF TABLES

LIST OF ABBREVIATIONS

Abbreviation	Description
a.m.s.l	Above mean sea level
CanESM2	The Second Generation of Earth System Model
CGCM3	Third Generation Canadian Global Climate Model
DMC	Double-Mass Curve
FAO	Food and Agriculture Organization
GCM	Global Climate Model
GHG	Green House Gas
HRU	Hydrological Response Unit
IPCC	Intergovernmental Panel on Climate Change
MCM	Million Cubic Meter
MWI	Ministry of Water and Irrigation
MK	Mann-Kendall
MW	Mann-Whitney
NCEP	National Center for Environmental Prediction
RCM	Regional Climate Model
RCP	GHG Representative Concentration Pathway
SDSM	Statistical DownScaling Model
SP	The Super Predictor
SRES	Special Report on Emission Scenarios
Tmax	Maximum Temperature
Tmin	Minimum Temperature
WEAP	Water Evaluation and Planning Model
WWTP	Waste Water Treatment Plant
YR	Yarmouk River
YRB	Yarmouk River Basin

ABSTRACT

THE SPATIAL AND TEMPORAL SIMULATION OF THE HYDROLOGICAL WATER BUDGET FOR YARMOUK RIVER BASIN UNDER CURRENT AND PROJECTED FUTURE CLIMATE

By

Alham Walid Saud Al-Shurafat

In this study, the potential climate change over the trans-boundary Yarmouk River Basin (YRB) has been projected. The basin extends between Jordan and Syria and is relatively large of approximately 7004 km^2. The basin climate is semi-arid that causes the basin to highly depend on irrigation. The climate has been downscaled and projected using the statistical downscaling model (SDSM). The scenarios used to drive SDSM are GHGs Representative Concentration Pathways (RCPs) using CanESM3 GCM and Special Report on Emissions Scenarios (SRES) A1B and A2 using CGCM3 GCM. All scenarios have agreed that the annual rainfall rate will continue to decrease while the temperature will continue to increase generally. There was a good statistical confidence in the projections based on the uncertainty analysis results that have been performed. Thus, the projections can be adopted with satisfying confidence for any intended climate change impact study in the YRB.

After that, the projected climate change scenarios have been used to anticipate the climate change impacts on the YRB hydrological water cycle temporally and spatially. For this goal, the physically process-based semi-distributed hydrological model Soil and Water Assessment Tool (SWAT) has been used. The basin was modeled at two conditions: (1) The basin as if it has stayed without any manmade changes (pre-development) and (2) The basin as it gets changed in the real life (post-development). The modeling evaluation measures indicated a satisfactory performance at the monthly scale. Under the pre-development conditions, the impacts are believed to be somehow disproportionate and of high risk. This can be ascribed to the inadequate SDSM ability to reproduce the actual precipitation pattern. Under the post-development conditions, the impacts were of much less risk. In general, the results indicated that the YRB watershed hydrology is vulnerable to climate change. The major impact will be the spread of drought conditions without certain knowledge how severe it could be. In terms of political boundaries, the Jordanian side is expected to be the least vulnerable and even, on the contrary, its territories are expected to increase in rainfall.

Chapter One: Introduction

1.1 Problem Statement and Significance

The main surface and groundwater water resources of fresh water in Jordan are shared with neighboring countries. This is let Jordan to be involved in water conflicts and unfair conventions due to either the rivers headwaters presence in the shared countries or the balance of power difference. This situation lets inadequate fresh water available for Jordan comparing to what historically i.e. before the 1950s has been. In the meantime, the pressure on water resources has been increasing due to the fast population growth rate, massive influxes of refugees from the neighboring countries and the rapid economic development. These factors combined have emerged water scarcity as the most detrimental environmental issue Jordan have to face at present and in the future. Currently, Jordan is considered one of the ten poorest countries in water worldwide. So far, water deficit has been handled through the unsustainable practice of overdrawing highland aquifers, resulting in lowered water tables and declining water quality. Nowadays, there is a large awareness about the seriousness of the situation led to tremendous efforts by governmental and non-governmental organizations. Main practiced ways in Jordan to sustain water include the efficient developments of new water supplies, water harvesting, small-scale desalination, reuse of wastewater for the agricultural sector, and water demands reduction (Abu-Jaber 2003; Hadadin 2010).

Climate change is another recent decisive issue due to the demonstrated vulnerability of natural systems toward it. Consecutive droughts with varying severity within the different basins/regions have been detected over Jordan, though drought was never announced during the past decade. The only time that a state of drought was declared nationwide in the history of modern Jordan was in 1998/1999; when the country was hit by extreme drought (with rainfall representing 30% of the annual average) for two consecutive water years until 2000 (Khordagui 2014; Shatanawi 2013). Therefore, for more profound sustainable management of water resources, projected changes in climate and their potential impacts on watershed hydrology has become indispensable Within this context, this study has been designed to project the future climate and evaluate its potential implications on a major surface water resource, the trans-boundary Yarmouk River Basin

(YRB). The basin riparians are Jordan and Syria as well as Israeli occupation of around 1% of the basin after 1981. The study aiming at simulating climate changes and its impacts on the basin hydrology during the 21st century under various conditions spatially and temporally. To achieve this, the most reliable modeling tools combined with the best available data and approaches have been used. Such evaluation can help in enhancing the basin management and propose different adaptation schemes to possible extreme climate change conditions.

1.2 Thesis Objectives

The main objectives of this study for the YRB are: (1) to detect the climate change trends in the available records of climatological data, (2) to downscale and project the climate change using SDSM and address the model skill in downscaling such a semi-arid climate and (3) to analyze the impacts of the projected climate change on the YRB using SWAT

1.3 Thesis Structure

This dissertation is organized into seven chapters to address the research objectives with the first chapter introducing and providing organizing context to the dissertation. Chapter 2 contains a literature review related to the climate change, climate change models, the downscaling technique for climate change projections, hydrological modeling and a general literature review on downscaling and hydrological modeling related to the study area.

Chapter 3 details description of the study area, input data sets used throughout the study, a comprehensive description of the used models and the underlying theory as well as the methods used for examining historical climate trends, developing climate change predictions and hydrologic simulation. In addition to that, all evaluation indices and criteria have been described thoroughly.

Chapter 4 summarizes the historical trend analysis results to address the reality of climate change at the watershed scale.

Chapter 5 outline the results of climate downscaling model calibration, validation, and the associated uncertainties, as well as the climate, changes projected along the 21st century under various carbon dioxide emission scenarios.

Chapter 6 shows the hydrological modeling and climate change impact results temporally and spatially under the projected climate change scenarios.

Finally, Chapter 7 summarizes the overall conclusions and provides recommendations for future research related to this study.

Chapter Two: Literature Review

2.1 Climate Change

2.1.1 Climate Change Phenomena

The 5th Assessment Report (AR5) of the Intergovernmental Panel on Climate Change (IPCC) reported that the globe average temperature has already increased by 0.85^{o}C (0.65–1.06^{o}C) during the period of 1800–2012. In addition to that, substantial changes in precipitation patterns and amounts have been already detected worldwide spatially and temporally. These changes are attributable to the increased emissions of greenhouse gasses (GHGs) such as carbon dioxide, methane and others that followed the Industrial Revolution with the beginning of the eighteenth century due to primarily the fossil fuel burning and secondarily deforestation and air pollution. It has been observed that the Earth temperature had been cooling somehow before this sudden warming. The major GHG emitters are China, the USA, and India with approximately 50% of the total world GHGs emissions. Generally, what has been observed and also forecasted by climate change models is that wet areas are becoming wetter while dry areas are becoming drier. However, precipitation patterns haven't changed that much because the changes in winds are still modest (Flato 2013; Dore 2005; Trenberth, 2011).

The change in climate extremes events which are typically defined as floods and droughts are what actually the most influential due to their larger adverse impacts on the globe than averages (Field 2012; Katz, 1992). Easterling et al. (2000) examined painstakingly tremendous studies of climate extremes change in observations, modeling, and impacts. Their findings underlined the reality of climate change through evident total precipitation and temperature extremes change that is responsible for uncommon recent flooding damages, water scarcity, and biological species climate-induced extinctions, apparent gradual biological changes and species range shifts. Therefore, the prediction of climate for the twenty-first century have been attracting strong interest because those predictions are the vital key input for present and future impact studies worldwide. This is important for long-term planning, mitigation and adaptation strategies at all levels making their reliability a very critical issue (Meehl, 2007).

Regarding the climate change in the Middle East specifically, a high-level workshop performed a comprehensive reliable analysis of the trends in extreme precipitation and temperature indices change in the region. The workshop reported that for 1950–2003, there have been statistically significant and spatially coherent warming trends in extreme temperature indices. In the other hand, for extreme precipitation indices, the trends in the extreme events were found weak and do not have spatial coherence (Zhang, 2005). For Jordan in particular, Smadi (2006) detected trends and abrupt changes in the mean Tmax and Tmin after studying the oldest major Jordanian meteorological station Amman Airport between 1922 and 2005. Their results revealed the occurrence of sudden climate changes in 1957 and 1967 which after gradual significant warming trend of 0.038^{o}C/year was found to be happening. Al-malabeh et al. (2016) studied the Jordanian Badia, Syrian Badia and Saudi neighboring areas at 9 representative stations which are Mafraq, Safawi, Rwaished, Azraq, Um El-Jumal, Ramtha in Jordan, Dara'a at south Syria, and Turaif and Guriat at North Saudi-Arabia. Their results outlined with significant confidence that air temperature is increasing at annual rate 0.02-0.06^{o}C/year while precipitation is decreasing at annual rate 0.5-2.6 mm/year.

For the 21st century projection of climate change, Evans (2009) has used 18 global climate models (GCMs) partaking in the IPCC Fourth Assessment Report (AR4) to scrutinize the future projections in the middle east under the Special Report on Emission Scenarios (SRES) A2 emission scenario. His findings predicted warming and highlighted that overall temperature may increase around 1.4^{o}C and 4^{o}C by mid- and late-century respectively while precipitation is expected to decrease widely especially in the Cyprus, Greece, Lebanon, Syria, Palestine, Israel, Turkey, Egypt Jordan, Libya, Turkey, Syria, and Northern Iran. Nevertheless, there would be a slight increase in the southernmost areas because of the Northward movement of the Inter-Tropical Convergence. Those predictions are consistent with those of Lelieveld et al. (2012) who had examined long-term meteorological datasets as well as regional climate model projections under the SRES A1B scenario speculating that droughts would increase in terms of intensity and frequency and rainfall would decrease in terms of days and amount in the region. This future picture of pronounced increase of temperature and decrease in precipitation under various scenarios is attributed to increased anticyclonic circulation resulting in increasingly stable conditions and is associated with a northward shift of the Atlantic storm track (Giorgi, 2008). Consequently, it is well conceded that middle east will be one of the most expected regions for profound climatic change (Stocker 2013; Giorgi, 2008). Major direct impacts of these

projected climate changes would encompass mainly heat stress and more fresh water scarcity particularity in the Levant (Lelieveld, 2012). However, should keep in mind that there is a big "if" surround those projections due to the inherent uncertainties in the climate models at this regional scale specifically in terms being unable to capture orographically-induced fine scale region structure (Prudhomme 2009; Giorgi, 2008).

2.1.2 Climate Change Mitigation

Climate change due to man-made changes that are reflecting in the unnatural high GHG emissions can be reduced or even stopped totally through various possible mitigation ways as most scientists confirmed. Climate change mitigation has become a common phrase that refers to all efforts to reduce or prevent the emission of GHGs. Mitigation can mean using new technologies and renewable energies that can replace fossil fuels, making older equipment more energy efficient, or change management practices or consumer behavior (IPCC, 2011). The bulk of the burning of fossil fuels is to generate electricity. Therefore, IPCC has assessed most efficient electricity generation mitigation technologies that included coal- and gas-fired power plants, solar power technologies, hydropower, wind power, and geothermal. Nuclear power was found to be of the largest mitigation potential and have the second lowest mitigation costs after hydropower. Currently, nuclear power is used within 29 countries and produce 15% of the world's electricity, thus, saving is 20% of the globe GHGs emissions. Accordingly, many countries are increasingly turning to develop a peaceful, civilian nuclear energy programs. However, there are risks associated with an increasing use of nuclear power including mainly the operational safety concerns, uranium mining risks, unresolved waste management issues, nuclear weapon proliferation concerns, and adverse public opinion (IPCC 2015; IPCC, 2007; Jordan Atomic Energy Commission (JAEC) 2011).

Europe is the pioneer in the renewable energy sector with having Germany, Denmark, and Sweden as the leading countries (Jacobsson, 2009). For example, the Denmark produces most days more than 100% of the need of electricity using the renewable energy. Denmark and Sweden are planning to become first-fuel free nations in the world by 2050 due to the immense public campaigns to stop climate change (The Offical Website of the Denmark, 2016; The Government of Sweden, 2016). The main challenge to renewable energy worldwide spread is the investment high capital costs though actually as soon as one invest in the renewable energy, it will become free of charge forever making it very profitable. This is leaving the main hinder of the spread the

renewable energy, in reality, is the systematic resistance campaigns by the powerful fossil fuel companies for the sake of their interests and profits (Peidong, 2009). The USA is the least country in taking action toward the climate change because the USA barely believes in climate change though it is one of the main GHG emitters (McCright, 2013; Betsill, 2001).

One of the most effective mitigation opportunities is stopping the rainforests cut for the sake of commercial products that can be dispensed with because those forests play a key role in maintaining the stability of the climate of the earth via absorbing and storing a huge portion of the atmosphere carbon dioxide (Canadell, 2008). Another opportunity is to replace a large part of cows breeding for meat production purposes with other varieties such as chicken since cows breeding is the main source of the methane that its molecule is equivalent to 23 carbon dioxide molecule (Goodland, 2009).

Scientists believe that if the GHGs emissions that resulting from human activities stops, the Earth will be able in a short time to restore its climate and the poles will regain quickly the ice that has melted through the last few decades due to global warming. Within this framework, several climatic summits have been to address the reality of the climate change and the possibilities of mitigation and adaptation, which finally culminated in the Paris Climate Change Summit agreement 2015. The agreement was within the United Nations Framework Convention on Climate Change (UNFCCC) in which 93 UNFCCC members have signed the treaty of following all the possible climate change mitigation and adaptation measures, as well as financing by the year 2020 with 100 members, have already ratified the treaty (United Nations Framework Convention on Climate Change (unfccc) 2015). Jordan is among the countries who ratified Paris treaty and plan to have sustainable, environmentally friendly long-term economic growth. To achieve this goal, Jordan established a nuclear power plant program to provide a reliable energy source with very low GHGs emissions. Two planned nuclear reactors are under construction and will be in operation by 2025 to provide nearly half the country's electricity (Jordan Atomic Energy Commission (JAEC) 2011).

2.2 Downscaling

Currently, Global Climate Models (GCMs) are the commonly used approach to project the climate change on global and continental levels under various GHGs emission scenarios. IPCC assessment reports are all based on large data sets of future climate projections provided by many modeling groups worldwide who run several GCMs under various experiments and GHGs emissions scenarios (Fowler 2007; Semenov, 2010). However, the GCMs has a low capability to capture complex topographical features and meteorological processes at regional (50×50 km) and local (0–50 km) scales due to its coarse resolutions (100–500 km). Accordingly, the GCMs output is considered of no use for climate change impact studies at subgrid scales (Gu 2012; Xu, 1999). For example, it's common to predict potential climate change at the watershed scale because comprehending climate change impacts on watershed hydrology is a valuable knowledge toward managing freshwater resources within any watershed (Oni, 2014).

To overcome this problem, downscaling techniques have emerged to build relationships between GCMs output and subgrid climate variables such precipitation and temperature which are what impact assessors require (Wilby, 1997). There are two broad approaches of downscaling which are either dynamical or statistical. The dynamical approach employs fine-resolution regional climate models (RCMs) and nests it into the GCMs over a limited area, thus become able to capture physical processes at a subgrid resolution. In the other hand, the statistical approach provides statically relationships between GCMs large-scale variables (predictors) and subgrid observed scale climate variables (predictands). Both approaches of downscaling have been reviewed thoroughly in a number of key papers. The reviewers agreed that the statistical approach is the preferred because of its implementation ease, low cost and relative fewer computations while maintaining an acceptable level of accuracy (Maraun 2010; Wilby, 1997; Wilby, 2002).

One of the most recommended statistical downscaling tools currently available is the Statistical Downscaling Model (SDSM) for both mean and extreme climate change impact assessment studies (Gachon, 2005; Dibike, 2008; Khan, 2006; Wilby, 2007; Wilby, 2002; Hashmi, 2011). SDSM is a hybrid of multi-regression based methods and stochastic weather generator that facilitates the rapid development of multiple, low-cost, single-site scenarios of daily surface weather variables under present and future climate forcing. SDSM is the most ubiquitous statistical downscaling software used in the scientific

literature with over 200+ studies in over 39 countries. Though SDSM reliability as decision support tool has already been demonstrated, its skill in simulating temperature is much better than precipitation (Wilby, 2002; Gachon, 2005). Therefore, to overcome that, it is recommended simulating the largest possible number of rainfall stations in the targeted area and examine carefully the quality of the SDSM input rainfall data. Furthermore, future climate projection is accompanied with a high amount of uncertainties that originated from the GCMs and the downscaling technique itself (Prudhomme 2009). Those uncertainties that are connected to the GCMs are the greatest (Chen, 2011). Therefore, conducting uncertainty analysis is inevitable in climate change impacts studies because the potential transformation of existing biases in baseline simulation to future simulations is a decisive matter (Prudhomme, 2009).

2.3 Hydrologic Modeling

Hydrology is the study of earth's waters motion through the hydrologic cycle, as well as constituents (e.g. sediment and pollutants) transport with the water flow (Maidment, 1996). Many models have been developed over the past decades in order to simulate and predict the hydrological water budget within any region and at any scale (Arnold, 1996). The first widespread hydrologic models generation has been the not very physically-based lumped models that consider the watershed as a single unit with a single rainfall input and based on the unit hydrograph (UH) concept assuming the rainfall excess is only what generate runoff. The UH can be derived from recorded hydrologic data or statistical parameters based on the watershed physical characteristics. Afterward in the 1970s, what called black box models have evolved and it included primarily two types: the autoregressive models and artificial neural network models. Both types based on the concept of time series analysis but the second type is able to incorporate information based on available data. Because of the many inherent simplifications of these models, it is not possible to capture the heterogeneity within the watershed thus very high uncertainties in its output. Nowadays after the technology has evolved dramatically, it became possible obtaining a comprehensive spatial knowledge of wide variety of variables representing a study area at fine resolution (100-500m) and handling this enormous information in a very short time. This led to moving toward the physically-based distributed models in which variables spatial variability is integrated thus modeling more faithfully and accurately the hydrologic processes that happen within a watershed. These models are complex and require the identification of tremendous of spatial parameters that should be estimated

from field data as possible, otherwise, should be calibrated. Then those calibrated parameters are incorporated in the distributed model to apply the hydrologic processes equations to each resolution unit and later aggregate the neighbor units' output. The hydrological models constitute the most effective tools for the study of climate change or management practices impacts over any hydrological units (Singh, 1989).

One of the most used worldwide distributed hydrologic model is the Soil and Water Assessment Tool (SWAT). SWAT is continuously under development at the USDA-ARS and the Texas AgriLife Blackland Research Center in Temple, Texas, as well as other research sites in North America and in other regions by multiple user groups that keep developing the model itself, its use and the calibration and validation approaches such as SWAT, ArcSWAT, VizSWAT, SWAT-CUP, Latin American, southeast Asia, Africa, Iran, and Brazil user groups. SWAT various applications have been documented by an immense number of publications that outlining the model high efficiency to predict the effect of climate and management decisions on water, sediment, nutrient and pesticide yields with reasonable accuracy on large, ungagged river basins. Many official institutes have adopted SWAT as the main model to study any climate or management impacts on a watershed such as NRCS (Temple and other Locations), EPA, Environmental Consulting Firms, Texas River Authorities, universities, NOAA as well as many similar entities worldwide (USDA Agricultural Research Service 2016; Arnold, 2012).

2.4 Related Studies to the Study Area

Kunstmann et al. (2007) have downscaled dynamically the ECHAM4 GCM climate output for the Upper Jordan basin under the scenario B2 with the meteorological model MM5 to a final resolution of 18 km. The climate projections were used then to drive the distributed, physically-based hydrological model WaSiM. It was found that by 2070–2099 relative to 1961–1990 period, mean annual temperature will increase up to 4.5^{o}C, and mean annual precipitation will decrease down to 25%. The impacts will be total runoff decrease by 23%, and a significant groundwater recharge decrease.

Abdulla et al. (2009) used various climate conditions included ±20% rainfall change, and 1^{o}C, 2^{o}C and 3.5^{o}C average temperature increase in run the distributed model BASINS-HSPF for the Zarqa River Watershed (ZRW). The ZRB is one of the major tributaries of the Jordan River Basin that is characterized by a semi-arid climate. The obtained results indicated warming can be influenced by changes in rainfall significantly and can dramatically impact runoffs and groundwater recharge.

Samuels et al. (2010) have used a technique based on the statistical correction of observed and modeled climate to downscale the regional climate model RegCM3 precipitation output to the station level in the Jordan River basin under the SRES A1B scenario. After that, the climate change projections were integrated into a watershed model called the Hydrological Model for Karst Environment (HYMKE). The results have been suggested slight changes in precipitation and potential evaporation during 2010-2035. By 2060, a precipitation decrease of about 10% and evaporation increase of about 5% can occur. These changes will reduce the Jordan River and its tributaries daily mean baseflow by10%–11% and the streamflow by 17%.

Wade et al. (2010) quantified the impact of climate change on the water resources of Jordan by the end of the 21st century via driving a suite of hydrological models with the output scenarios regional climate model, HadRM3. The projections illustrated there will be an increase in mean annual winter precipitation and increase in mean annual near-surface air temperatures causing further reduction in the groundwater recharge. However, the extreme flood flows will not be affected in the upper River Jordan substantially.

Smiatek et al. (2011) estimated the future climate conditions in the Jordan River region, using a nested dynamic downscaling approach using the National Center for Atmospheric Research–Penn State University meteorology model. SRES A1B emission scenario from Hadley Centre global circulation model was used to drive the dynamical model for the period 1960–2099. The results showed good reproduce of the mean temperature and precipitation patterns but limited precipitation seasonality reproduction. The projections showed mean annual mean temperature increase/precipitation decrease of 2.1ºC/−11.5% for 2031–2060 and 3.7ºC/−20% for 2070–2099 relative to the baseline period 1961–1991. In addition, the results expected a larger interannual precipitation variability and more heat waves. Therefore, it was concluded that water availability in the Jordan River region will vulnerable to the risk of significant reduction.

Samuels et al. (2011) presented results from regional climate model simulations with RegCM3 and MM5 for the Jordan River region of the Middle East to project changes in frequency and intensity of extreme events. The results showed that maximum daily summer temperature is expected to increase 2.5-3ºC, with an increase in warm spell length. Precipitation extremes are expected to increase with longer dry spells, shorter wet spells, and more heavy rainfall.

Chenoweth et al. (2011) investigated the likely impacts of climate change on the water resources within the eastern Mediterranean and Middle East region using a high-resolution regional climate model (PRECIS). The projections showed approximate 10% decrease in precipitation across the study area by the middle and the end of the 21st century. In the Middle East, climate change coupled with population growth is likely to reduce per capita water resources considerably. Among the countries of the highest need for adaptation were Syria due to its large agricultural workforces and Jordan due to its low per capita water resources coupled with limited options for desalination.

Smiatek and Kunstmann (2015) have used climate change data from five different RCM models run in two Coordinated Regional Climate Downscaling Experiments (CORDEX) experiments to evaluate its impacts on the future discharge of the Upper Jordan River. Impacts were modeled using the hydrological simulation model WaSiM-ETH. The results indicated an annual mean temperature increase/precipitation increase of 2.6^{o}C/-20% and discharge decrease of -25.3% by 2071-2100 relative to 1971-2000.

Raggad et al. (2016) have statistically downscaled different GCMs to examine the impact of the current climatic conditions on the variability of groundwater recharge in Ajlun Highlands in Jordan along the 21st century. Groundwater recharge was modeled using the J2000 water budget model. The results showed that on average, the precipitation will decrease by 18.7% while maximum and minimum temperatures will increase by 1.7^{o}C and 2.2^{o}C respectively by the year 2050. This will cause the groundwater recharge to reduce by 27% less than current recharge. This in turn with the continuous over-pumping will reduce the saturated aquifer thickness by 20 to 65%.

Chapter Three: Study Area, Data Sets and Methodologies

At the outset, this chapter will explain enough the nature of the study area. Subsequently, the chapter will detail all the data necessary to conduct the study followed by an adequate explanation of the used method.

3.1 Study Area

The surface Yarmouk River Basin (YRB) extends within two countries Jordan and Syria in a semi-arid region. The basin is of volcanic origin overlies basalts plateau covering around 78% of its area featuring mountainous and plains regions (Burdon 1954). The basin total area is approximately 7004 km^2 of which 1424 km^2 (21%) lies inside Jordan while 79% lies in Syria of which 10% (Golan Heights) is under the Israeli occupation as seen in Figure 3.1. The basin extends from Jabal al-Arab heights to the east, Ghabaghab to the north and the city of Qatna to the northwest in the Syrian territories and to include northern and eastern Irbid, and western Mafraq in the Jordanian territories. The altitudes in the basin vary from 1858 m a.m.s.l at Jabal al-Arab then fluctuates between 500 and 650 a.m.s.l in the plain in the basin middle to the lowest point 212 m b.m.s.l at the confluence with the Jordan River which is the basin outlet. The basin's middle plains contain many hills in the mid-north of the western edge, such as the Harah, Jaybah, Jumu', Al-Ahmar Al-Sharqi, Al-Ahmar Al-Gharbi, and other hills.

The basin seasonal rivers and valleys drain into the approximately 60 km narrow and shallow perennial Yarmouk River (YR) forming the border between Jordan and Syria. The river is the largest tributary of the Jordan River (JR) joining it below Lake Tiberias measuring its largest width of 9 m and depth of 1.5m. The river main tributaries are the seasonal streams Allan and Ruqqad from the north and Harir, Dahab and Zeidi from the east within the Syrian territories (AL-Momani, 1993). The river mean annual historic flow was estimated at 450-500 MCM up to the 1950s which after has been declining to reach 83-99 MCM at present due to the construction of a series of infrastructure and diversion schemes. However, the river has a highly variable torrential flow with a very low baseflow that ranges currently from 0.5 to 5 m^3/s and prone to irregular flooding caused by rain storms of about 71 MCM.

Syria and Jordan have signed a bilateral treaty over the sharing of the YR in 1987 in preparation for the construction of the Al-Wehda dam on the border between the two countries. Much of the flow of the YR is diverted by Syria, leaving only a small share to Jordan amounting to only about one-third of the proposed share as per treaties and agreements (Ministry of Water and Irrigation, 2016). Jordan uses 290 MCM/yr of water from JR and YR and diverts it to the King Abdullah Canal to be used for irrigation of crops in the Jordan Valley and for domestic use in the Jordan capital Amman**.** Currently, the YRB undergo increasing intensive urban, industrial and agricultural activities and plays a central role in socioeconomic development for both Jordan and Syria (UN-ESCWA, 2013).

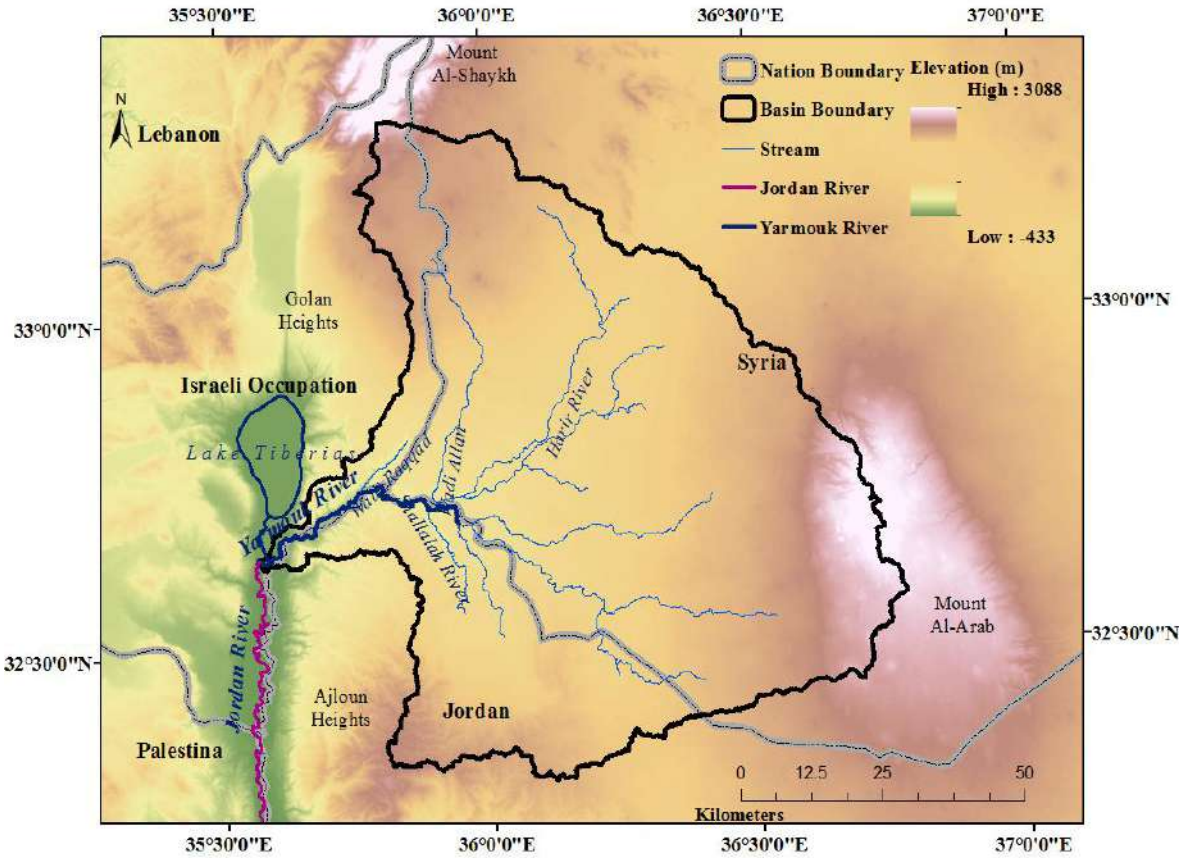

Figure 3.1: Location map of Yarmouk River Basin (YRB)

The climate prevails in the YRB is classified as Mediterranean subtropical climate (CSA) that has moderate seasonality (Kottek, 2006). The seasons are December of the previous year to February (winter), March to May (spring), June to September (summer) and October to November (autumn). Summers are dry and hot because of subtropical high-pressure systems domination while winters have moderate temperatures and changeable, rainy weather due to the polar front. The observed mean precipitation and temperature

along the year (1981-2009) are depicted in Figure 3.2. Spatially, average annual rainfall ranges approximately from 106 mm in the southern lowlands (Jordanian desert) up to 486 mm in the northern west (Golan Heights). Average Tmax-Tmin ranges from 30-13ºC in the low western lowlands (Jordan Valley) and 18-10ºC in the highlands.

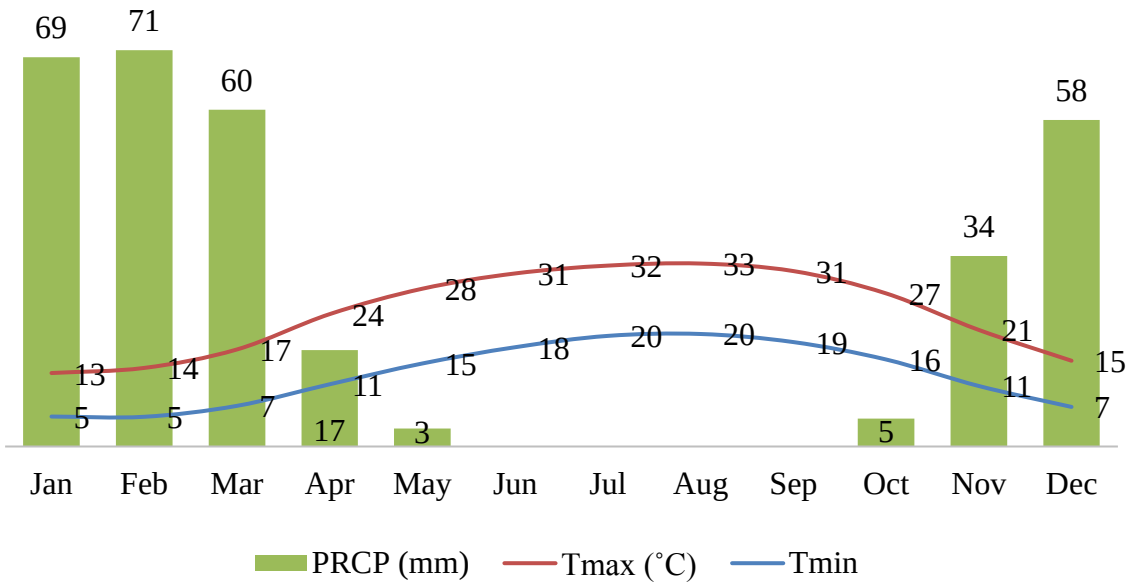

Figure 3.2: Mean monthly climate diagram of YRB as observed (1981-2009)

3.2 Data Sets

3.2.1 Basin Delineation

The delineation was done using 1 arc-second (approximately 30m) resolution Digital Elevation Model (DEM) from the Advanced Spaceborne Thermal Emission and Reflection Radiometer (ASTER). One-degree tiles covering the study area were downloaded from USGS Earth Explorer website (http://earthexplorer.usgs.gov/) and then processed using tools within ArcGIS 10.2.1 (©1999–2013 Esri Inc.) into voids sink and mosaicked DEM The DEM was projected to the Universal Transverse Mercator (UTM) projection system in northern hemisphere zone 36N that encompass the study area. The YRB basin boundaries were extracted from the DEM using ArcSWAT interface for the Soil and Water Assessment Tool (SWAT) 2012. The basin is shown in Figure 3.1. %

3.2.2 Basin-Scale Observed Climate Data (Predictands)

Local observed daily climate (natural variability) at 13 stations for precipitation (PRCP) and 5 stations for maximum temperature (Tmax) and minimum temperature (Tmin) were obtained from the Jordanian Ministry of Water and Irrigation (MWI),

Department of Meteorology. Other ten stations for annual rainfall amounts from 1960 to 1984 were obtained from the Syrian Meteorological Department in 1985 by the Jordanian MWI for the Project of Water Resources Investigation in North Jordan (Yarmouk, Amman-Zarqa, and Azraq Basin) to represent the Syrian part of the YRB. The total 28 stations are shown in Figure 3.3 while Table 3.1 and Table 3.2 summarize the stations' information, their geographic characteristics and the temporal span of data availability. Other climate information including wind speed, solar radiation and dew-point were taken from the gross meteorological stations Irbid and Baqoura.

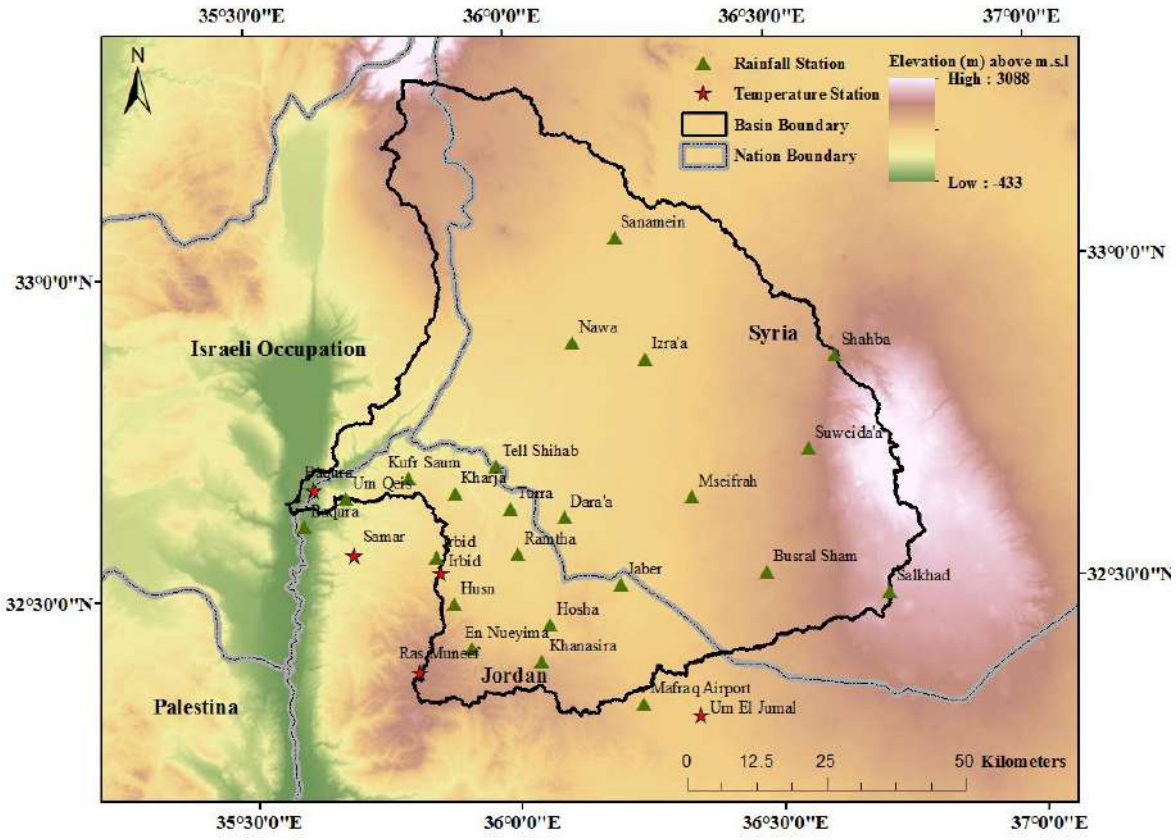

Figure 3.3: The YRB meteorological stations that have been used in the study

Table 3.1: Geographic characteristics and the temporal span of data availability of the meteorological stations for precipitation that used in the study

Station ID	Station name	Elevation (m)	Latitude	Longitude	Data availability	Record length (yr.)	Country
AE0001	Irbid	616	32° 33' 33"	35° 50' 57"	1938-2009	71	JO*
AD0003	Kufr Saum	423	32° 41' 2"	35° 47' 55"	1981-2009	29	JO
AD0005	Um Qeis	351	32° 39' 16"	35° 40' 45"	1981-2009	29	JO
AD0008	Kharja	441	32° 39' 29"	35° 53' 13"	1981-2009	29	JO
AD0010	Husn	637	32° 29' 12"	35° 52' 50"	1981-2009	29	JO
AD0011	En Nueyime	748	32° 25' 2"	35° 54' 43"	1981-2009	29	JO
AD0012	Ramtha	513	32° 33' 39"	36° 0' 12"	1981-2009	29	JO
AD0013	Khanasira	810	32° 23' 38"	36° 2' 40"	1981-2009	29	JO
AD0019	Mafraq	667	32° 19' 20"	36° 14' 10"	1981-2009	29	JO
AD0021	Turra	446	32° 37' 53"	35° 59' 29"	1981-2009	29	JO
AD0022	Hosha	589	32° 27' 2"	36° 3' 40"	1981-2009	29	JO
AD0023	Jaber	571	32° 30' 36"	36° 11' 60"	1981-2009	29	JO
AD0032	Baqura	-227	32° 36' 45"	35° 35' 49"	1981-2009	24	SYR**
AD0400	Izra'a	575	32° 51' 30"	36° 15' 26"	1961-1984	24	SYR
AD0401	Nawa	563	32° 53' 12"	36° 7' 7"	1961-1984	24	SYR
AD0403	Sanamein	750	33° 2' 53"	36° 12' 21"	1961-1984	24	SYR
AD0405	Shahba	1250	32° 51' 17"	36° 37' 13"	1961-1984	24	SYR
AD0408	Tell Shihab	299	32° 41' 53"	35° 58' 2"	1961-1984	24	SYR
AD0409	Suweida'a	1010	32° 42' 40"	36° 33' 53"	1961-1984	24	SYR
AD0412	Dara'a	500	32° 36' 58"	36° 5' 40"	1961-1984	24	SYR
AD0413	Mseifrah	685	32° 38' 29"	36° 20' 24"	1961-1984	24	SYR
AD0414	Busral Sham	800	32° 31' 22"	36° 28' 36"	1961-1984	24	SYR
F-S1	Salkhad	1447	32° 29' 3"	36° 42' 37"	1961-1984	24	SYR

*JO=Jordan **SYR=Syria

Table 3.2: Geographic characteristics and the temporal span of data availability of the meteorological stations for the temperature that used in the study

Station ID	Station name	Elevation (m)	Latitude	Longitude	Data availability	Record length (yr.)	Country
AD0032	Baqura	-227	32° 40' 0"	35° 37' 0"	1970-2005	35	JO*
AD0034	Samar	332	32° 33' 54"	35° 41' 28"	1981-2009	28	JO
AE0001	Irbid	616	32° 32' 4"	35° 51' 18"	1970-2005	35	JO
AH0003	Ras Muneef	1150	32° 22' 49"	35° 48' 41"	1976-2005	29	JO
AL0059	Um El Jumal	650	32° 18' 8"	36° 20' 39"	1976-2009	33	JO

*JO=Jordan

3.2.3 Large-scale Atmospheric Variables (Predictors)

Twenty-six large-scale observed and modeled atmospheric variables (predictors) were downloaded from the Canadian Climate Change Scenarios Network (CCCSN) website (www.**cccsn**.ec.gc.ca/). Modeled predictors were obtained for two GCMs due to the downscaling input files availability in formats compatible with the statistical downscaling model (SDSM). Both GCMS were developed by the Canadian Centre for Climate Modelling and Analysis (CCCma) in Canada. One model is the Coupled Global Climate Model (CGCM) that generates climate change scenarios using Greenhouse Gases (GHG) Special Report on Emissions Scenarios (SRES). The other model is the second generation of Earth System Model (CanESM2) that generates climate change scenarios using GHG Representative Concentration Pathways (RCPs).

The SRES scenarios were published in 2000 and IPCC had adopted them for its Third Assessment Report (TAR) in 2001 and Fourth Assessment Report (AR4) in 2007. SRES are expressing changes in GHG emissions that accompany specific possible future socioeconomic, technological, demographic, and political storyline of developments and radiative forcing. Both A2 and A1B scenarios that have been adopted in this study belong to the economic focus family and expect the emissions to continue to increase along the 21st century (Figure 3.4). By the end of 21st, the storyline A2's CO_2 concentration is expected to reach approximately 840 ppm while the moderate storyline A1B will reach 700 ppm.

RCPs have been adopted by the IPCC for the Fifth Assessment Report (AR5) in 2014 to supersede SRES projections. RCPs reflect GHG concentration (not emissions) trajectories of possible climate futures of anthropogenic (i.e., human) GHG emissions. In other words, RCPs are not based on predefined storylines as it's the case of SRES but instead RCPs radiative force change can have resulted from a variety of possible combinations of economic, technological, demographic, and policy developments with the years to come will reveal which trajectory is the most possible. The used RCPs in the study, RCP2.6, RCP4.5, and RCP8.5, are expressing possible radiative forcing values increase (+2.6, +4.5, and +8.5 W/m2, respectively) relative to pre-industrial values by the year 2100. The radiative forcing in the friendliest pathway RCP2.6 will peak at approximately 3 W/m2 (~400 ppm CO_2) and then declines to 2.6 W/m^2 (~330 ppm CO_2) in the year 2100. The moderate pathway RCP4.5 radiative forcing will keep increasing up to approximately 4.5 W/m^2 (~540 ppm CO_2) by the end of the 21st century. The worst pathway RCP8.5

radiative forcing will continue to rise until peaking at around 8.5 W/m^2 (~940 ppm CO_2) in the year 2100 (Stocker, 2013; Flato, 2013; Sillmann, 2013). All SRES and RCPS carbon dioxide (CO_2) concentrations trajectories as observed in the 20th century and projected along the 21st century are displayed in Figure 3.4 (Sillmann, 2013).

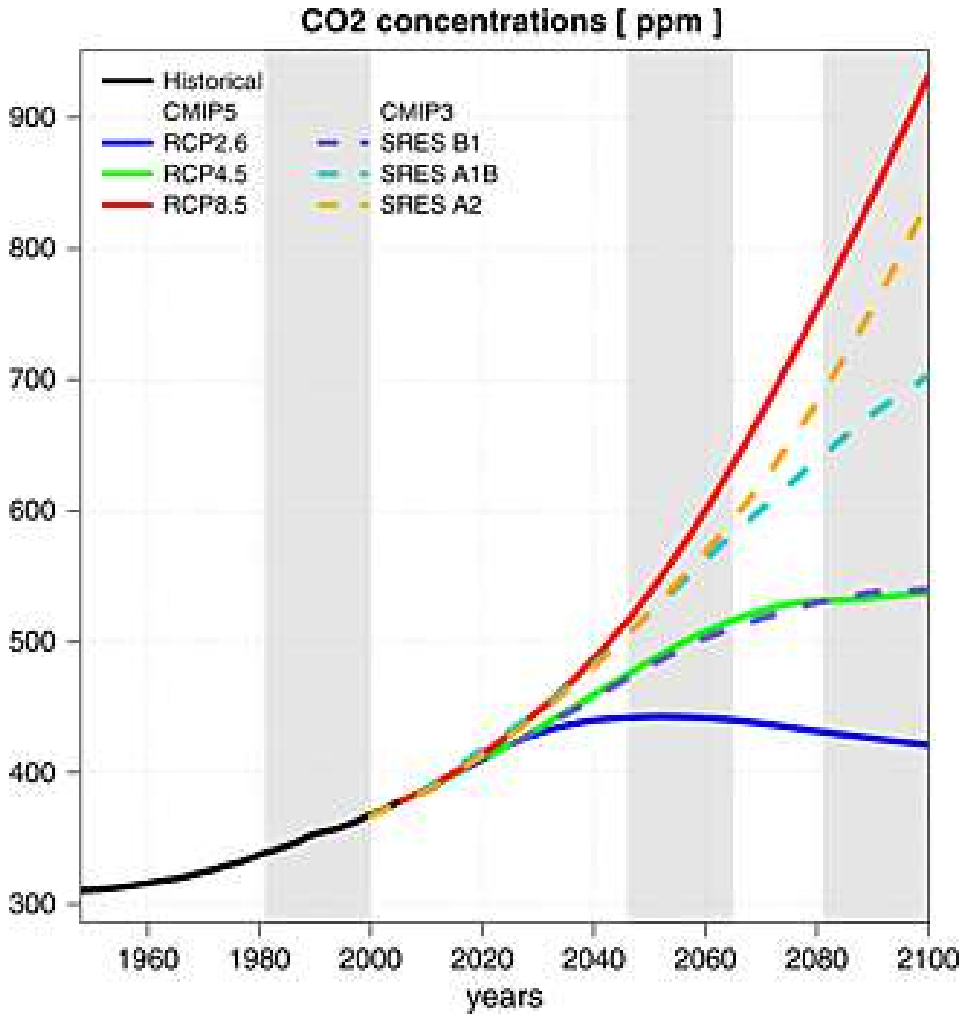

Figure 3.4: CO_2 concentrations in ppm that used do drive climate change scenario simulations by the IPCC (Sillmann 2013).

More details about the used two GCMs and it's grid boxes that cover the YRB are summarized in Table 3.3 while Figure 3.5 shows the GCMs grid boxes that overlaid YRB. The downloaded dataset from each model contain the observed predictors that are derived from the National Center for Environmental Prediction (NCEP) re-analysis dataset that is re-gridded to the same coordinate system as the corresponding GCM and normalized with respect to their respective 1961-1990 mean; the 26 predictors available are listed in Table 3.4.

Table 3.3: The GCMs and the GHGs scenarios used in the study (Network 2007)

Official name	Resolution (Lon x Lat)	Grid box centroid		Scenarios	Simulation type	Period
		Lon(E)	Lat(N)			
CGCM3_1 (CGCM3)	3.75° x 3.75°	35.26°	33.75°	20C3M	Historical	1961-2000
				A1B	Future	2001-2100
				A2	Future	2001-2100
CanESM2 / CGCM4 (CanESM2)	2.813° x 2.813°	36.562°	32.091°	20C3M	Historical	1961-2005
				RCP2.6	Future	2006-2100
				RCP4.5	Future	2006-2100
				RCP8.5	Future	2006-2100

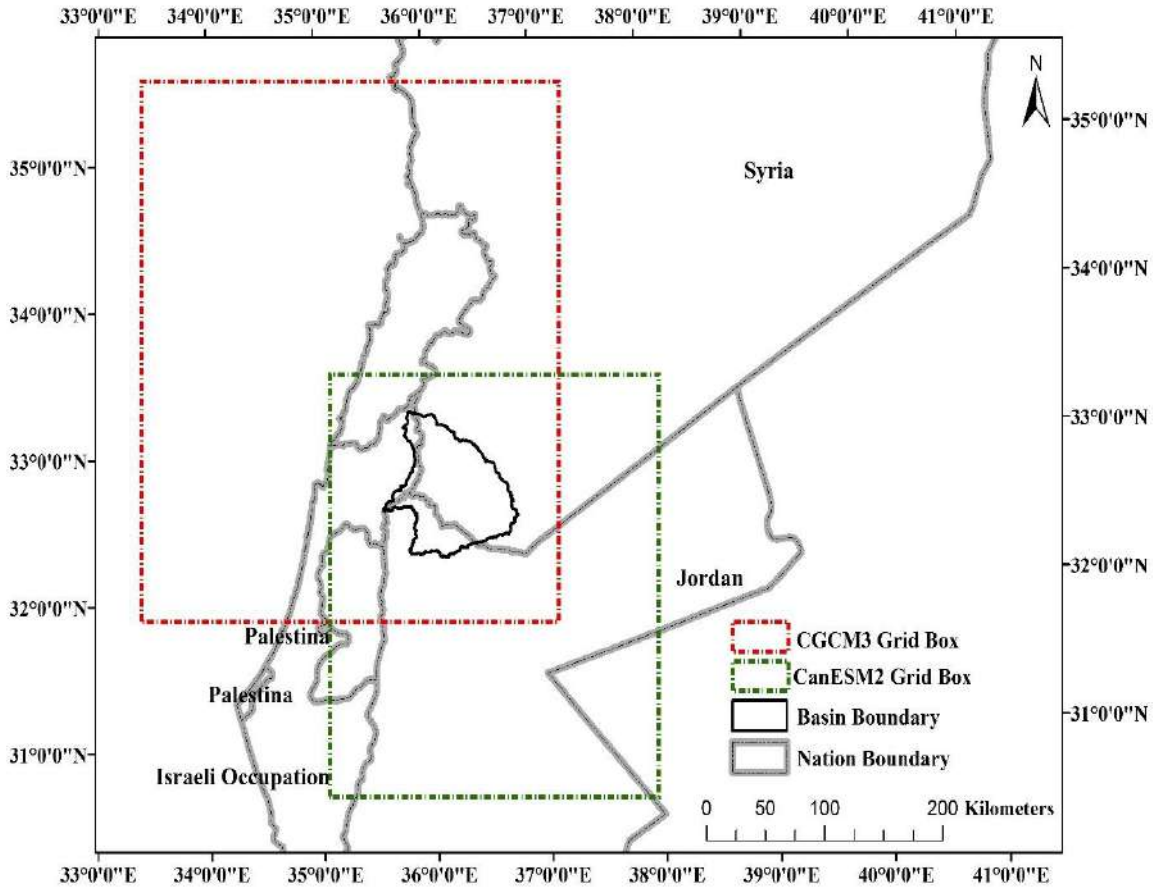

Figure 3.5: CGCM3 and CanESM2 data grid boxes that overlaid YRB

Table 3.4: List of the predictor variables from NCEP Reanalysis and GCMs datasets

Predictor code	Description	Predictor code	Description
p500	500 h Pa Geopotential height	p_th	1000 h Pa Wind direction
p8_v	850 h Pa Meridional velocity	p5_f	500 h Pa Wind speed
s500	500 h Pa Specific humidity	p5_z	500 h Pa Vorticity
shum	1000 h Pa Specific humidity	p8_f	850 h Pa Wind speed
p5_u	500 h Pa Zonal velocity	p5zh	500 h Pa Divergence
p_u	1000 h Pa Zonal velocity	p8_z	85 0 h Pa Vorticity
p5_v	500 h Pa Meridional velocity	p_f	1000 h Pa Wind speed
s850	850 h Pa Specific humidity	temp	Screen (2 m) air temperature
p–v	1000 h Pa Meridional velocity	p8zh	850 h Pa Divergence
p8_u	850 h Pa Zonal velocity	p__z	1000 h Pa Vorticity
mslp	Mean sea level pressure	p8th	850 h Pa Wind direction
p850	850 h Pa Geopotential height	p_zh	1000 h Pa Divergence
p5th	500 h Pa Wind direction	precp	Precipitation

3.2.4 Yarmouk River Discharge Data

The YR discharge data for the gauging Addasiya station that locates near the confluence with the Jordan River (YRB outlet point) (see Figure 3.1) was obtained from the Jordanian MWI. The records that had been obtained expanded an interval from 1928 till 2000. The discharge records from this gauging station almost cannot reflect the prior 1950s historical flow conditions because of many dams on the Syrian upstream tributaries and the shared large Wahdah Dam that opened in 2006 (UN-ESCWA 2013).

Two types of discharge data were prepared, the first are the observed station data and the second are hypothetical discharge data reflect the conditions if no manmade changes have occurred. To establish the hypothetical discharge data, the observed discharge date from 1928 to 1950 (reflects historical conditions) used to establish a relation between the annual rainfall and annual YR discharge. These relations had been used then to extrapolate the discharge values beyond the 1950s so can reflect flow regime as if the YRB had remained without manmade changes. This is because one of this study aims is to assess how manmade changes affect the YRB basin vulnerability to climate change

3.2.5 Land Cover and Soil Data

The YRB basin land cover information was extracted from the 0.5-km representative global land cover map that based on 10 years (2001-2010) of Collection 5.1 Moderate Resolution Imaging Spectroradiometer (MODIS) Land Cover Type (MCD12Q1) data (Broxton 2014). The land cover map that re-gridded to a regular latitude-longitude grid was downloaded from the USGS Land Cover Institute (LCI) website (http://landcover.usgs.gov/global_climatology.php). This raster map is classified into 16 classes namely water, evergreen needle leaf forest, evergreen broadleaf forest, deciduous needle leaf forest, deciduous broadleaf forest, mixed forests, closed shrublands, open shrublands, woody savannas, savannas, grasslands, permanent wetland, croplands, urban and built-up, cropland/natural vegetation mosaic, snow and ice and barren or sparsely vegetated (Broxton, 2014). Those classes should be redefined into SWAT generic land covers that defined in SWAT database.

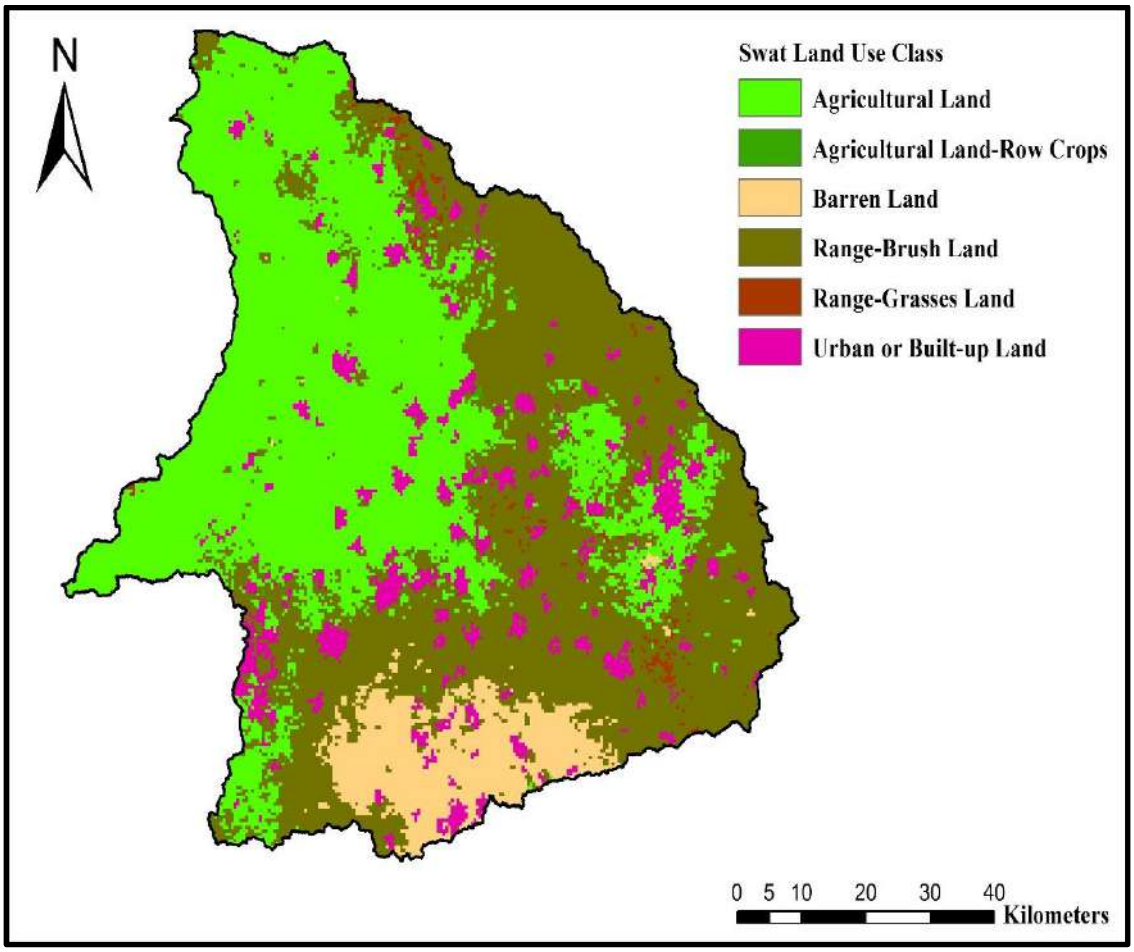

Figure 3.6: A map shows the land use within the YRB

Soil map and its average weighted two layers' properties were extracted from the Food and Agriculture Organization of the United Nations (FAO/UNESCO) Digital Soil Map of the World version 3.6 that was released in January 2003. This digital map has a coarse scale equal to 1:5000000 and was downloaded from the FAO GeoNetwork website which is http://www.fao.org/geonetwork/srv/en/metadata.show?id=14116. The shallow layer depth is 300 mm while the total soil profile depth is 1000mm with average porosity of 0.5. Other properties of the FAO soil profile in Yarmouk basin that affect the soil moisture content are shown in Table 3.5.

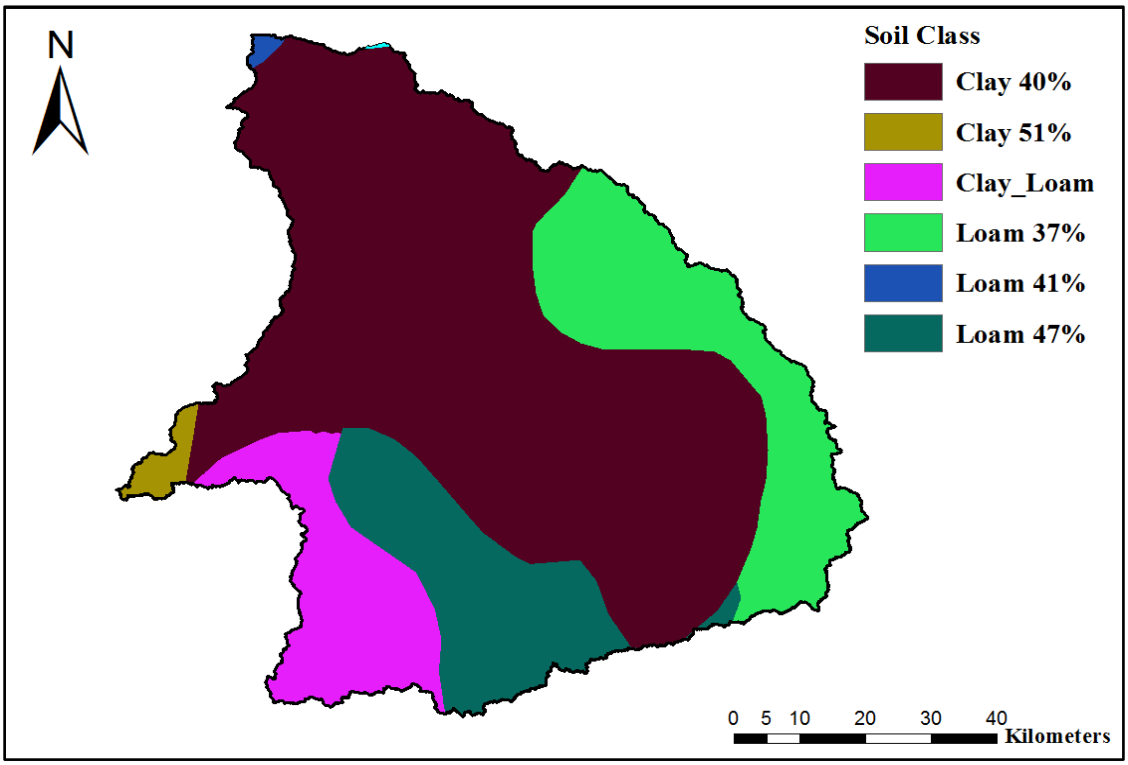

Figure 3.7: A map shows the soil types within YRB based on FAO soil map

Table 3.5: The YRB FAO soils main properties

Soil class	FAO soil class	Ks* mm/hr	Bulk density g/cm^3	Hydrologic group	Clay %	Silt %	Sand %
Clay 40%	Bv15-3b-3501	1.49	1.6	D	40	33	27
Loam 37%	I-Yk-2ab-3135	4.46	1.4	D	26	37	37
Loam 47%	Kl2-2a-5571	9.21	1.3	C	21	47	33
Clay_Loam	Lk5-3ab-3534	4.18	1.4	D	30	35	35
Clay 51%	Vc46-3a-3560	1.85	1.6	D	51	28	21
Loam 41%	I-Xk-2c-3133	7.66	1.3	D	25	41	34

* Ks is the saturated hydraulic conductivity (mm/h).

3.2.6 The Dams Data

Thirty-nine dams were modeled that have been identified to be in operation during the study period 1986-2000. Three of them was Jordanian and their information's was obtained from the Dams Operation and Maintenance Directorate, MWI, Jordan. The other 37 Syrian dams physical characteristics and operation was evaluated based on many reports such as the basin evaluation report by Al-Momani (1993), ESCWA Inventory of Shared Water Resources in Western Asia (UN-ESCWA, 2013) (see http://waterinventory.org/surface_water/jordan-river-basin), AQUASTAT - FAO's Information System on Water and Agriculture that provides a rich database (see http://www.fao.org/nr/water/aquastat/dams/index.stm), the EU-funded Trans-European Mobility Program for University Studies (TEMPUS) Study 2005-2006 project report and Food and Agriculture Organization (FAO) Syrian water report (Food and Agriculture Organization (FAO) 2009). The main dam dates were the year of opening, the principal volume, principal surface area, emergency spillway volumes, emergency spillway surface area, the uses and how the dam water being consumed generally. the More about the dam's water consummation was evaluated after consulting the Dams Operation and Maintenance Directorate in Jordan. The dams' locations along the main YRB streams are shown in Figure 3.8.

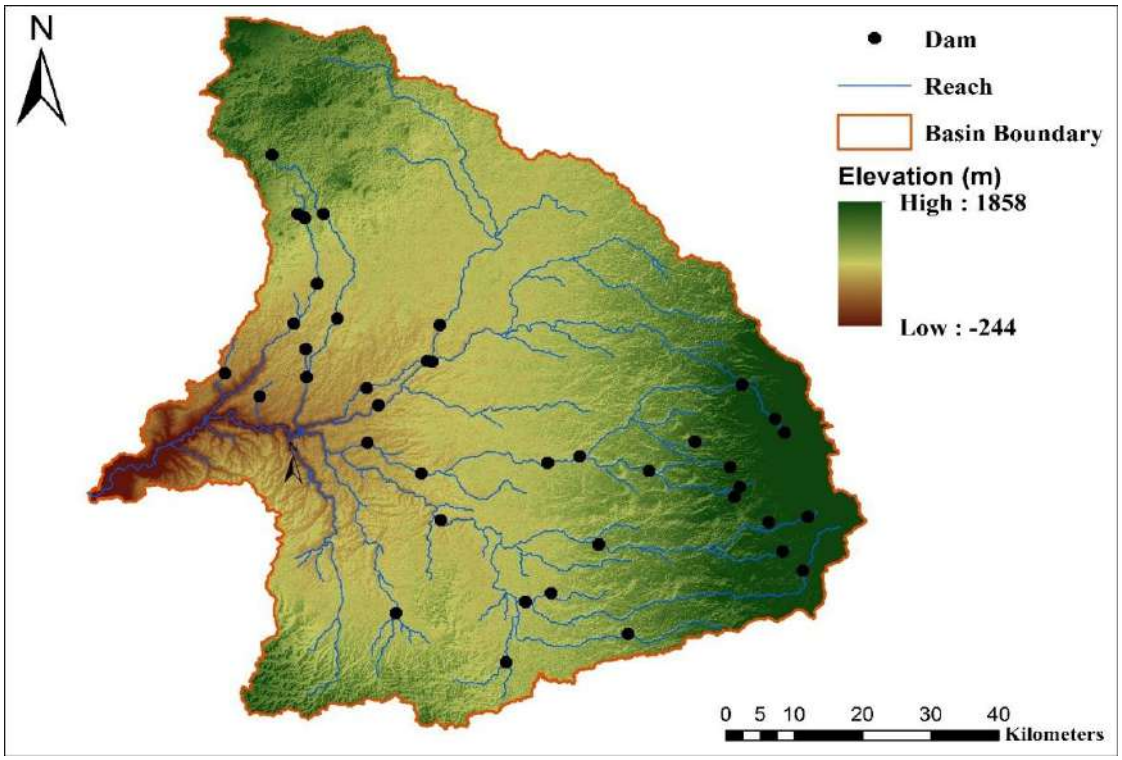

Figure 3.8: A map showing the main modeled dams in the YRB during the study period

3.3 Methodologies

3.3.1 Data Sets Preparation

The Jordanian stations' metrological data series (PRCP, Tmax, and Tmin) were examined for its quality and then used to develop daily PRCP series for the 10 Syrian stations from their 23 years annual PRCP data from 1960 to 1982. This is necessary because the downscaling technique that had been used in the present study requires daily scale time series. The following two sections 3.3.1.1 and 3.3.1.2 are going to detail how this had been done.

3.3.1.1 Jordanian Data Sets Inspection

All times series of PRCP, Tmax and Tmin were checked out for outliers and distribution normality.

For daily Tmax and Tmin time series, lag-1 serial correlation coefficient (r_1) was calculated using Equation (3.1) where x_t is a variable value in day t (t=1,2,3, 4…n), x_{t+1} is the variable value in next day and $\bar{x}$ is the variable series mean. This equation is simple and suitable when n is large which is the case for the considered time series in the study (De Smith 2015).

$$r_1 = \frac{\sum_{t=1}^{n-1}(x_t - \bar{x})(x_{t+1} - \bar{x})}{\sum_{t=1}^{n}(x_t - \bar{x})^2} \tag{3.1}$$

Testing autocorrelation presence entail that the computed r_1 is between critical upper and lower limits that are calculated according to Equation (3.2). If r_1 is within the limits, then the time series data set has no significant autocorrelation and pattern and it is random.

$$\frac{-2}{\sqrt{n}} \leq r_1 \leq \frac{2}{\sqrt{n}} \tag{3.2}$$

For the PRCP data series, inhomogeneities, data consistency, and abrupt breaks were detected using the simple, visual and practical double-mass curve (DMC) analysis. This method was used for the first time to analyze PRCP data by Merriam (1937) in the USA then later a theoretical explanation of the method was provided by Searcy and Hardison (1960). In a DMC analysis, the targeted station cumulative PRCP magnitude is plotted against the average of cumulative PRCP of the other stations in the study area during the same period. If the plot manifests approximate straight line, the series will be considered consistent with minor random errors in data observing or recording. However, notable slope change in the plot indicates errors in data and entails adjusting the slope that is

evaluated to be wrong. DMC analysis can smooth a time series and eliminate random errors, showing the main trends in the time series. In this study, DMC analysis of PRCP was performed for each Jordanian station time's series during the period of the station data availability.

3.3.1.2 Developing Daily PRCP Series for Syrian Stations

There are ten representative rainfall stations in the Syrian part of YRB. Twenty-three years' annual rainfall data from 1960 to 1985 were obtained from the Syrian Meteorological Department for these stations. The missing annual PRCP data of Syrian rainfall stations for the interval 1986-2000 were estimated using the rainfall data of Jordan rainfall stations exist in the YRB. That had been done by coupling similar stations and applying "Straight-Line Regression" during the years 1980-1985 in which annual PRCP data are available for both Jordanian and Syrian stations. The stations coupling was identified after regressing each Syrian station with all the Jordanian stations and then selecting the one of the best regression based on the coefficient of determination R^2. The Jordanian station that gives highest R^2 is the more similar and should be selected. The regression equations were used for the correlated stations, are shown in Table 3.6. After that, the modeled Syrian annual PRCP were distributed to the daily scale using the assumption that PRCP occurs in same days as the relevant Jordanian station with similar day/annual PRCP ratio as the Jordanian station.

Table 3.6: The relevant stations between the Syrian and Jordanian rainfall stations

Stations	Equations	Correlation coefficient (R^2)
Izraa' (AD0400) Vs. Turra (AD0021)	y = 0.7852x	0.6921
Kufr Saum (AD0003) Vs. Nawa (AD0401)	y = 1.1078x	0.608
Salkhad (F-S1) Vs Um El Quttein (F0001)	y = 1.9489x	0.7506
Ramtha (AD0012) Vs. Sanamain (AD0403)	y = 0.8576x	0.7157
Shahba (AD0405) Vs. Kharja(AD0008)	y = 0.7952x	0.5334
Turra (AD0021) Vs. Tell Shihab (AD0408)	y = 0.7027x	0.699
Ramtha (AD0012) Vs. Mseifrah (AD0413)	y = 0.7729x	0.7707
Suweida'a (AD0409) Vs. Um Qeis (AD005)	y = 1.2528x	0.7073
Dara'a (AD0412) Vs. Ramtha (AD0012)	y = 1.2868x	0.7686
Busral Sham (AD0414) Vs. Ramtha (AD0012)	y = 1.2479x	0.629

3.3.2 Trend Analysis

In the present study, two non-parametric methods which are Mann-Kendall and Sen's slope estimator were implemented to find out the trends and its significance for annual times series of PRCP, Tmax, and Tmin for each Jordanian station. Syrian stations were modeled (not observed) as shown in section 3.3.1.2 through the trend study period (1981-2009) so can't serve the target of dedication observed trends. The software XLSTAT (Addinsoft™ XLSTAT v. 2014.5.03, Paris, France, 2014) was utilized to execute MK test and Sen's slope test for the time series at a confidence level of 0.05.

3.3.2.1 Mann-Kendall (MK) Trend Test

Mann-Kendall (MK) test is a premium rank-based non-parametric statistical test for climatologic and hydrologic time series trend analysis (Mann, 1945; Stuart, 1968). The popularity of MK test stemmed from its suitability in analyzing skewed data distributions and its minimal sensitivity to inhomogeneities and outliers in the data series and have been used widely for hydro-meteorological time series (Yue, 2002). However, MK test entail independence and randomness in the data series where autocorrelation can mislead by detection significant trends though their absence and vice versa. Consequently, autocorrelation analysis or serial correlation is a requisite antecedent requirement before a climatic trends analysis to detect if an appreciable correlation is existing between a variable and itself over successive time intervals (Karmeshu, 2012). Though the time series in the study showed no noteworthy autocorrelation, a modified MK test suggested by Hamed and Ramachandra Rao (1998) was implemented for trend analysis in which the data ranks autocorrelation is calculating after removing the apparent trend.

MK test null hypothesis H_0 is no trend (i.e., an unchanging climate) while the alternative hypothesis H_1 assume a trend of changing climate. Briefly, the computations begin with calculating the MK test statistic S using Equation (3.3) and (3.4) given an ordered temporally equally spaced time series of n data points having values such as x_i and x_j with time points $i > j$.

$$S = \sum_{i=1}^{n-1} \sum_{j=i+1}^{n} sign(x_j - x_i) \tag{3.3}$$

$$\text{sign}\,(x_j - x_i) = \begin{cases} +1, & \text{if } (x_j - x_i) > 0 \\ 0, & \text{if } (x_j - x_i) = 0 \\ -1, & \text{if } (x_j - x_i) < 0 \end{cases} \tag{3.4}$$

It's more indicative to use the standard normal test statistic Z_S instead of the statistic S. Z_S is calculated using Equations (3.5) - (3.7). N is the number of data points in the series, NS^* is the effective number of data points to account for autocorrelation in the data, $P_s(i)$ is the autocorrelation between the data points ranks for lag i, and P is the maximum time lag under consideration. Z_S can be positive or negative indicating upward and downward trends respectively. The trend analysis had been performed at significance level (α) of 0.05, which at, if $|Z_S| > Z_{1-\alpha/2}$, the null hypothesis will be rejected elucidating a time series significant trend presence. The value of $Z_{1-\alpha/2}$ is 1.96 for α=0.05 as obtained from the standard normal distribution table.

$$Z_s = \begin{cases} \dfrac{S-1}{\sqrt{Var(S)}}, if\ S > 0 \\ 0, \qquad if\ S = 0 \\ \dfrac{S+1}{\sqrt{Var(S)}}, if\ S < 0 \end{cases} \tag{3.5}$$

$$\text{Var [S]} = \frac{1}{18}[N(N-1)(2N+5)]\frac{N}{NS^*} \tag{3.6}$$

$$\frac{N}{NS^*} = 1 + \frac{2}{N(N-1)(N-2)}\sum_{i=1}^{P}(N-i)(N-i-1)(N-i-2)P_s(i) \tag{3.7}$$

Yue et al. (2002) investigated the power of MK test for monotonic trends detecting in general. They deduced that the test gets very powerful as the trend magnitude get bigger, the sample size increases and the data variations decreases.

3.3.2.2 Sen' Estimator Approach (TSA)

Inasmuch as trend magnitude (change per unit time) cannot be estimated utilizing MK test, non-parametric Sen's slope estimator statistical test that developed by Sen (1968) was chosen for this objective. Trend magnitude estimation using Sen's slope is considered the most powerful; particularly comparing to the classical least-squares method regression coefficient. This characteristic is attributed to Sen's slope estimator trivial sensitivity toward outliers or extreme values that exist in the data series. Sen's slope (Q_k) is calculated given equally spaced date series in temporal ascending order of n data points using Equation 3.8 in which x_i and x_j are data values at time points $i > j$.

$$Q_k = \frac{x_j - x_i}{j - i}\ for\ k = 1, \dots, N \tag{3.8}$$

The overall N values of Q_k where $N < \frac{n(n-1)}{2}$ are then ranked in ascending order and the median of slope (i.e. Sen's slope estimator) is calculated using Equation 3.9. After that a tow-sided test is applied to the calculated Sen's slope at 95% confidence interval to obtain the lower and upper confidence limits Q_{min} and Q_{max}. If the limits have the same sign, then Sen's slope would be statistically different than zero.

$$Q_{med} = \begin{cases} Q_{(N+1)/2} & \text{if N is odd} \\ \frac{Q_{N/2} + Q_{(N+2)/2}}{2} & \text{if N is even} \end{cases} \quad (3.9)$$

3.3.3 SDSM Downscaling

3.3.3.1 SDSM Model Description

Statistical Downscaling Model version 4.2 (SDSM 4.2) was downloaded freely from http://co-public.lboro.ac.uk/cocwd/SDSM/index.html. Daily maximum temperature (Tmax), minimum temperature (Tmin) and precipitation (PRCP) (the predictands) were downscaled for each station standalone. The general steps are quality control, data transformation, screening of predictor variables, model calibration, weather generation (observed predictors), statistical analysis and scenario generation (climate model predictors). Among them, screening of predictors is the most central step to obtain the least-uncertainties downscaling (Wilby 2002; Huang 2011). More detailed steps of the downscaling process in SDSM are outlined in **Figure 3.9**.

SDSM do the temperature modeling with unconditional one step process in which a linear regression model is created between daily $Tmax_i$ or $Tmin_i$ temperatures and predictors (P_is) for day i as shown in equations 3.10 and 3.11, where δ and γ are linear least squares regression parameters while ξ and ζ are random or modeling errors (Wilby 1999).

$$Tmax_i = \delta_0 + \delta_T Tmax_{i-1} + \delta_1 P_{1+} \ldots + \delta_k P_k + \xi_i \quad (3.10)$$

$$Tmin_i = \gamma_0 + \gamma_T Tmax_{i-1} + \gamma_1 P_{1+} \ldots + \gamma_k P_k + \zeta_i \quad (3.11)$$

Precipitation modeling is a conditional process with no autoregression and its algorithm is summarized into two steps. At first, a linear regression relation is established between observed predictors (NCEP) and precipitation occurrence probability in a day i (O_i). So O_i is calculated first using equation (3.12) where $\propto_i$s are linear least squares regression parameters, P_is are the selected predictors and k is a counter of days. After that,

a uniformly distributed random number r ($0 < r < 1$) that generated using a stochastic process is used to determine the weather condition where if $r \leq O_i$ then the day is wet and precipitation happens, otherwise the weather is considered dry (Wilby 1999).

$$O_i = \propto_0 + \propto_{i-1} O_{i-1} + \propto_1 P_1 + \cdots + \propto_k P_k \quad (3.12)$$

In case the precipitation happens, then the second step will be performed in which an another linear regression model between daily precipitation amount (predictand) (R_i) that always greater than zero and the selected predictors (P_i) will be created as shown in Equation (3.4) where β_is are linear least squares regression parameters, P_is are the selected predictors, *k* is a counter of days and ε_i random or modeling error (Wilby 1999).

$$R_i = \exp(\beta_0 + \beta_1 P_1 + \cdots + \beta_k P_k + \varepsilon_i \quad (3.13)$$

SDSM can produce 20 simulations in a single run with the same probability of appearance called together as an ensemble and each simulation is called ensemble member.

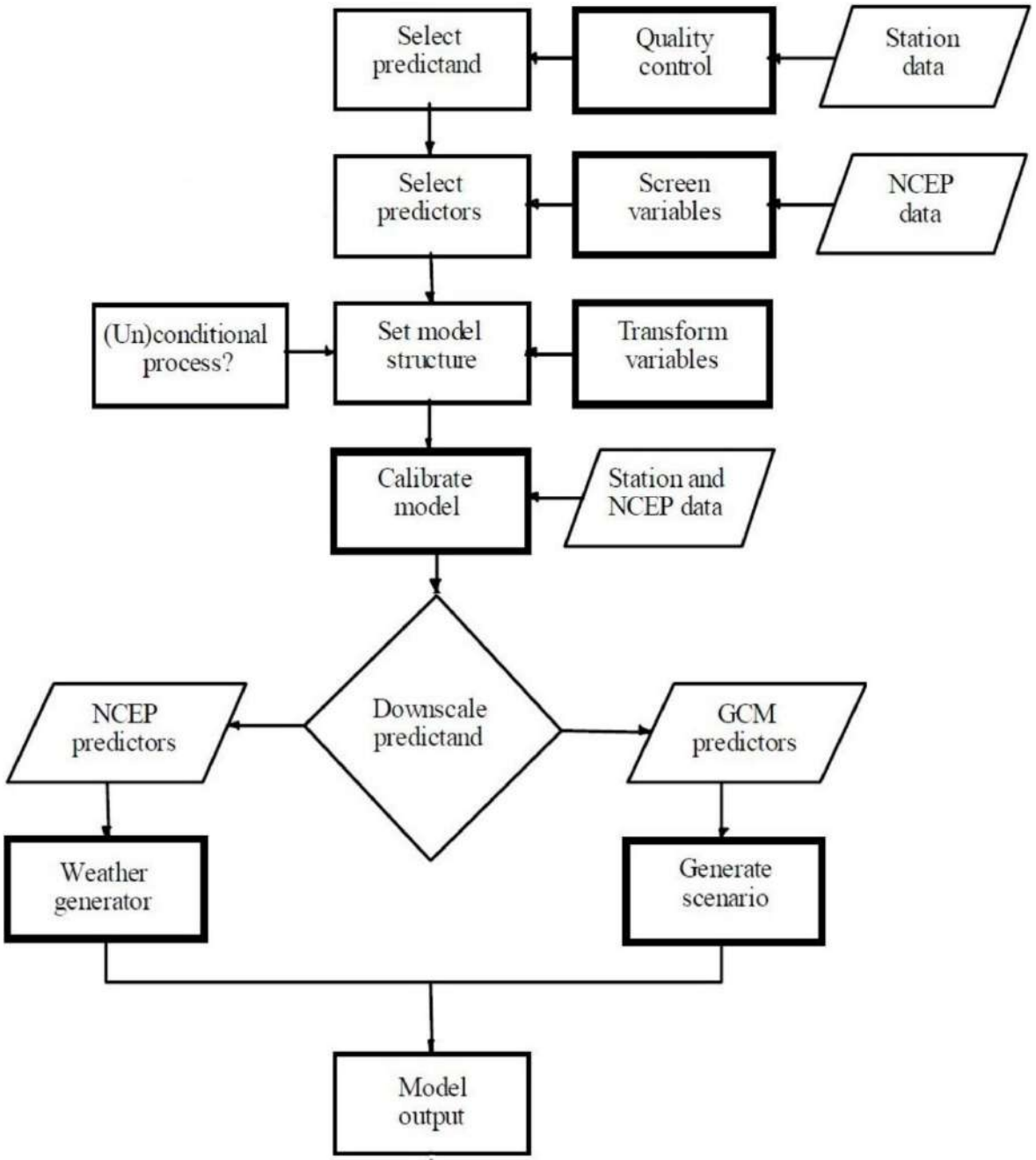

Figure 3.9: SDSM climate scenario generation general steps (Wilby, 2002)

3.3.3.2 Screening of Predictors

The procedure to select the relevant predictors (large-scale variables) to the predictand (local station variable) was performed using a suggested procedure in the literature that combine the correlation matrix, partial correlation, and P value within the SDSM that found to have a significant enhanced effect on the model's performance (Gagnon, 2005; Huang, 2011; Mahmood, 2013). The screening steps start with selecting the first and most suitable large-scale variable and then selecting the second, third, fourth, and so on such that the predictors are not collinear and still have significant effect on the

model parameters, the procedure with minor modification is as follow and was performed at confidence level of 95%:

1. Generate a correlation matrix between the 26 NCEP predictors and the predictand, and then the 12 predictors (SDSM matrix limit of predictors) with the highest correlation coefficient (r_c) with the predictand are selected and re-arranged in descending order. The predictor with the highest r_c is defined as the super predictor (SP).
2. Generate r_c between the predictor and predictand, absolute partial correlation coefficient (r_p) and P value by regressing the 12 predictors to the predictand.
3. Remove first the predictors of P value greater than 0.05 so leaving the statistically significant predictors and then remove the highly correlated predictors to leave out any multi-co-linearity. In the present study, r_c between predictors up to 0.7 was accepted as suggested by Pallant (2007). After this step, a set of predictors with the highest partial correlation is left. If the set is with a number up to 6 predictors, the set will be chosen as a final set (Souvignet, 2011), otherwise, step 4 is performed.
4. Determine the next super predictor using the percentage reduction in an absolute partial correlation (PRP) with respect to absolute correlation for each predictor using Equation (3.14), where r_p is the absolute partial correlation coefficient and r_c is the correlation coefficient between the predictor and the super predictor (SP). The predictors of the minimum PRPs are selected as the most suitable predictors.

$$PRP = \frac{r_p - r_c}{rc} \tag{3.14}$$

3.3.3.3 SDSM Calibration and Validation

The observed PRCP, Tmax and Tmin (predictands) and the selected NCEP predictors were used to calibrate the monthly downscaling sub-models for each predictand at each station for both GCMs. According to the common time series length of the predictands between the stations (1981-2009) and the common NCEP time series length between the GCMs (1961-2000), the calibration was chosen to be 15 years (1/1/1981-31/12/1995) and validation is 5 years (1/1/1996–31/12/2000) for comparison purposes. Tmax and Tmin sub-models were unconditional and not transformed because it is normally distributed and 1-day lag had autoregressived since its data series are autocorrelated (Wilby, 2002). PRCP sub-models were conditional and transformed to the

fourth root because of its skewed distribution (Wilby, 2002). For the conditional process, wet day is defined when the precipitation amount is 0.1mm or more as recommended for arid or semi-arid climates by Liu et al. (2011) after downscaling using several wet day thresholds. To overcome SDSM overflow error from popping out when to calibrate at monthly scale because the summer months (June, July, August, and September) are of zero PRCP in the YRB, the summer months were filled with fake trivial amounts. Then the summer months' models parameters in the calibration files had been reset to zero manually. SDSM had been run to produce 20 simulations (ensemble number), then one ensemble member was used for the later downscaling performance evaluation because it will have more similar characteristics to the actual time series.

The models were evaluated in the validation period using commonly used measures which are time series plots, the Pearson's coefficient of determination (R^2) and root mean square error (RMSE) for mean monthly Tmax and Tmin and PRCP monthly sum. R^2 quantify variability proportion within the observed data accounted for the modeled data while RMSE quantifies the model errors between the observed and modeled time series. R^2 and RMSE were calculated using Equation (3.15) and (3.16) respectively; where x_i is the observed variable in day *i*, $\acute{x_\iota}$ is the molded variable in day *i*, $\overline{x}$ in the observed variable time series mean and *n* the total number of values in the time series. RMSE ranges between zero 0 (perfect model) and infinity while R^2 ranges between 0 and 1(perfect model) (Maidment, 1992).

$$R^2 = 1 - \frac{\sum_i^n x_i - \acute{x_\iota}}{\sum_i^n x_i - \overline{x}} \tag{3.15}$$

$$RMSE = \frac{\sqrt{\sum_i^n (x_i - \acute{x}_i)^2}}{n} \tag{3.16}$$

In addition, its ability to simulate mean and extreme climate conditions was evaluated by comparing mean climate indices versus extreme climate indices that shown in Table 3.7. The mean indices were selected mostly as recommended by Maraun et al. (2010). The extreme indices were selected from the 27 core indices that the World Meteorological Organization Joint Expert Team on Climate Change Detection and Indices (ETCCDI) promoted for climate extremes analysis around the world (see http://etccdi.pacificclimate.org/indices.shtml for detailed information) (Peterson, 2008).

Table 3.7: Evaluation indices of mean and extreme events

	Index full name	Index short name	Unit
Precipitation mean indices	Mean precipitation sum	Mean_PRCP	mm
	Mean dry spell length	Dry_spell	days
	Mean wet spell length	Wet_spell	days
	Percentage of wet days(>0.1mm)	Wet_days	%
Precipitation extreme indices	Monthly maximum consecutive 5 days' precipitation	Rx5day	mm
	Maximum length of dry spell	Max_dspel	days
	Maximum length of wet spell	Max_wspel	days
Temperature mean indices	Mean daily maximum temperature	Mean_Tmax	^{o}C
	Mean daily minimum temperature	Mean_Tmin	^{o}C
Temperature extreme indices	Monthly maximum value of daily maximum temperature*	Max_Tmax	^{o}C
	Monthly maximum value of daily minimum temperature*	Max_Tmin	^{o}C
	Monthly minimum value of daily maximum temperature**	Min_Tmax	^{o}C
	Monthly minimum value of daily minimum temperature**	Min_Tmin	^{o}C

*Warm extremes indices, **Cold extremes indices

In order to investigate the ability of the models to simulate extreme events at various return period comparing to the observed extremes events, frequency analysis was performed in which statistical distribution is fitted to observed and modeled data. For our study of extremes, the generalized extreme value (GEV) distribution was the most suitable that is calculated using Equation (3.17); where x is the predictand value and ξ, β and k are location, scale and shape parameters respectively which are calculated from the predictand data series (Souvignet 2011).

$$F(x) = exp\left\{-exp\left[\frac{-(x-\xi)}{\beta}\right]^{\frac{1}{k}}\right\} \quad (3.17)$$

3.3.3.4 Uncertainty Analysis

The aim of uncertainty analysis is to investigate the GCMs predictors' ability to regenerate the current climate state to build confidence in the GCMs future climate scenarios (Khan, 2006). The total 20 years of the observed meteorological variables (1981-2000) was used as a baseline scenario. The downscaled current climate using GCMs predictors was generated by a twentieth-century experiment (20C3M) which is usually called the historical scenario which corresponds to a greenhouse gasses change as observed up to 2000 (Hegerl, 2003).

In addition to the same measures that have been used and explained in detail in section 3.2.2.3, Mann-Whitney (MW) hypothesis test was performed on mean monthly Tmax and Tmin and PRCP sum**.** The Mann–Whitney (MW) is powerful non-parametric hypothesis test seeks the equality of median between two populations (Mann, 1947). MW test null hypothesis H_0 is that the median between two populations is equal while the alternative hypothesis H_1 assume the opposite. As other non-parametric tests, MW tests is insensitive to outliers, distribution normality and autocorrelation because its theory states that ranks sum (instead of variable amount) above and below the median should be the same to accept the null hypothesis. For a significance level of α (0.05 used in the present study), If $p>\alpha$ then the null hypothesis is accepted with 1-α% (95% in the present study) confidence that there is no difference between the two population medians. The test was performed using XLSTAT software (Addinsoft™ XLSTAT v. 2014.5.03, Paris, France, 2014).

3.3.3.5 Future Climate Change Scenarios Generation

Future modeled local-scale predictand (PRCP, Tmax, and Tmin) were generated for CGCM3 and CanESM2 GCMs under the climate change scenarios that were mentioned in Table 3.3 along the 21st century (2006-2100). The PRCP percentage difference, mean Tmax and Tmin absolute difference and frequency were calculated for three future time periods of approximately thirty years which are the 2020s (2011-2040), 2050s (2041-2070) and 2080s (2071-2099).

All evaluation measures mentioned throughout the downscaling validation and uncertainty analysis were performed for each predictand at each of the 28 station for both GCMs to consider the surface and climate conditions spatial differences between the stations and then averaged to represent the general downscaling performance. All measures were averaged normally by summing the values and then dividing by its number

except those measures of PRCP amount which were averaged instead by Thiessen polygons method. Thiessen polygons is areal averaging method in which at first lines between the stations is drawn and then divided by other lines that define the influence area of each PRCP station so the averaging then is calculated using the ratio of the influence areas (subbasins) to the total basin area as Equation (3.18) states; where $PRCP$ is the average PRCP over the basin, A_T is basin total area, A_i is subbasin area, j is station counter and m is the total number of stations (Thiessen, 1911). The Thiessen polygons network that cover the whole YRB is shown in Figure 3.10.

$$R_A = \sum_{j}^{m} \frac{A_i}{A_T} R_i \tag{3.18}$$

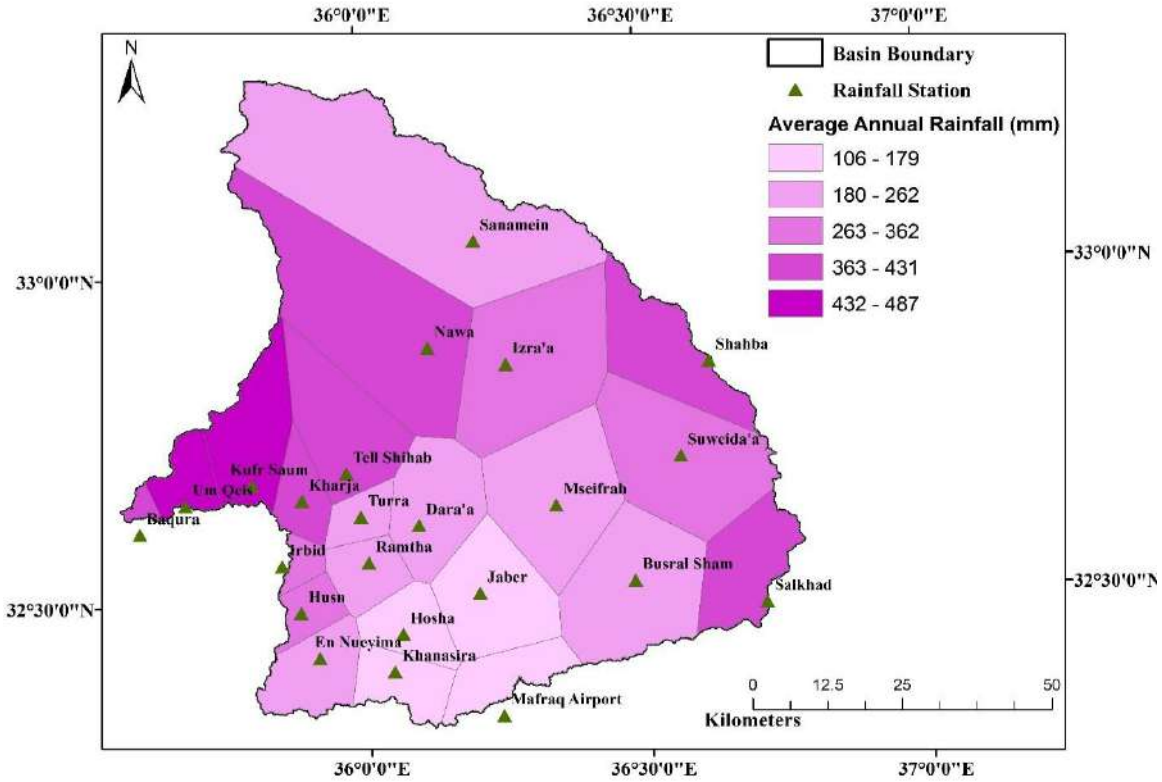

Figure 3.10: Thiessen polygons network for the whole YRB

3.3.4 SWAT Hydrologic Modeling

3.3.4.1 Hydrologic Model Description

The Soil and Water Assessment Tool (SWAT) is a process based distributed model that has been developed by the US Department of Agriculture–Agricultural (USDA) Research Service (USDA–ARS). SWAT enable performing long continuous-time, spatially distributed modeling of a basin hydrologic cycle and its water quality at even

daily time step. This is, in turn, would help water-resources managers to evaluate management approaches in large river watersheds (Arnold, 1998). SWAT divide a basin into subbasins each with the main channel and then the subbasins are furthermore divided into homogenous units in terms of land use, soil and slope called hydrological response units (HRUs). SWAT model building unit HRU water balance budget compromise five components which are canopy interception, snowfall, soil profile, shallow aquifer, and deep aquifer. Simulation of basin hydrologic response is separated into two phases: land and in-stream. In the land phase, the HRUs generate flows that then aggregated via weighted average across its containing subbasin. In the in-stream phase, those flows let to be routed through channels, ponds, and/or reservoirs till the outlet of the basin (Arnold, 1993; Arnold, 2012; Ficklin, 2009). SWAT entail four spatial input dataset which are Digital Elevation Model (DEM), Land use/Land cover, soil, and basin/subbasin outlets discharges and/or quality data. The model has been used in several large area projects by EPA, NOAA, NRCS and others to estimate the climate and management impacts on water use, non-point source loadings, and pesticide contamination (Arnold, 1998). Moreover, Most studies involved SWAT demonstrated its capability of providing realistic watershed-scale analysis over diverse small and large watersheds and its accuracy depending upon the data availability (Jha, 2004). The hydrologic cycle in SWAT is based on the following water balance (equation) in which SW_f is the final soil water content, SW_o is the initial soil water content, t is the simulation period (days), R_i is the precipitation, Q_{surf} is surface runoff, E_a is evapotranspiration, W_{deep} is deep aquifer recharge and Q_{gw} is the return flow where all these hydrologic processes are calculated on each day i and have the unit of mmH_2O (Githui, 2009).

$$SW_f = SW_o + \sum_{i=1}^{t} R_i - Q_{surf} - E_a - W_{deep} - Q_{gw} \tag{3.19}$$

In this study, a solely hydrologic response modeling of the YRB using SWAT model has been conducted at monthly time step driven by the downscaled 21st-century climates for predevelopment conditions (i.e. before the 1950s) and post-development conditions.

3.3.4.2 Setting up SWAT

The simulation of the YRB hydrology that forced under the projected climate change has been evaluated for two different conditions during the study period from 1981 to 2000:

(1) Pre-development conditions: These are notional conditions and assume there has been no substantial human intervention alters the YRB historical hydrology and water circulation. In reality, the basin has remained under its historical conditions until the 1950s, where the communities were still small, and their normal lifestyle was either nomadic or simple peasant (Burdon, 1954). After the 1950s, the communities have started turning into urban communities experiencing high population growth and rapid economic development rates. In summary, these conditions assuming that the basin remained the same and has no expansion of urbanization, agriculture, dams' construction, harvesting systems and water diversion. Under these conditions, the hydrologic simulation should match as possible the YRB historical hydrologic water cycle as was evaluated by Burdon, (1954).

(2) Post-development conditions: These conditions represent the real changes in YRB because of human intervention that affected the basin hydrologic water cycle. The main changes that have been simulated included the main dams, water harvesting and patterns of agriculture through the basin. Under these conditions, the hydrologic water cycle simulation should match as possible what have been observed during the study period.

The goal of simulating the basin under both pre-development and post-development conditions is to evaluate how manmade changes affect the basin vulnerability to climate change.

3.3.4.2.1 Pre-Development Conditions

The YRB was divided into 25 subbasins that delineate the river attributes valleys that most of them are dry except in the rainy season and then was further divided into 531 HRUs. Partitioning into surface runoff and infiltration was quantified using a modification of the SCS curve number method and variable storage method was used to route water through the basin. Hargreaves method was used to calculate the evapotranspiration which driven by daily climate input data series for precipitation and maximum/minimum air

temperature. SWAT assign automatically the nearest precipitation and temperature station to a subbasin centroid. Each run included 5 years of warming up to make the model able to capture the hydrological water cycle adequately before starting calculating various hydrological quantities. In addition, other climate information including wind speed, solar radiation and dew-point were generated from weather generator using monthly values from the nearest standardized weather station to be used if needed.

3.3.4.2.2 Post-Development Conditions

Thirty-nine dams were modeled after had been identified to be in operation during the study period 1986-2000. The basin was divided into 47 subbasins that drain the dams subbasins and the river main attributes valleys and then was further divided into 731 HRUs. Surface runoff and evapotranspiration were calculated using a modification of the SCS curve number method and Hargreaves method respectively. Water routing through channels was evaluated using the Muskingum Method. The irrigation timing and application amount in an HRU had been scheduled automatically by SWAT in response to water deficit in the soil. The specified sources of the irrigation water were either the dams or the shallow aquifer.

3.3.4.3 Calibration, Validation and Sensitivity Analysis

Calibration is a subjective process that is linked intimately to the uncertainties and no unique calibration can be obtained. The prime issues related to calibration of distributed model specifically are parametrization, objective function definition, non-uniqueness (uncertainty), parameter conditionality, positioning observed outlets and time constraint (Abbaspour, 2007). Generally, the requirement of a calibrated watershed model to do climate change analysis is the model be able to simulate the dominant hydrologic processes and their interactions as simply and realistically as possible (Arnold, 2005).

In this study, a process-based calibration for the basin hydrological processes has been performed for both pre-development (the natural historical conditions) that had been prevailing the basin till the 1950s (Burdon, 1954) and post-development conditions. The SWAT processes of the hydrological water balance in the watershed involve surface runoff, ET, lateral flow, return flow, tile flow (if present), channel transmission losses, and deep aquifer recharge. Hence, an actual physical knowledge of the watershed before calibration is an indispensable matter (Arnold, 2012). Burdon (1954) had already quantified the Yarmouk basin water balance processes through an intensive field and office research

using comprehensive field data sources including runoff gauges, 172 spring gauges, rainfall maps, 77 boreholes as well as the most accurate geology and soil maps available at the time. Burdon investigation had quantified the basin water balance ratios as follow: 0.81 ET/precipitation, 0.1 infiltration/precipitation (0.02 lateral flow and 0.08 return flow after percolation) and 0.09 surface runoff/precipitation. The historical annual streamflow used to be 450-500 MCM that is partitioning into 0.55 baseflow and 0.45 surface runoff. Burdon depiction of the general hydrological cycle of the whole basin is shown in Figure 3.11 in which he had summarized different processes quantities. The calibration had been implemented into two procedures; first manual calibration procedure and second automated procedure for a single outlet model at the Addasiya station that is located near the confluence with the Jordan River (YRB outlet). The single outlet calibration approach was demonstrated by Niraula et al. (2015) to be significantly indifferent from spatially-calibrated (SC) models (using multiple stations) for analyzing the streamflow absolute and relative changes under climate change scenarios.

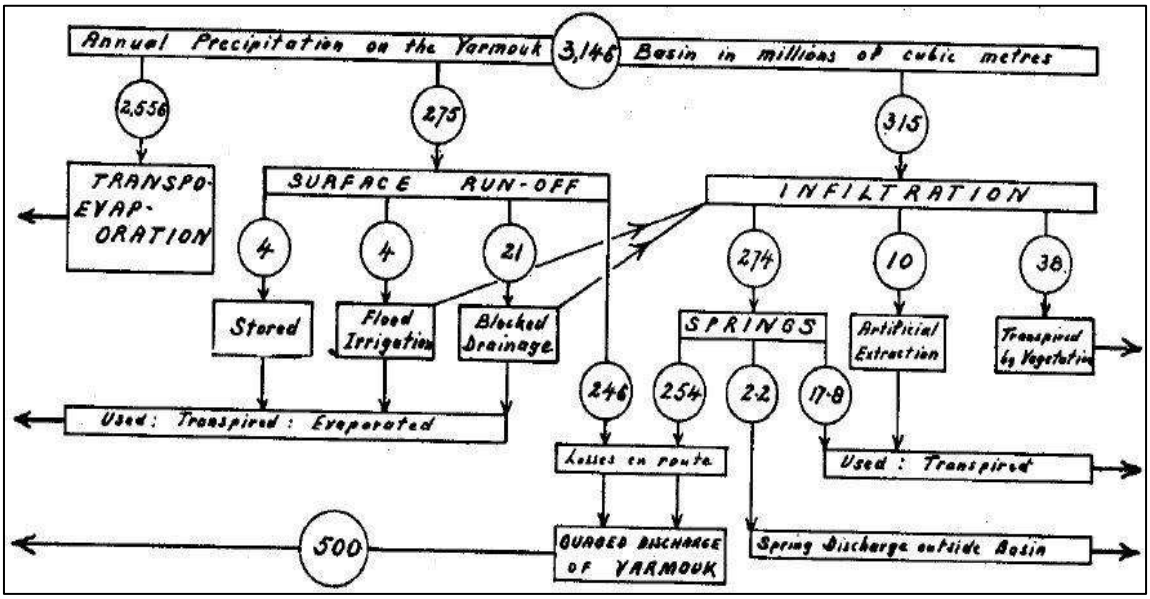

Figure 3.11: General hydrological cycle of the historical YRB (Burdon 1954)

The manual calibration is to initially parameterize the model based on the available data, literature, and analyst's expertise to achieve as a possible match in water balance ratios and quantities. At first, the curve number (CN2) had been adjusted till satisfactory runoff/precipitation ratio was achieved. Afterward, the soil evaporation compensation factor (ESCO), depth from soil layer 2 surfaces to the bottom (SOL_Z2) and soil available water capacity (SOL_AWC) as well as the Groundwater revap coefficient (GW_REVAP) were adjusted to obtain satisfactory ET/precipitation ratio. The groundwater delay

(GW_DELAY) was then adjusted to match the observed flow regime as possible, especially the dry months' baseflow. Finally, the high unreasonable peaks in the simulated flow regime were reduced by increasing the channel hydraulic conductivity (CH_K2) and the baseflow alpha factor (ALPHA_BF) till peaks become reasonable. The model which had been obtained after finishing the manual calibration was used as default input model for the automated procedure. This default model had been assured to be not drastically different from the observed because it was demonstrated that automated calibration will be of little help for poor default models (Abbaspour, 2015).

The automated procedure is to adjust the parameters within realistic uncertainty ranges iteratively between autocalibration runs as well as to provide parameter sensitivity analysis and goodness-of-fit statistics. The automated calibration used the Sequential Uncertainty Fitting (SUFI2) procedure in the decision-making framework calibration, validation, sensitivity, and uncertainty analysis software SWAT-CUP that was developed by the Swiss Federal Institute of Aquatic Science and Technology Eewag (Abbaspour, 2007). SUFI2 compromise various uncertainties such those related to a parameter, conceptual model, and input via encompassing the observed data as possible into the 95% prediction uncertainty (95PPU) that is calculated at the 2.5% and 97.5% levels of the output variable cumulative distribution. P-factor and R-factor are the indices SUFI use to evaluate the goodness of fit between the model simulation 95PPU band and observed date plus its error band. The P-factor that is varying between 0 and 1 (perfect model) indicates the percentage of observed data plus its error that is bracketed by the 95PPU band simulation. on the other hand, the R-factor - that is ranging from 0 (perfect model) to ∞ - measures the ratio between 95PPU band average width and the observed variable standard deviation. For stream discharge modeling, P-factor >0.7 and R-factor < 1.5 is considered satisfactory but those are subjective criteria depending on the watershed and the study conditions and a balance should have obtained between them because higher P-factor can lead to higher R-factor. After several iterations, one should achieve the best R-factor and P-factor at which the resulted new parameter ranges will be taken as the calibrated parameters. SUFI-2 provides ten objective functions to be employed as targets during the iterative calibration (Abbaspour, 2015). Four objective functions had been selected for model uncertainty evaluation which is Nash-Sutcliffe efficiency (NSE), percent bias (PBIAS), ratio of the root mean square error to the standard deviation of measured data (RSR) as well as the common statistic coefficient of determination (R^2). Those objective functions have been recommended by Moriasi et al. (2007) after their profound and

comprehensive review of the model application and evaluation methods in the literature. They recommended NSE ≥ 0.50, RSR ≤ 0.70, and PBIAS ≤ ±25% to consider a stream discharge modeling satisfactory. The calibrated parameters were then validated with an independent set of data during a 5 years' period from 1996 to 2000 without further changes to the parameters. The following equations indicate how NSE, RSR, and PBIAS are going to be calculated in which Q_i^{obs} is the observed discharge on day i (m^3/s), Q_i^{sim} is the simulated discharge in day i (m^3/s) and Q^{mean} is the observed discharge mean value (m^3/s).

$$NSE = 1 - \frac{\sum_{i=1}^{n}(Q_i^{obs} - Q_i^{sim})^2}{\sum_{i=1}^{n}(Q_i^{obs} - Q^{mean})^2} \tag{3.19}$$

$$PBIAS = \frac{\sum_{i=1}^{n}(Q_i^{obs} - Q_i^{sim}) * 100}{\sum_{i=1}^{n} Q_i^{obs}} \tag{3.20}$$

$$RSR = \frac{\sqrt{\sum_{i=1}^{n}(Q_i^{obs} - Q_i^{sim})^2}}{\sqrt{\sum_{i=1}^{n}(Q_{i=1}^{obs} - Q^{mean})^2}} \tag{3.21}$$

After the automatic calibration, for only the post-development conditions, a remaining tuning of the flow regime has been performed by adjusting the dams average daily consumptive use parameters (WURESN), the number of days required to release any water surplus from a reservoir (NDTARGR) and the maximum average daily outflow for the month (OFLOWMX) for each dam.

The sensitivity method that had been used in this study is the global sensitivity analysis that was introduced by Van Griensven et al. (2006). This method combines a Latin-hypercube and one-factor-at-a-time sampling methods that also has been adopted for calibration and sensitivity analysis tool SWAT-CUP.

Chapter Four: Precipitation and Temperature Trend Detection

One of the essential steps in the climate change impact studies is the analysis of trends in the available records of climatological data for the selected stations. However, before the trend analysis, the data quality and characteristics have to be checked thoroughly. In addition, the knowledge of autocorrelations will be of great benefit when setting the downscaling model for PRCP, Tmax, and Tmin. Therefore, this Chapter has been devoted to present the autocorrelation, DMC as well as the trend analysis results for the annual PRCP, Tmax and Tmin time data series of the metrological stations within the YRB.

4.1 Annual PRCP, Tmax and Tmin Autocorrelation

Inasmuch the non-parametric MK trend test and Sen's slope perform powerfully if the time series itself is independent (no pattern and random), autocorrelation analysis was performed for the Jordanian stations so can build more confidence in the resulted trends (Mann, 1945; Gocic, 2013). Lag-1 serial correlations (correlation of variable with itself day ago) plots for annual PRCP (23 stations), Tmax (5 stations) and Tmin (5 stations) between 1981 and 2009 are depicted in Figure 4.1.

PRCP showed no significant and almost negative autocorrelation at 85% of the stations because lag-1 serial correlation coefficient (r_1) lies within its upper and lower limits at 0.05 significance level. Consequently, enough confidence can be dragged in the PRCP data series independency. This will, in turn, make the trend statistical tests able to give results at the lowest possible uncertainties for PRCP time data series.

In general, Tmax and Tmin data series showed positive autocorrelations (upward influence on itself over time). Tmax showed the strongest autocorrelation; almost all the stations have or close to have significant autocorrelations. Tmin has accompanied with no significant autocorrelations at all. This may lead to some extent to generate some uncertainty in the results of trend statistical tests for Tmax time data series.

Anyway, the statistical tests MK and Sen's slope were applied so as to be able to remove or reduce any apparent autocorrelations.

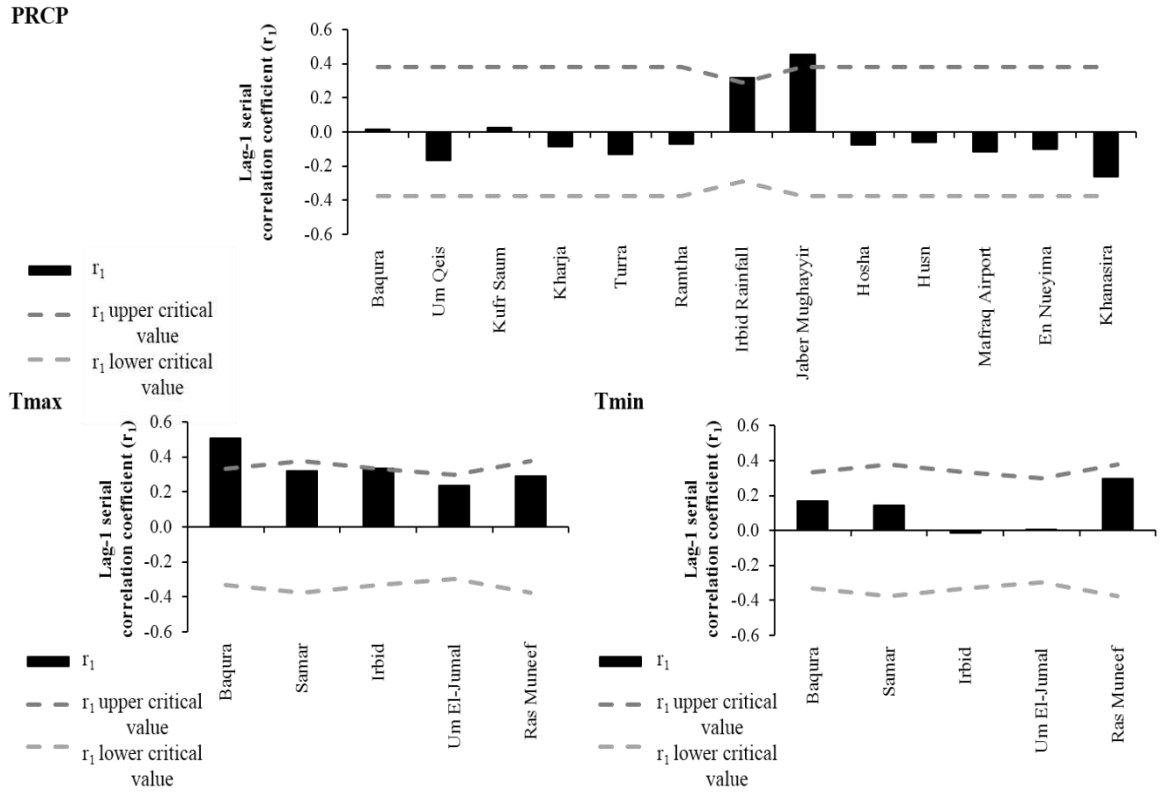

Figure 4.1: The lag-1 serial correlation coefficient (r_1) and its upper and lower limits of the confidence interval at 0.05 significance level for annual PRCP, Tmax and Tmin (1981-2009)

4.2 Double-Mass Curve Analysis for Daily PRCP

Input good quality of the climate variables data series can reduce uncertainties within the climate change impact studies substantially (Prudhomme, 2009). Therefore, all PRCP, Tmax, and Tmin daily records were extensively examined for consistency and outliers and to fill any missing day by averaging the previous and next day. In addition to that, in order to get better PRCP time series, inhomogeneities (abrupt change) were analyzed using the double mass curve (DMC) method.

The double-mass fit curves (Figure 4.2) that obtained from the DMC analysis showed consistent close relationships without substantial slope alterations for the 13 Jordanian rainfall stations. These results indicate minor errors in site recording methods and in the data processing for precipitation records. This indicates that the rainfall stations data across the YRB can be considered consistent. In addition, this supports the same finding for whole Jordan after a DMC analysis had been performed for 13 meteorological

stations distributed across the country by Dahamsheh and Aksoy (2007) in order to analyze the structure of annual precipitation data.

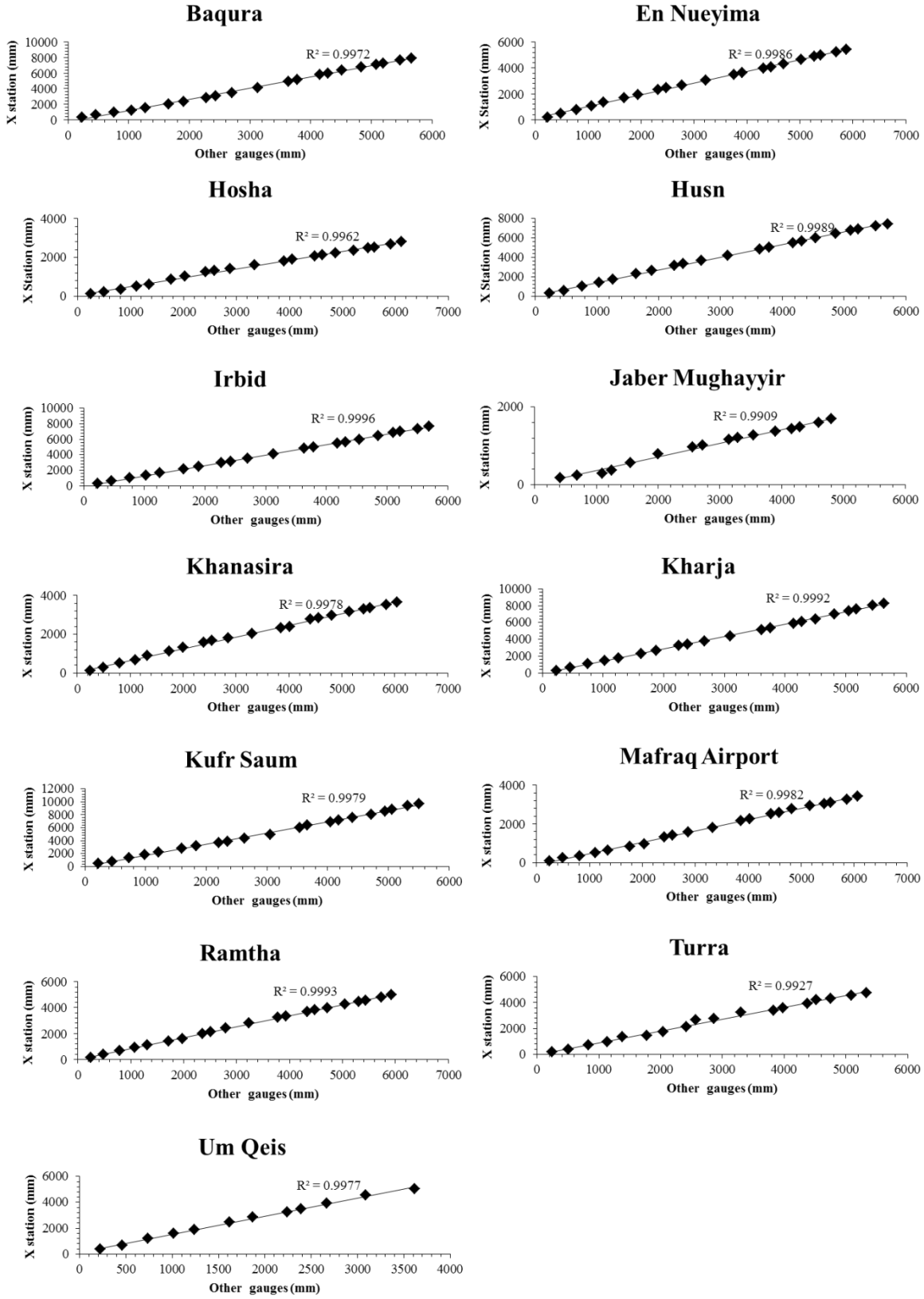

Figure 4.2: Double-mass curves (DMCs) of accumulative PRCP for the Jordanian stations

4.3 Trends in PRCP, Tmax, and Tmin

The resulted normalized MK test statistic Z_S (a measure of the significance of trend) and Sen's slope estimator Q_{med} (a measure of the trend magnitude) are presented in Table 4.1 and Table 4.2 to identify monotonic upward or downward trends in annual PRCP, Tmax and Tmin data series between 1981 and 2009 (20 years) at each station.

In general, PRCP showed no significance downward trends (negative Z_S) for the majority of the stations of an average magnitude of -0.70 mm/year. In particular, Baqura (27 years) and Irbid (using its longest record of 70 years) trends were detected previously using 7 statistical tests by Hamdi et al. (2009). Their results are in agreement for Baqura station but indifferent for Irbid station that showed an insignificant downward trend. Therefore, it can be reported with confidence that annual PRCP in YRB has no significant apparent downward trend and fluctuates between dry and wet years. Tmax showed upward significant trends at 4 of the 5 stations of average magnitude 0.04ºC/year while Tmin showed almost no significant trends of 0.02oC/year. Baqura and Irbid annual Tmax and Tmin trends in the study of Hamdi et al. (2009) were also in agreement. Therefore, it can be reported with confidence that annual Tmax has significant warming trend while Tmin has an insignificant warming trend.

For the longest record at Irbid station, the natural variability is plotted for mean annual PRCP (Figure 4.3), Tmax (Figure 4.4) and Tmin (Figure 4.5). The plots clearly show that there is a downward trend in rainfall and an upward trend in temperature.

Table 4.1: MK statistic measure Z_S and Sen's slope estimator Q_{med} (mm/year) for PRCP

Station	Test	Annual PRCP	Station	Test	Annual PRCP
Baqura	Z_S	-0.533	Jaber Mughayyir	Z_S	1.734
	Q_{med}	-1.662		Q_{med}	4.847
Um Qeis	Z_S	-0.731	Hosha	Z_S	0.459
	Q_{med}	-1.701		Q_{med}	0.254
Kufr Saum	Z_S	-0.929	Husn	Z_S	-1.561
	Q_{med}	-4.393		Q_{med}	-4.732
Kharja	Z_S	-0.059	Mafraq Airport	Z_S	-1.146
	Q_{med}	-0.6		Q_{med}	-1.184
Turra	Z_S	-0.119	En Nueyima	Z_S	-0.532
	Q_{med}	-0.482		Q_{med}	-1.184
Ramtha	Z_S	-0.457	Khanasira	Z_S	-0.31
	Q_{med}	-0.926		Q_{med}	-0.676
Irbid Rainfall	Z_S	-2.174*			
	Q_{med}	-2.269*			

* Statistically significant trends at 0.05 significance level ($|Z_S| > 1.96$)

Table 4.2: MK statistic measure Z_S and Sen's slope estimator Qmed (°C/year) for Tmax and Tmin

Station	Test	Annual Trends	
		Tmax	Tmin
Baqura	Z_S	2.150*	-0.722
	Q_{med}	0.026*	-0.010
Samar	Z_S	3.497*	-0.257
	Q_{med}	0.066*	-0.003
Irbid	Z_S	3.877*	4.601*
	Q_{med}	0.038*	0.04*
Um El-Jumal	Z_S	-1.716	-1.901
	Q_{med}	-0.022	-0.035
Ras Muneef	Z_S	2.382*	0.957
	Q_{med}	0.028*	0.012

* Statistically significant trends at the 5% significance level ($|Z_S| > 1.96$).

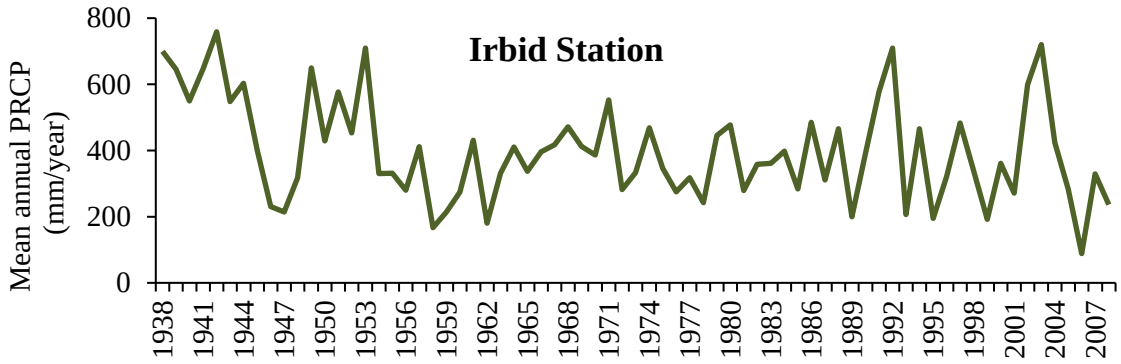

Figure 4.3: 70 years' records of PRCP at Irbid station

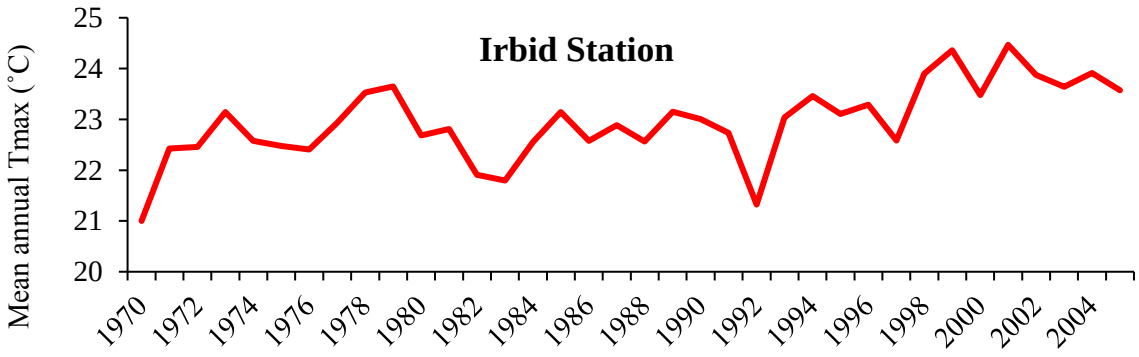

Figure 4.4: 37 years' records of Tmax at Irbid station

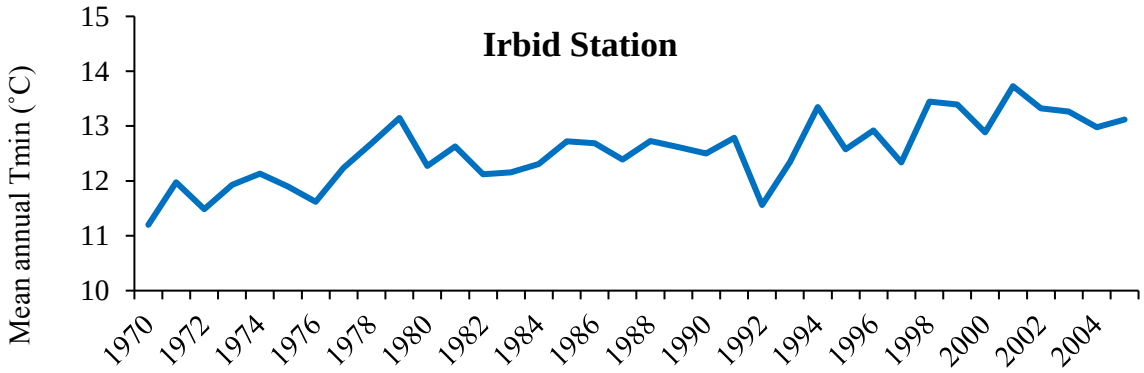

Figure 4.5: 37 years' records of Tmin at Irbid station

Chapter Five: Downscaling and Scenarios Projection

This chapter introduces the SDSM skill in downscaling PRCP, Tmax, and Tmin for the semi-arid YRB basin using CGCM3 and CanESM2 GCMs. In addition, the chapter presents the projected climate changes using the downscaled models.

5.1 Downscaling Using SDSM

5.1.1 Screening NCEP Predictors

The selection of the most relevant predictors is the highest-impact and challenging step when downscaling a predictand using SDSM (Wilby, 2007). In this study, the screening took into account the results of the statistical tests for the evaluation of predictand-predictors relationships and the physical meaningful relationships. The predictors choice has varied from station to another either due to the characteristics of the large-scale atmospheric circulation and/or the local station characteristics. Both CCCma GCMs of different generations gave almost the same predictors. Moreover, for the same predictand, most of the stations relied on the same relevant predictors. For the station-scale PRCP, the screening showed that 10 of the available 26 NCEP predictors are the most relevant with a confidence level of 95%. The number of the screened predictors were between two and seven for each station. Summary of the relevant predictors and the frequency of being selected for the rainfall stations is shown in The predictors screened for daily PRCP are almost in agreement with predictors selected under similar semi-arid climate by Cavazos and Hewitson (2005) and Anandhi et al. (2008).

Table 5.1. The highest influential predictor (super predictor) was either the 850 h Pa or 500 h Pa geopotential heights (p850 or p500) having linear correlation coefficients (r_c) between 0.12 and 0.31 with the PRCP. The other influential significant predictors with no appreciable collinearity were 1000 hPa vorticity (p_z), 500 hPa vorticity (p5_z), mean sea level pressure (mslp), 1000 hPa wind speed (p_f), 1000 hPa meridional velocity (p_v), zonal velocity (p_u) and 500 hPa specific humidity (s500). These high-pressure predictors were expected due to the strong physical relationship between high-pressure systems and YRB hot Mediterranean/ dry-summer subtropical climate (Kottek, 2006). Grid box PRCP

predictor (prcp) was found to have very low correlation with the local-scale PRCP in spite of the expected meaningful physical relationship.

The predictors screened for daily PRCP are almost in agreement with predictors selected under similar semi-arid climate by Cavazos and Hewitson (2005) and Anandhi et al. (2008).

Table 5.1: List of the screened predictors from NCEP and frequency of getting selected among the 23 rainfall stations

CGCM3		**CanESM2**	
Predictor code	**Frequency**	**Predictor code**	**Frequency**
p850	13	p850	17
p_z	11	p1_z	13
mslp	11	prcp	11
p_f	10	s500	10
p_u	10	p1_f	10
p500	10	p1_u	10
p_v	9	p1_v	9
p5_z	9	p5_z	9
s500	8	p500	7
prcp	2	mslp	6

Two to four predictors were screened for daily Tmax and Tmin at each station. The super predictor is the 2m air temperature (temp) that reflect the strong physical relationship as seen in Table 5.2. The linear correlation coefficient (r_c) between the daily observed Tmax and Tmin and the predictor temp ranged from 0.86 up to 0.95. In addition, 500 hPa vorticity (p5_z), 500 hPa specific humidity (s500) and 500 hPa wind speed were of significant influence with no collinearity with the super predictor temp. Those selected predictors are almost similar to many studies for downscaling temperature for such semi-arid climate including Toews and Allen (2009); Souvignet and Heinrich (2011) and Abbasnia and Toros (2016).

Table 5.2: List of the screened predictors from NCEP and frequency of getting selected in the 5 Tmax and Tmin stations

CGCM3				CanESM2			
Tmax		**Tmin**		**Tmax**		**Tmin**	
Predictor code	**Frequency**	**Predictor code**	**Frequency**	**Predictor code**	**Frequency**	**Predictor code**	**Frequency**
temp	5	temp	5	temp	5	temp	5
p5_z	4	s500	2	s500	3	s500	3
s500	2	p8_v	2	p5_f	2	p5_f	1
p–v	2	p5_v	1	p8_v	1		
p8_u	2	p8_u	1	p5_v	1		
p_f	2	p5_z	1				
p8_v	1	p_f	1				
p8zh	1						

5.1.2 Calibration

The coefficient of determination (R^2) and the standard error (SE) at daily scale (calculated directly by SDSM) were used as indicators during calibration for performance check. The means of those indicators among the stations for PRCP, Tmax and Tmin are shown in Table 5.3. Both CGMs provided almost analogous power in downscaling at daily scale. PRCP was poorly modeled at a daily scale where annual R^2 ranged 0.50-0.02 with a mean of 0.19. Temperature calibration showed good performance given the obtained annual ranges of 0.78-0.57 for R^2 and 2.56-1.94^{o}C for SE among the stations. However, those results indicate the low SDSM capability of modeling PRCP comparing to the temperature at daily scale.

Table 5.3: Coefficient of determination (R^2) and the standard error (SE) of the calibrated model at daily scale

	CGCM3						CanESM2					
	PRCP		Tmax		Tmin		PRCP		Tmax		Tmin	
	R^2	SE (mm/d)	R^2	SE (ºC)	R^2	SE (ºC)	R^2	SE (mm/d)	R^2	SE (ºC)	R^2	SE (ºC)
Jan	0.13	0.42	0.62	1.96	0.40	2.14	0.13	0.42	0.64	2.06	0.40	2.14
Feb	0.15	0.40	0.68	2.23	0.36	2.30	0.13	0.40	0.59	2.41	0.37	2.28
Mar	0.17	0.38	0.66	2.49	0.47	2.64	0.13	0.39	0.68	2.75	0.47	2.63
Apr	0.26	0.36	0.73	2.60	0.47	3.27	0.25	0.35	0.69	2.85	0.48	3.24
May	0.55	0.34	0.69	2.49	0.28	3.12	0.70	0.28	0.46	2.51	0.28	3.11
Jun	-	-	-	-	-	-	-	-	-	-	-	-
Jul	-	-	-	-	-	-	-	-	-	-	-	-
Aug	-	-	-	-	-	-	-	-	-	-	-	-
Sep	-	-	-	-	-	-	-	-	-	-	-	-
Oct	0.29	0.27	0.73	2.02	0.33	2.81	0.29	0.28	0.75	2.21	0.34	2.78
Nov	0.14	0.42	0.78	1.93	0.21	2.54	0.15	0.42	0.64	2.06	0.27	2.43
Dec	0.22	0.40	0.69	2.01	0.34	2.16	0.19	0.41	0.65	2.17	0.33	2.19
Annual	**0.19**	**0.38**	**0.70**	**2.18**	**0.37**	**2.55**	**0.18**	**0.38**	**0.59**	**2.36**	**0.38**	**2.53**

5.1.3 Validation Using NCEP Predictors

NCEP predictors that re-gridded according to the corresponding GCM resolution are used to calibrate the SDSM. After that, the calibrated GCMs predictors are used to force SDSM for downscaling the climate variables of interest. To validate the downscaled PRCP, Tmax and Tmin using NCEP predictors, various measures were evaluated for mean and extreme characteristics at monthly scale during the validation 5 years' period 1996-2000. Should keep in mind that NCEP predictors are not used for climate change projections. However, understanding SDSM ability using NCEP predictors as opposed to GCM predictors can reveal potential deficiencies in GCM predictors when used within the SDSM environment.

5.1.3.1 PRCP Validation

SDSM showed better applicability using monthly, seasonal and annual time series, in comparison to the daily time series as the vast majority of previous studies (Mahmood, 2013; Khan, 2015). Agreement between observed and downscaled monthly PRCP time

series is obvious during the validation period as seen in Figure 5.1. The plots were accompanied with average R^2 of 0.71 and 0.73 and RMSEs of 18.2 and 16.8 mm/month comparing to observed range of 0 to 177.5 mm/month using CGCM3 and CanESM2 respectively. In addition, most of the mean PRCP monthly indices were reproduced accurately as shown in Figure 5.2. However, biases were existing to some extent at monthly scale but they are almost minor at seasonal and annual scale. Major rainy months (Jan, Feb, Mar, Apr, Oct, Nov and Dec) were simulated with good accuracy but May which is a month of very little observed PRCP was not. Generally using both GCMs/NCEP predictors, wet percentages were slightly overestimated along all major rainy months by the approximately total annual percentage increase of 1.5% (6 days) distributed 1-2 day/rainy-month increase. Mean dry-spell lengths in the rainy months were underestimated 0.6-2.7 day/per month while the dry spell in May has been overestimated by 5.8 days. Mean wet spells were simulated with high accuracy showing minor biases 0.03-0.34 days/month. However, since SDSM is calibrated with NCEP predictors, the downscaling using the GCMs predictors is expected to be accompanied with larger biases.

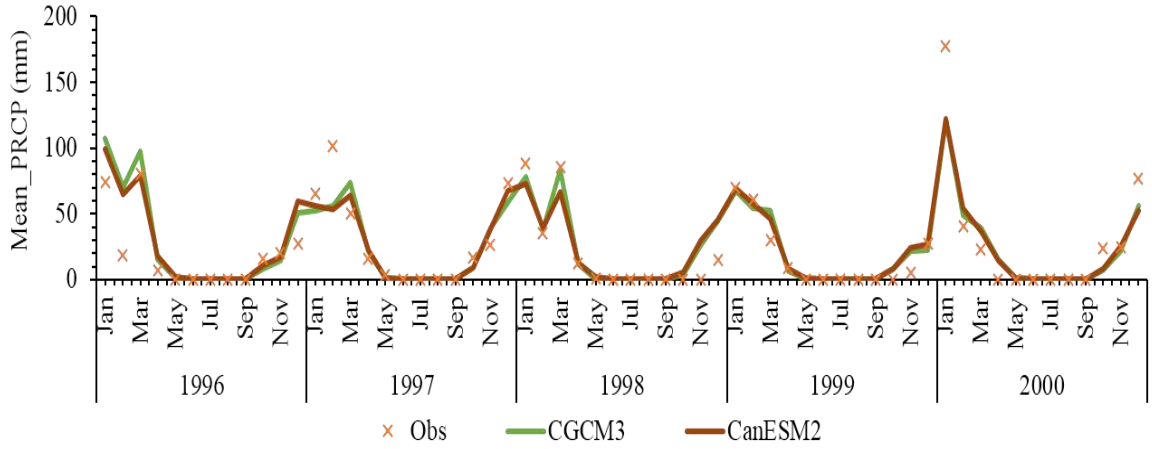

Figure 5.1: Monthly Mean_PRCP time series comparison between observed and downscaled PRCP using NCEP predictors (1996-2000)

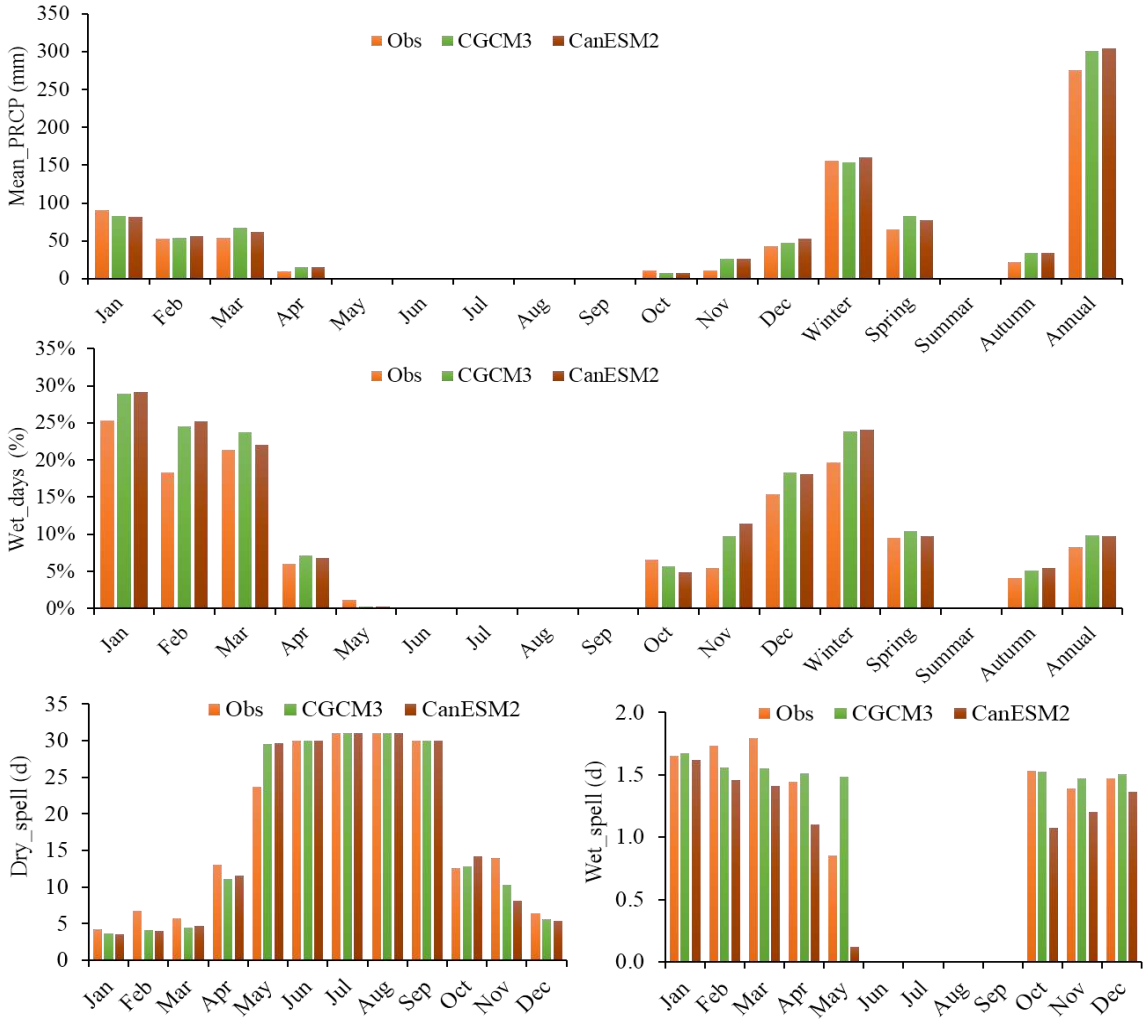

Figure 5.2: Comparison of mean indices between observed and downscaled PRCP using NCEP during the validation (1996-2000)

The reproduction of PRCP extremes indices (Figure 5.3) was of less accuracy in compare to the mean indices but the biases seem acceptable. Maximum total PRCP accumulated over 5-days (Rx5day) was mostly underestimated through the rainy months with annual biases that occur in winter of 11.5 and 13.8 mm using CGCM3/NCEP and CanESM2/NCEP respectively. Maximum dry spell length (Max_dspel) and maximum wet spell length (Max_wspel) were reproduced with good accuracy. However, biases are higher in the lowest rainy months (Mar, Apr, May, and Oct) in compare to highest rainy months (Jan, Feb, Nov and Dec). Generally, Max_dspel and Max_wspel were underestimated by 0.5-4.3 day/month and 0.12-1.1 day/month respectively.

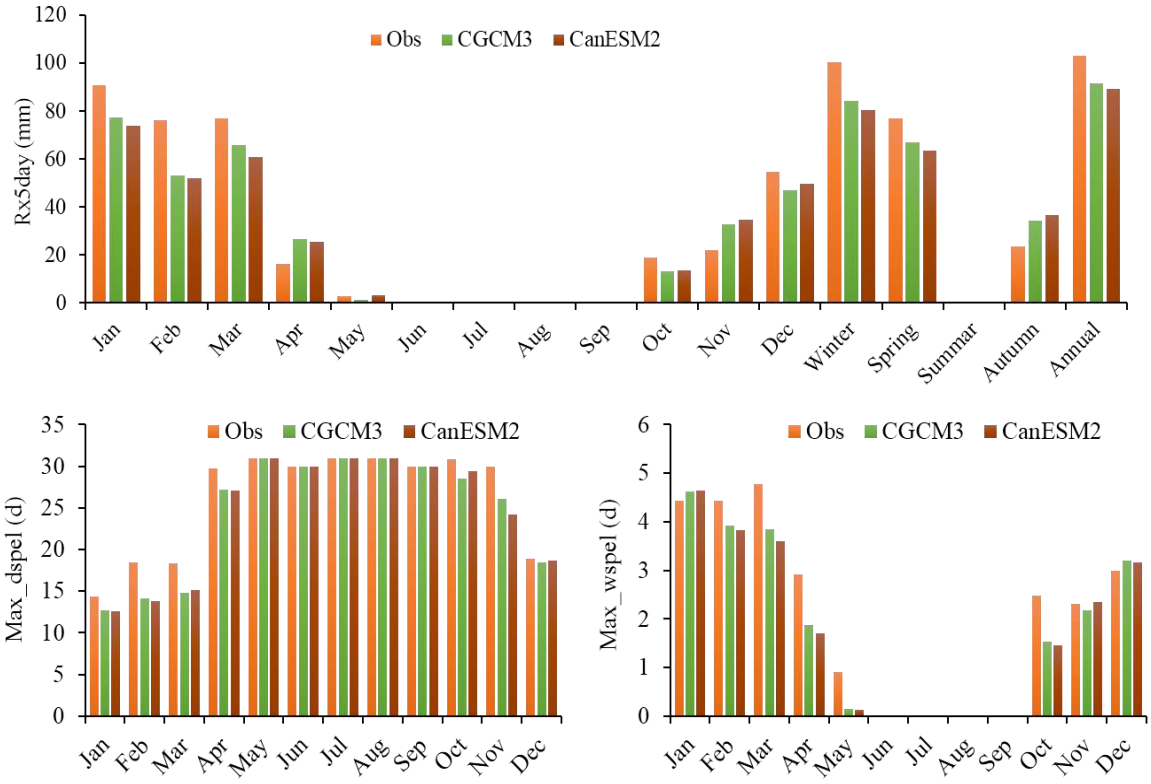

Figure 5.3: Comparison of extreme indices between observed and downscaled PRCP using NCEP through the 5 years' validation period (1996-2000)

The generalized extreme value (GEV) distributions and return period estimates for the observed and GCMs/NCEP downscaled maximum daily PRCP at 95% confidence level have been averaged over the 23 rainfall stations in the study area and depicted in Figure 5.4. The GEV distributions the distributions elucidate that generally using both CGCM3 and CanESM2/NCEP, the fit GEV distribution systematically underestimates the observed historical extreme events. In addition, both GCMs suggested an approximate upper bound of maximum daily PRCP amounting to 120 mm/day relative to the observed upper bound of 130mm/day given a bias of 10mm/day. This result was expected because the majority of studies on modeling extreme PRCP characteristics from GCMs/NCEPs have found that simulated daily PRCP tends to occur more frequently but is less intense than observed PRCP (Tryhorn, 2011). The derived average return period values from the GEV distribution of the PRCP extreme value series showed that short period extreme events up to 5 years were accurately reproduced while long return periods extreme events (> 5years) were poorly reproduced.

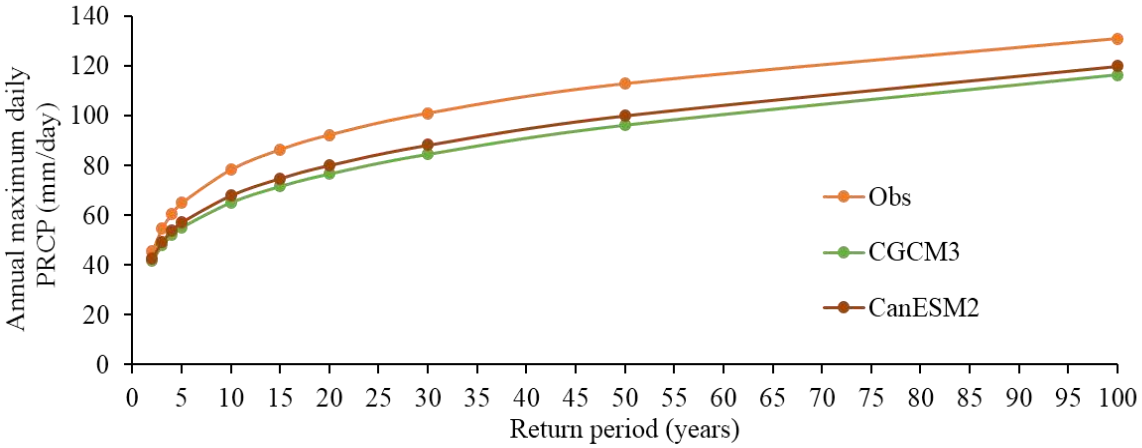

Figure 5.4: Frequency analysis for annual maximum daily PRCP between observed and downscaled PRCP using NCEP (1996-2000)

5.1.3.2 Tmax and Tmin Validation

Monthly mean Tmax and Tmin simulation using GCMs/NCEP predictors were of very high accuracy among all temperature stations as displayed in Figure 5.5. Comparing the observed and the simulated time series showed average Tmax-Tmin R^2 of 0.96-0.97 and 0.97-0.97 using CGCM3 and CanESM2 respectively. Extreme indices were accurately simulated for Tmin comparing to Tmax as shown in Figure 5.6.

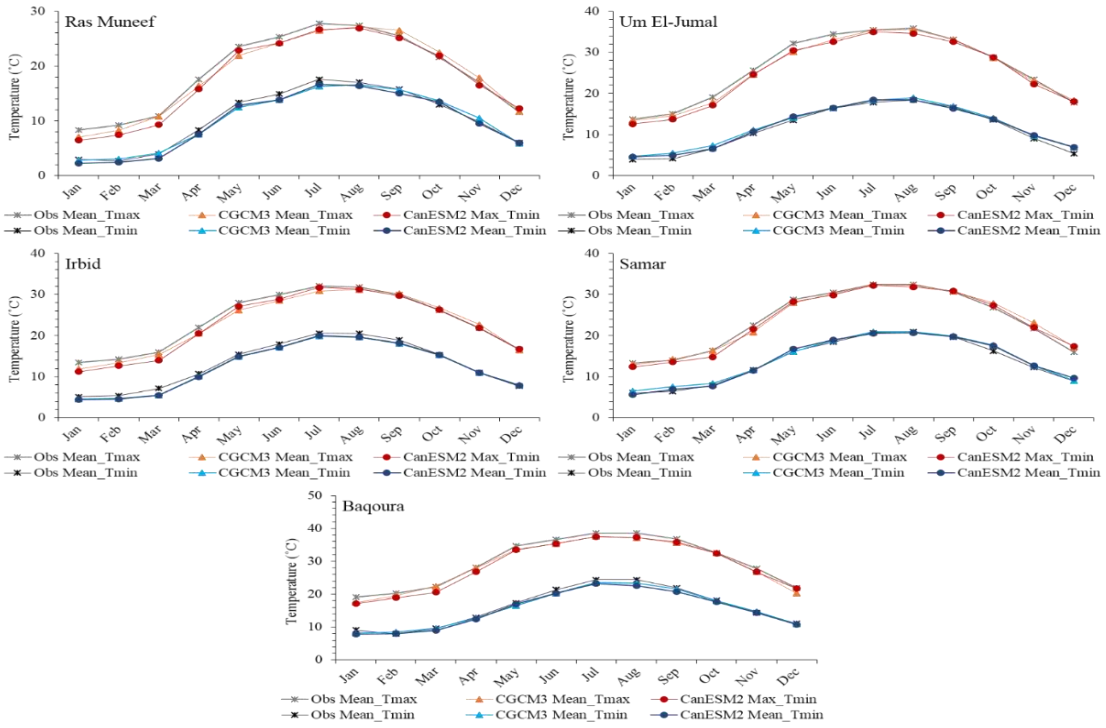

Figure 5.5: Comparison of mean indices between observed and downscaled Tmax and Tmin using NCEP through the 5 years' validation period (1996-2000)

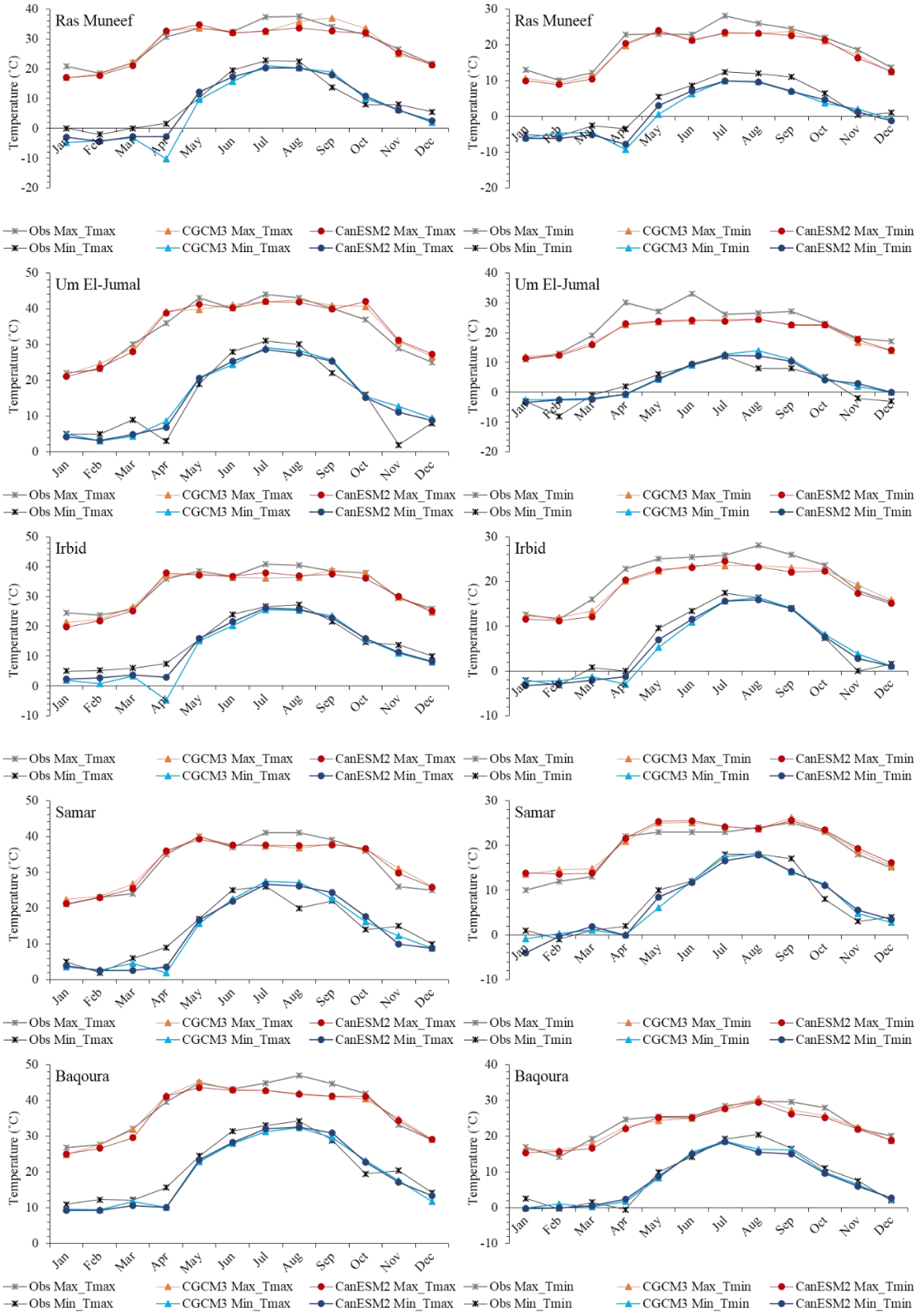

Figure 5.6: Comparison of extreme indices between observed and downscaled Tmax and Tmin using NCEP through the 5 years' validation period (1996-2000)

5.2 Uncertainty Analysis of Current Climate Reproduction

The confidence on the ability of the downscaling models that generated using GCMs predictors to simulate current climate is a prerequisite to being convinced in the future climate projection. Therefore, this section will explore the degree of which the downscaled output from CGCM3 and CanESM2 predictors for the climate of the twentieth-century experiment (20C3M) scenario did reproduce the observed mean and extremes events characteristics of the baseline observed scenario 1981-2000 at monthly scale.

5.2.1 Uncertainties in PRCP

The mean PRCP downscaling was not reasonably well fit showing an average R^2 of 0.31 and 0.35 and RMSEs of 31.3 and 35.8 mm/month comparing to observed range of 0 to 177.5 mm/month using CGCM3 and CanESM2 respectively. The PRCP time series plot (Figure 5.7) confirm to some degree a plausible agreement between simulated and observed but misses the observed extreme PRCP events. The mean PRCP indices were generally well reproduced as manifested in Figure 5.8. In general, CGCM3 was accompanied with slightly better skill. Based on this, the SDSM is considered underperformed and not able to reproduce with good skill the observed PRCP even at monthly scale as well as the case at the daily scale. This relatively low explained variance for PRCP underlines SDSM poor ability to reflect the stochastic nature of PRCP occurrence, magnitude, and the regime variability within the downscaling process (compared to temperature). This weakness has been suggested in many studies when downscale PRCP (Wilby, 1997; Gachon, 2005; Wilby, 2003; Dibike, 2008).

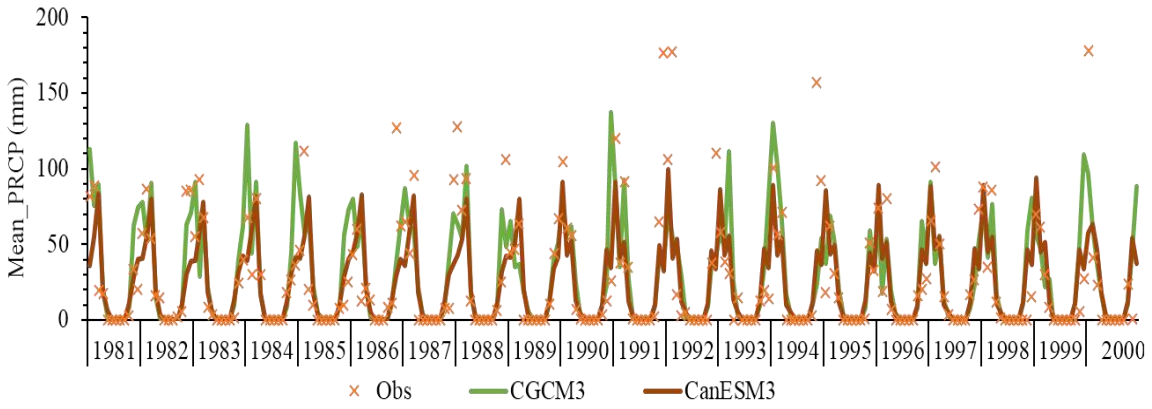

Figure 5.7: Monthly PRCP time series comparison between observed and downscaled PRCP using GCMs (1981-2000)

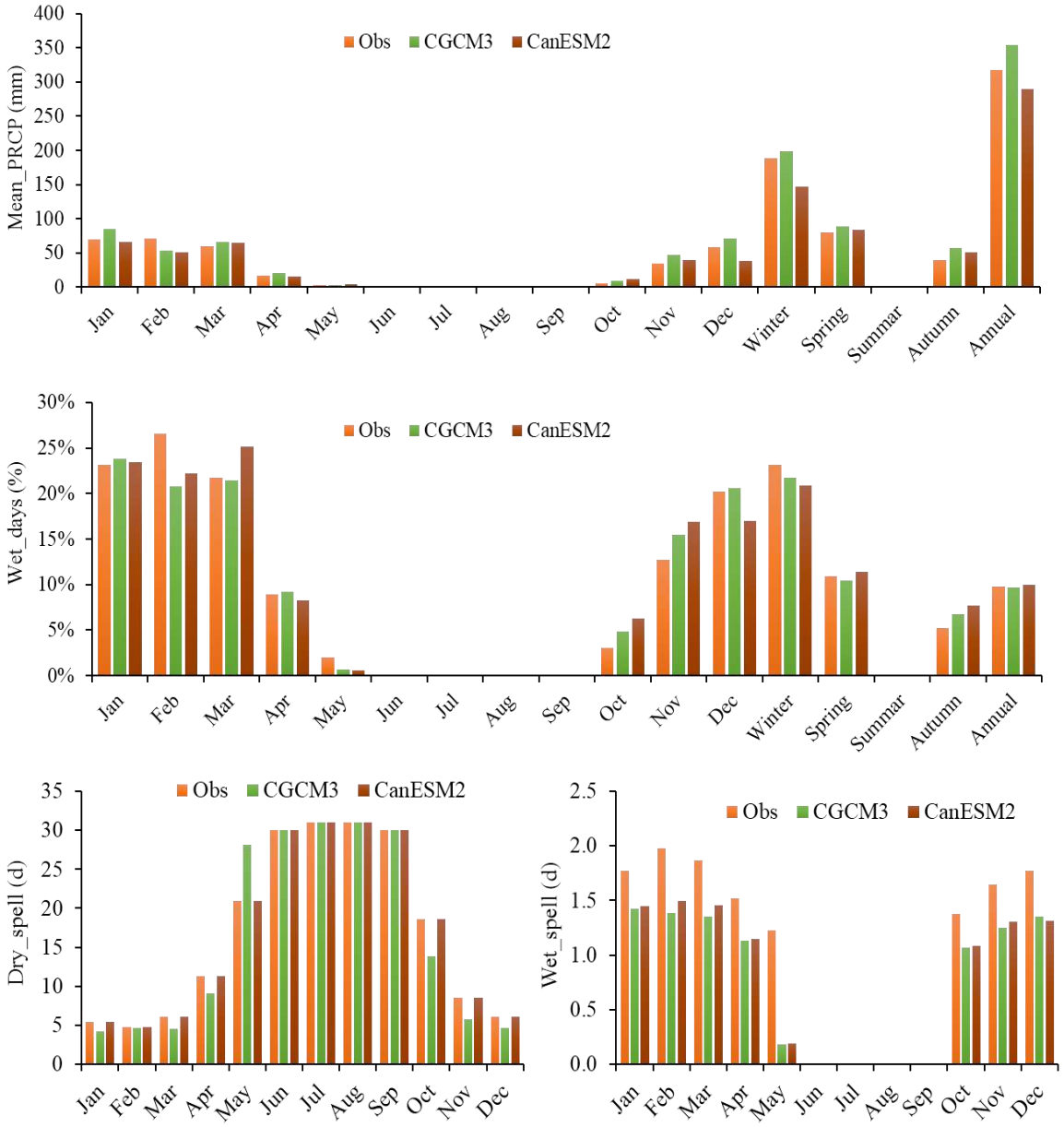

Figure 5.8: Comparison of mean indices between observed and downscaled PRCP using GCMs (1981-2000)

In general, the extreme events were not well reproduced using both GCMs. The monthly maximum consecutive 5 days PRCP (Rx5day) and maximum wet spells (Max_wspel) have been underestimated on average by around 25% and 37% respectively. On the other hand, maximum dry spells (Max_dspel) has been overestimated on average by around 3%. Therefore, no robust confidence can be dragged there between observed and GCMs downscaled PRCP extreme events. Accordingly, it can be stated that even a multi-model approach is still not able to capture extremities and thus lower confidence levels are given to their values. This is common when utilizing GCMs predictors, the IPCC TAR reported that low GCM resolution is an inhibiting factor for accurate and detailed

evaluation of PRCP extremities (Tryhorn, 2011). Souvignet et al. (2010) also concluded that SDSM was not a very robust method for the simulation of extreme PRCP after investigating the SDSM performance and ability to simulate extreme events in an arid mountainous watershed in Chile using the GCMs predictors. Liu et al. (2011) showed that SDSM performance is relatively poor on extreme events for dry stations with annual precipitation lower than 200 mm but fair enough for the wet stations. Even a nested dynamic downscaling approach that was used in Jordan River region underestimate the wet day frequency and the strong PRCP events (Smiatek, 2011). However, though the systematic errors that accompany the simulating extreme events for PRCP using SDSM, the results usually can be considered acceptable for practical applications (Chu, 2010).

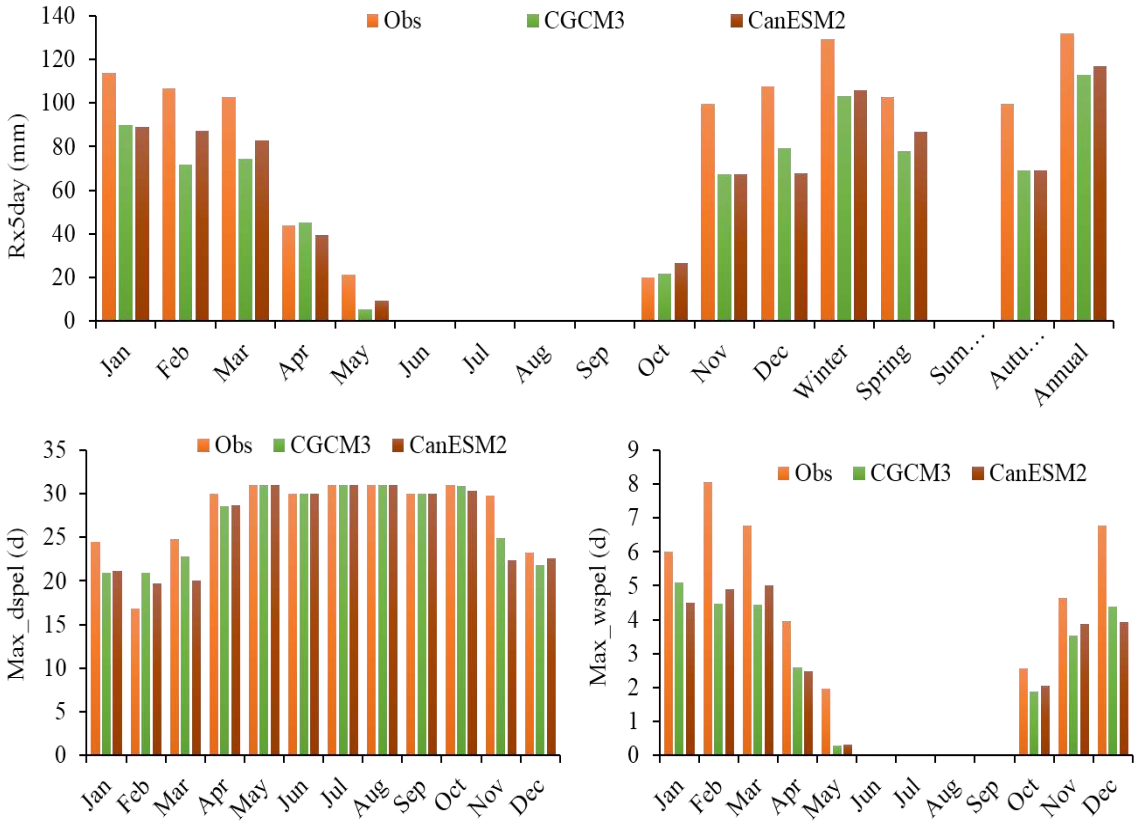

Figure 5.9: Comparison of extreme indices between observed and downscaled PRCP using the GCMs (1981-2000)

The generalized extreme value (GEV) distributions of the maximum daily PRCP that fit very well for the observed and GCMs downscaled PRCP are displayed in Figure 5.10. It elucidates that generally both CGCM3 and CanESM2 systematically underestimate the observed historical extreme events. The CGCM suggested an approximate upper bound of maximum daily PRCP amounting to 131 mm/year relative to the observed upper bound of 147mm/day given a bias of 16mm/day (12% underestimation). The CanESM suggested

lower upper bound of 112mm/day and thus higher bias of 35mm/day (25% underestimation). In addition, as the return period get shorter, extreme events become more accurately reproduced. CGCM3 had caught accurately extreme events up to 30 years in compare to 5 years by CanESM2. This makes CGCM more skilled for reproduction of PRCP extremities. On the other hand, long return periods extreme events were poorly reproduced by both GCMs. These results support the previously stated conclusion that long return period extreme events are hard to be reproduced using the GCMs predictors within the SDSM (Souvignet, 2011).

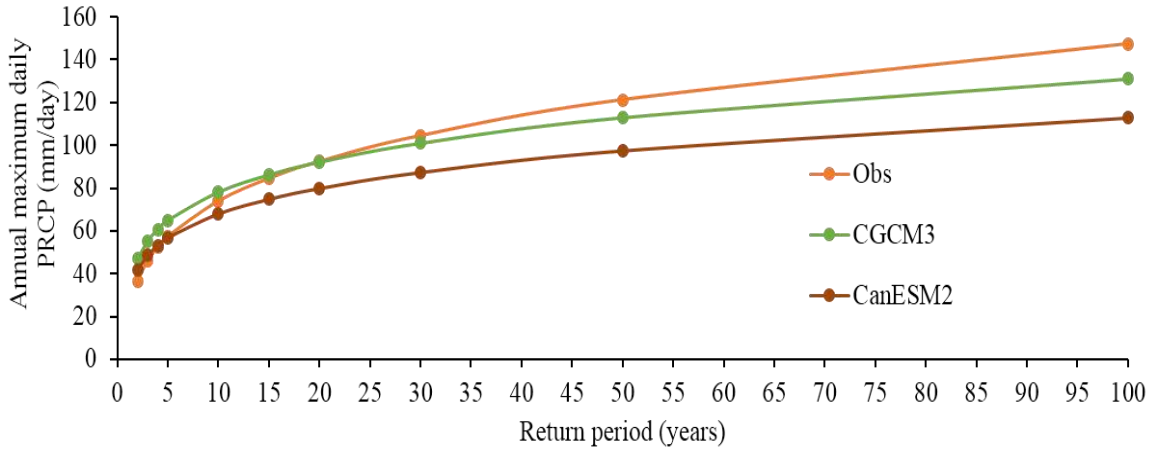

Figure 5.10: Frequency analysis for annual maximum daily PRCP between observed and downscaled PRCP using GCMs (1981-2000)

In summary, utilizing SDSM in integration with CGCM and CanESM predictors is able to reproduce the mean PRCP characteristics but is not for the PRCP extremities. The reproduction of the monthly and annually PRCP is much powerful than daily PRCP due to the hardship to capture the stochastic nature of PRCP. CGCM provided to some extent better skill in downscaling than the next GCM generation CanESM. Generally, the downscaling of PRCP seems acceptable; however, the power and weakness in driving a hydrological model will be further evaluated in Chapter 6.

5.2.2 Uncertainties in Tmax and Tmin

The results of the uncertainty analysis are reported for each temperature station because SDSM performance using GCMs predictors showed to vary significantly according to the station altitude. Ras Muneef is of the highest altitude (1150m a.m.s.l) while Baqura is of the lowest altitude (-227m b.m.s.l). The other stations have relatively moderate altitudes which are 650, 616 and 332 m a.m.s.l for Um El-Jumal, Irbid, and Samar respectively. The results in Table 5.4 indicate that as the altitude decreased, Tmax

and Tmin downscaling got more powerful. That was reflected through Tmax-Tmin R^2 increase from 0.77-0.78 up to 0.93-0.90 and from 0.84-.81 up to 0.89-0.92 using CGCM3 and CanESM2 respectively. This is in agreement with the finding of the nested dynamic downscaling approach that was implemented in Jordan River region by Smiatek et al. (2011) that showed a significant elevation dependence in the simulation of future climate temperature. The elevation dependency has been confirmed previously by Liu et al. (2009) after simulating and projecting 116 weather stations in the eastern Tibetan Plateau and its vicinity during 1961–2006to examine the relationship between climatic warming and elevation. The main finding was the elevation dependency is most likely caused by the combined effects of cloud-radiation and snow albedo feedbacks among various influencing factors.

Table 5.4: R^2 and RMSE of the reproduced Tmax and Tmin using the GCMs (1981-2000)

*Station	CGCM3				CanESM2			
	Tmax		Tmin		Tmax		Tmin	
	R^2	RMSE (ºC)	R^2	RMSE (ºC)	R^2	RMSE (ºC)	R^2	RMSE (ºC)
Ras Muneef	0.77	2.36	0.78	2.55	0.84	3.13	0.81	2.63
Um El-Jumal	0.84	3.20	0.85	2.32	0.86	3.28	0.84	2.25
Irbid	0.82	3.00	0.83	2.35	0.86	3.07	0.89	2.06
Samar	0.84	2.91	0.84	2.21	0.86	3.00	0.88	1.97
Baqoura	0.93	1.94	0.90	1.84	0.89	2.74	0.92	2.02

*The stations are ordered from the highest to the lowest altitude as it goes down.

Figure 5.11 and Figure 5.12 confirm the SDSM well skill to reproduce daily mean air temperature indices. Chu et al. (2010) results also showed that SDSM can reproduce very well the mean pattern and numerical values for mean temperature and precipitation. Mahmood and Babel (2013) also demonstrated the good applicability of monthly sub-models of SDSM for downscaling air temperature.

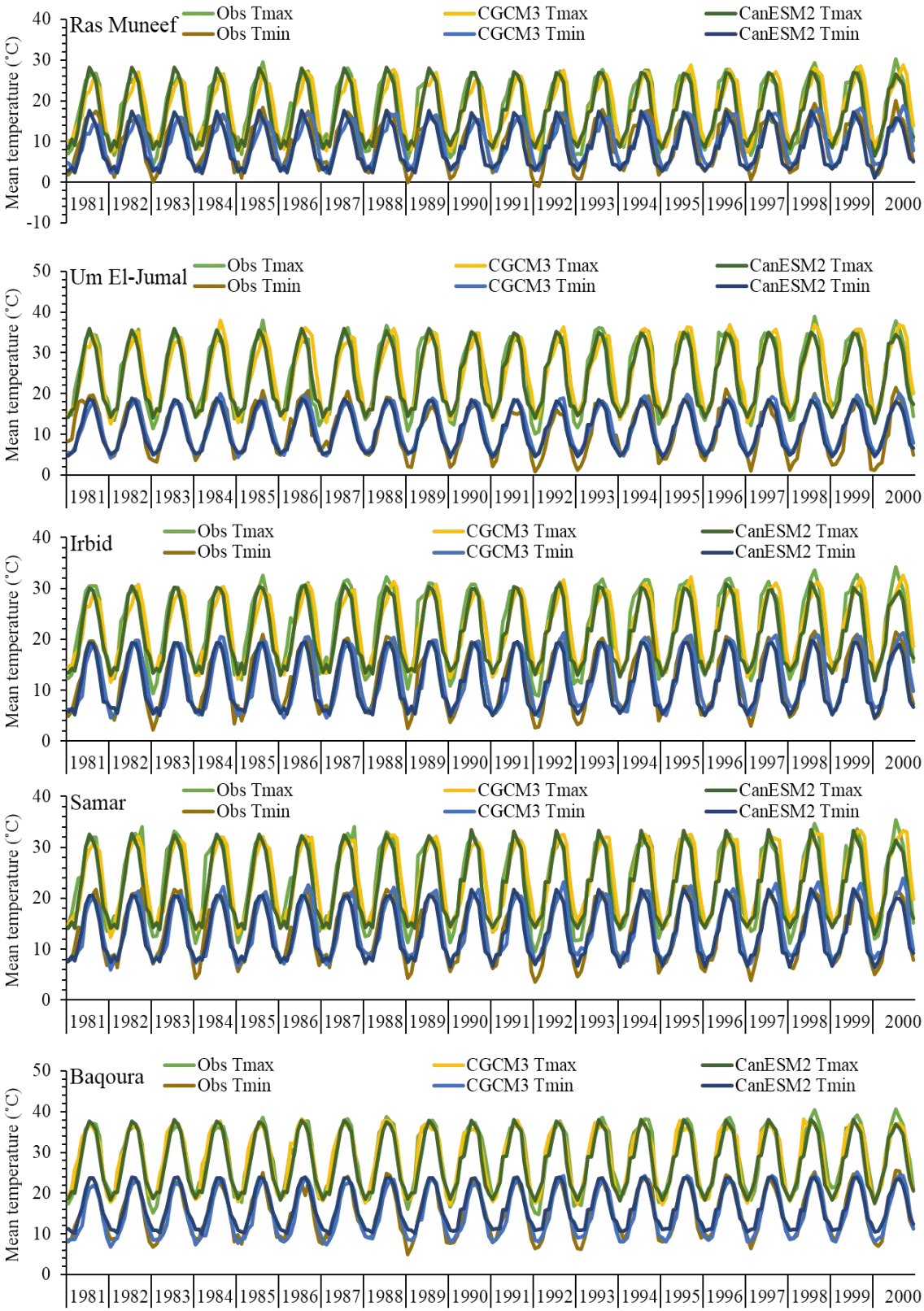

Figure 5.11: Mean monthly time series comparison between observed and downscaled Tmax and Tmin using GCMs (1981-2000)

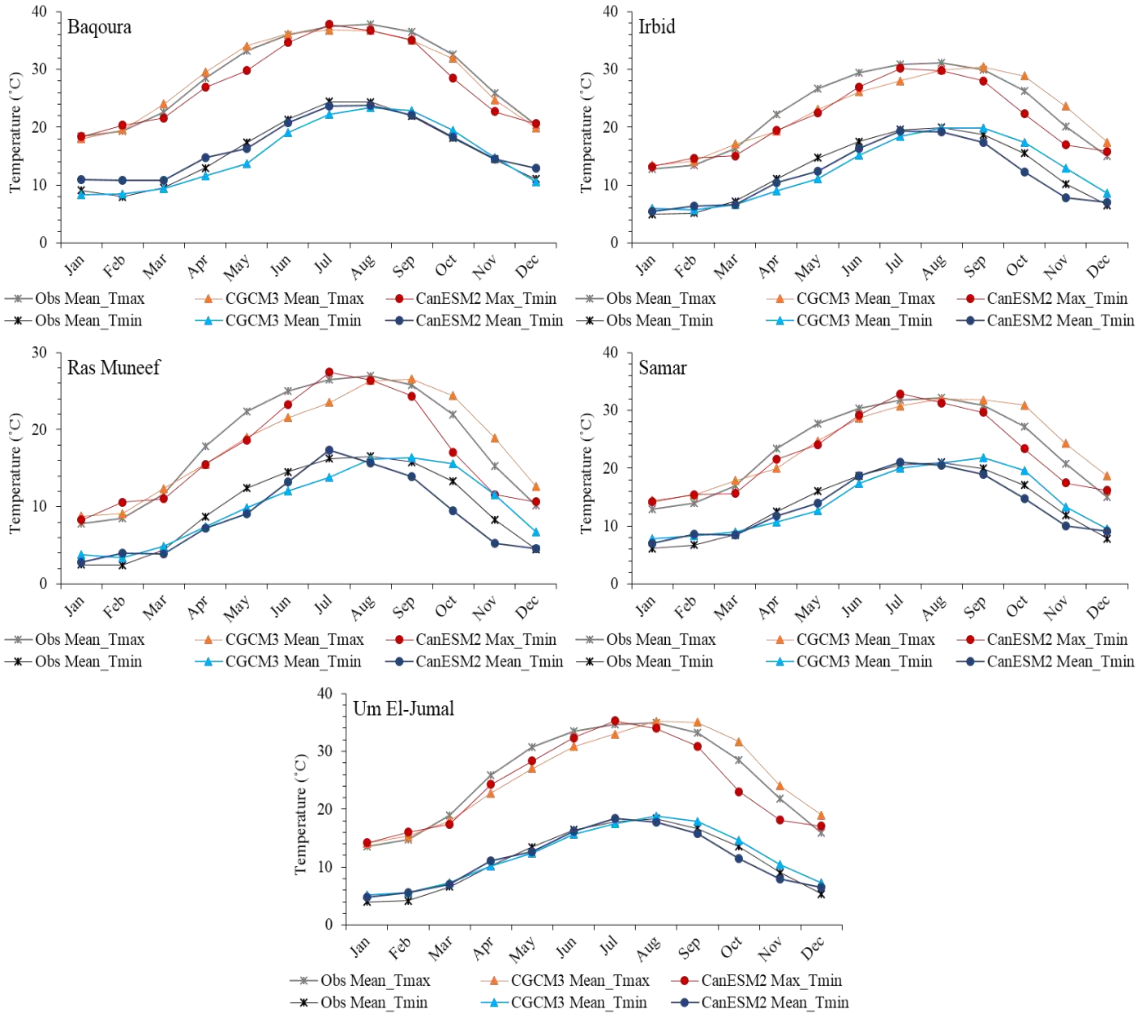

Figure 5.12: Comparison of mean indices between observed and downscaled Tmax and Tmin using GCMs through 20 years' uncertainty analysis (1981-2000)

The results of comparing extremes indices that displayed in Figure 5.13 suggest a lower GCM's capability of reproducing most of Tmin and Tmax extreme events compared to NCEP. The altitude influence is clear where the GCM's skill got enhanced as the station altitude decreased. CanESM2 was more powerful in Tmax and Tmin extremities reproduction.

In contrast to the systematics underestimation that appeared in the frequency analysis of PRCP, Tmax, and Tmin frequency analysis (Figure 5.14) showed no rule with no secured ability to reproduce extreme events. However, generally, the extremities of Tmax and Tmin are reproduced in acceptable agreement to some extent with the observed extremities using both CGCM3 and CanESM2. In addition, the short return period of <5 years' events is more accurate than long return period events.

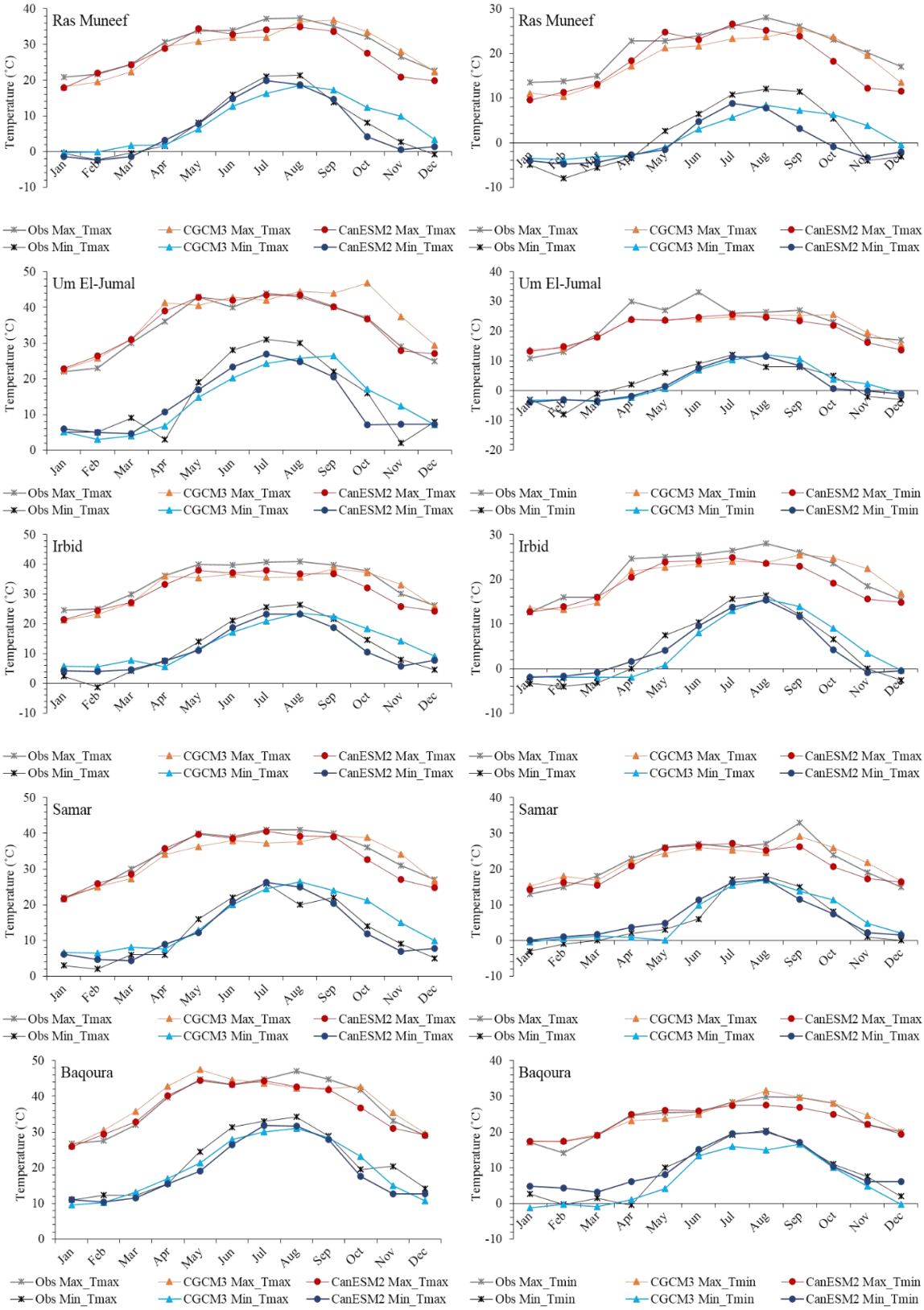

Figure 5.13: Comparison of extremes indices between observed and downscaled Tmax and Tmin using GCMs (1981-2000)

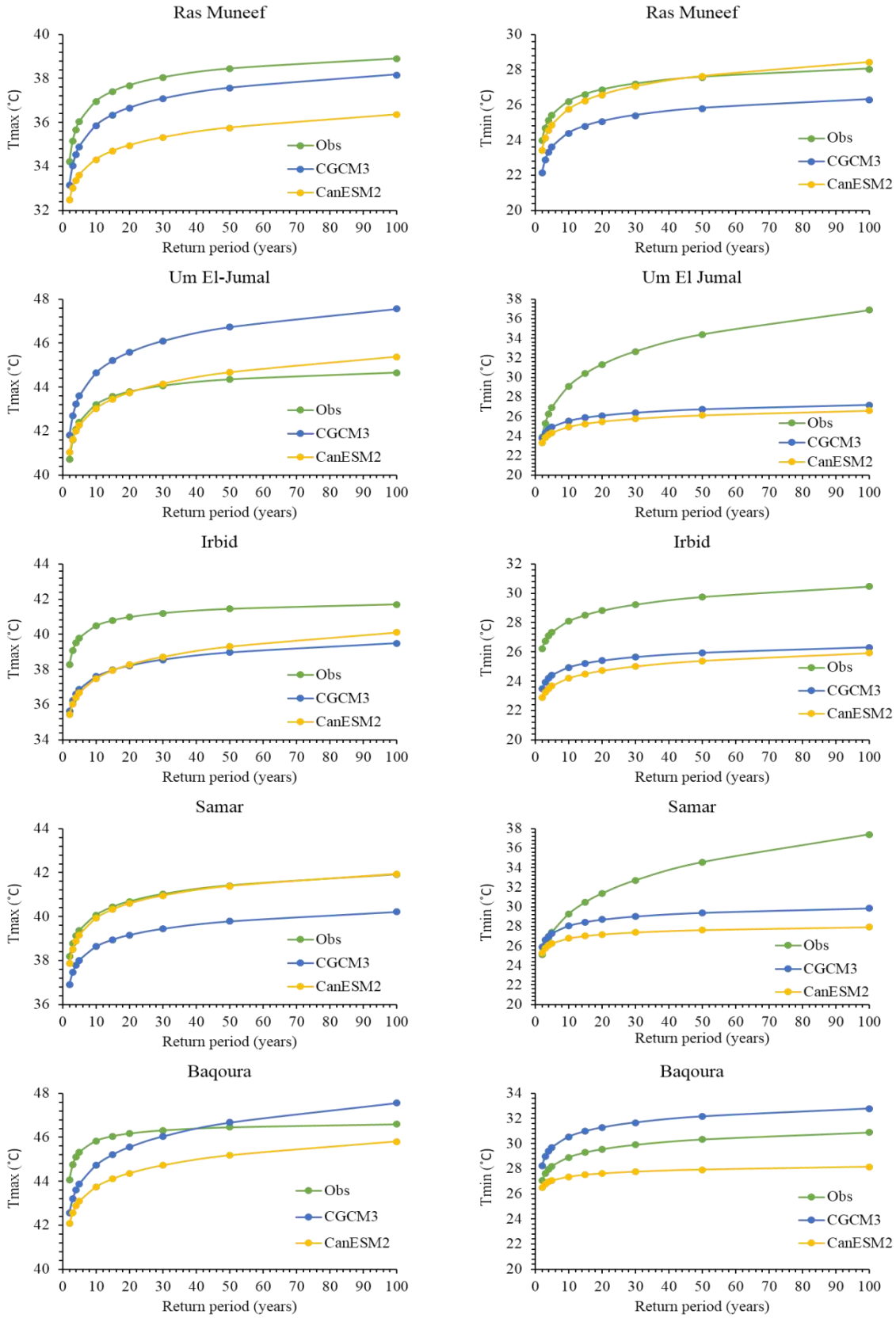

Figure 5.14: Frequency analysis for annual mean Tmax and Tmin between observed and downscaled series for the period 1981-2000 at each station

5.2.3 Equality of Median

The non-parametric Mann–Whitney (MW) test was performed for mean monthly PRCP, Tmax and Tmin in each station at the 95% confidence level to seek out the null hypothesis (H_0) that the difference of median between the observed and downscaled samples is equal to zero. The percentages of the stations accepting the test are displayed in Figure 5.15. The 100% of accepting test for Tmax and Tmin provide a very high confidence in the ability of CGCM3 in downscaling them. On the other hand, more uncertainties arise in the case of CanESM2 downscaling of Tmax and Tmin. Therefore, Tmax and Tmin choice of the GCM that used for downscaling is of important influence on the reproduction of the observed median. In the case of PRCP, both CGCM3 and CanESM2 showed similar significant reproduction percentages of the observed median by approximately 80%. Thus, a good confidence can be dragged in the ability of CGCM3 and CanESM2 in downscaling monthly PRCP.

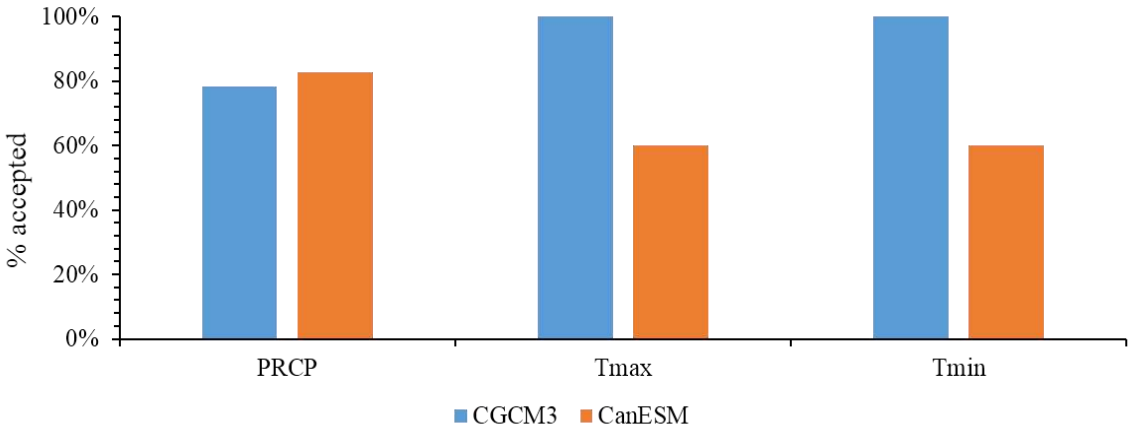

Figure 5.15: Percentage of accepting Mann–Whitney test (equality of median)

5.3 Climate Change Projections

The annual mean surface air temperature change and precipitation percentage change of projected downscaled climate scenarios along the 21st century relative to the simulated baseline period 1981-2000 are going to be presented hereafter. The projected PRCP is expected to increase slightly in the 2020s for both A1B and A2 scenarios and then decline after that. RCPs scenarios project continues declination in PRCP through as seen in Figure 5.16.

Downscaled mean Tmax and Tmin are projected to increase steadily under all scenarios as Figure 5.17 and Figure 5.18 display. In general, under the various scenarios, there will be a continuous reduction in precipitation and increase in temperature. This is

consistent with the previously quantified observed trends of precipitation and temperature in the YRB over the last decades of the 20th century. A summary of the projected scenarios combination annual temperature difference and precipitation percentage change during the intervals of interest in the 21st-century is shown in Table 5.5. The amount of increase in temperatures will range between 0.9°C and 3.7°C, while the percentage of change in precipitation will vary from +6% to -32% among the scenarios.

Generally, the basin is expected to undergo drought conditions that will increase in intensity and duration along the 21st century especially under the worst scenarios RCP4.5, RCP8.5 and A2 due to the increased evapotranspiration and thus surface drying. Meanwhile, the water holding capacity of air will increase due to more water vapor that was estimated previously by 7% increase in vapor per 1°C warming. This air moisture increase affects the various storm forms including individual thunderstorms, extratropical rain or snow storms, or tropical cyclones by causing more intense precipitation events even if precipitation quantities are decreasing as they say 'it never rains but it pours' (Trenberth, 2011). This is already have been observed to happen from time to time in the study area leading to potential increased risk of flooding (Khordagui, 2014). However, it is not necessarily that the projected climate is being likely. That is because there are various intrinsic uncertainties associated with the GCMs and the used downscaling technique (Prudhomme, 2009).

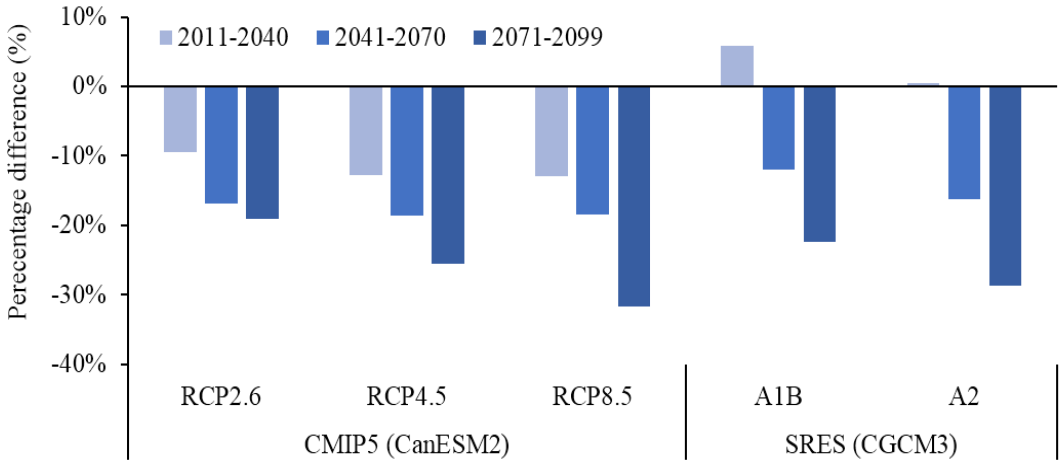

Figure 5.16: The projected percentage change in PRCP

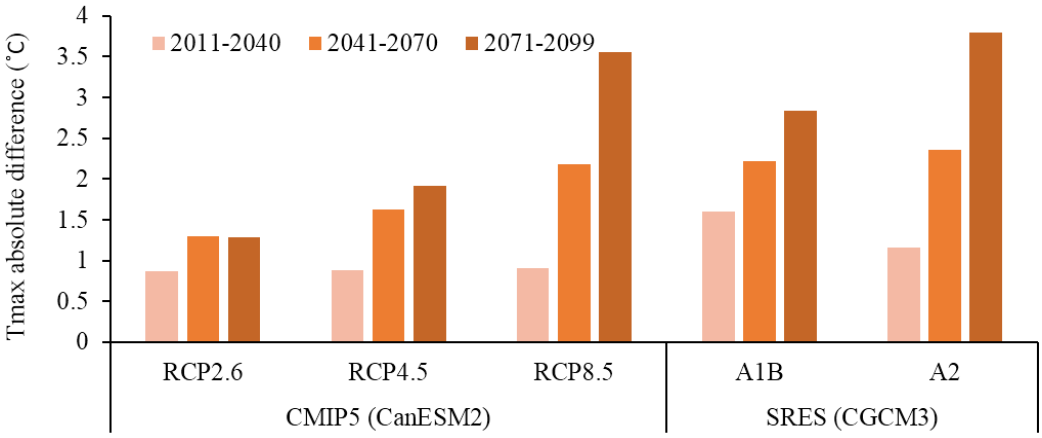

Figure 5.17: The projected difference change in Tmax

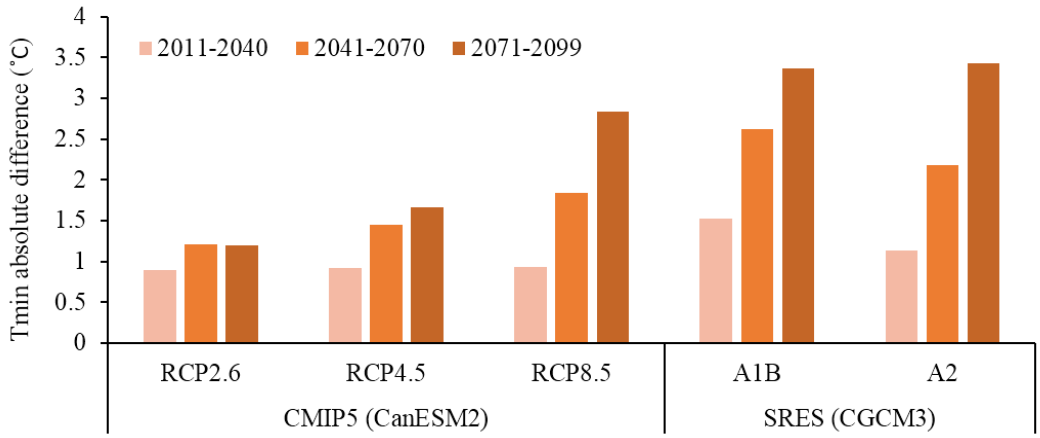

Figure 5.18: The projected difference change in Tmin.

Table 5.5: The projected scenarios using CGCM3 and CanESM2 GCMs

Period	RCP2.6	RCP4.5	RCP8.5	A1B	A2
2011-2040	+0.89˚C -9.5%P*	+0.90˚C -12.7%P	+0.92 ˚C -12.9%P	+1.56˚C, +5.9%P	+1.14˚C, +0.5%P
2041-2070	+1.25˚C -16.8%P	+1.54˚C -18.62%P	+2.01˚C, - 18.46%P	+2.42˚C -12.02%P	+2.27˚C -16.28%P
2071-2099	+1.21˚C -19.03%P	+1.79˚C -25.48%P	+3.20˚C -31.63%P	+3.10˚C -22.46%P	+3.61˚C, -28.66%P

P is the precipitation

Spatially, the climate changes were drawn at the hydrological response unit scale after delineating the basin using SWAT. This because those changes will determine the impact on the basin hydrology analysis under the current and future climate changes using SWAT. The map that shows the precipitation percentage change is depicted in Figure 5.19.

The maps that depict Tmax and Tmin difference change are shown in **Figure 5.20** and **Figure 5.21** respectively. The maps track the changes over the 30 years' intervals 2011-2040, 2041-2070 and 2071-2099 relative to the 15 years' simulated baseline climate (1986–2000).

It is clear that the amount of climate change varies from place to another. CGCM3 and CanESM2 GCMs consensus that there will be widespread precipitation decrease and temperature increase under all scenarios. Those changes are considered of negative impact on the basin hydrology. The PRCP special distribution showed that the PRCP decrease more from south to north. Even there will be an increase in PRCP in the basin far southeast and southwest which their current climate characterized with low precipitation <200mm/year. The PRCP percentage changes may vary from -60% to 100% of the various scenarios. Spatial distributions of Tmax and Tmin showed that temperature increase is higher wherever the elevation get lower. However, the spatial distribution of temperature is of lower accuracy in comparison to PRCP due to the low number of used temperature stations within the YRB. The difference change of temperature varies spatially between -1^{o}C and +5^{o}C among the various scenarios. RCPs projected climate changes show larger variations than the SRES scenarios. RCPs shows higher PRCP decrease toward the north but in the same time high PRCP increase toward the far south.

In general, highland areas are the least vulnerable to the warming even, in contrary the highlands may witness cooling conditions under low relativity CO_2 concentration increase scenarios. However, the spatial changes revealed no coherence where no clear spatial correlations can be derived. However, changes seem to get worse toward the northern-eastern territories. These wide spatial changes in the YRB support what Samuels et al. (2011) conclusion that due the Jordan River Basin complex topography, even small differences in the spatial scale will lead to different climate changes across the area. In terms of political boundaries, the Jordanian side is expected to be the least vulnerable and even, on the contrary, its territories are expected to increase in rainfall though it will be presented to high-temperature increases.

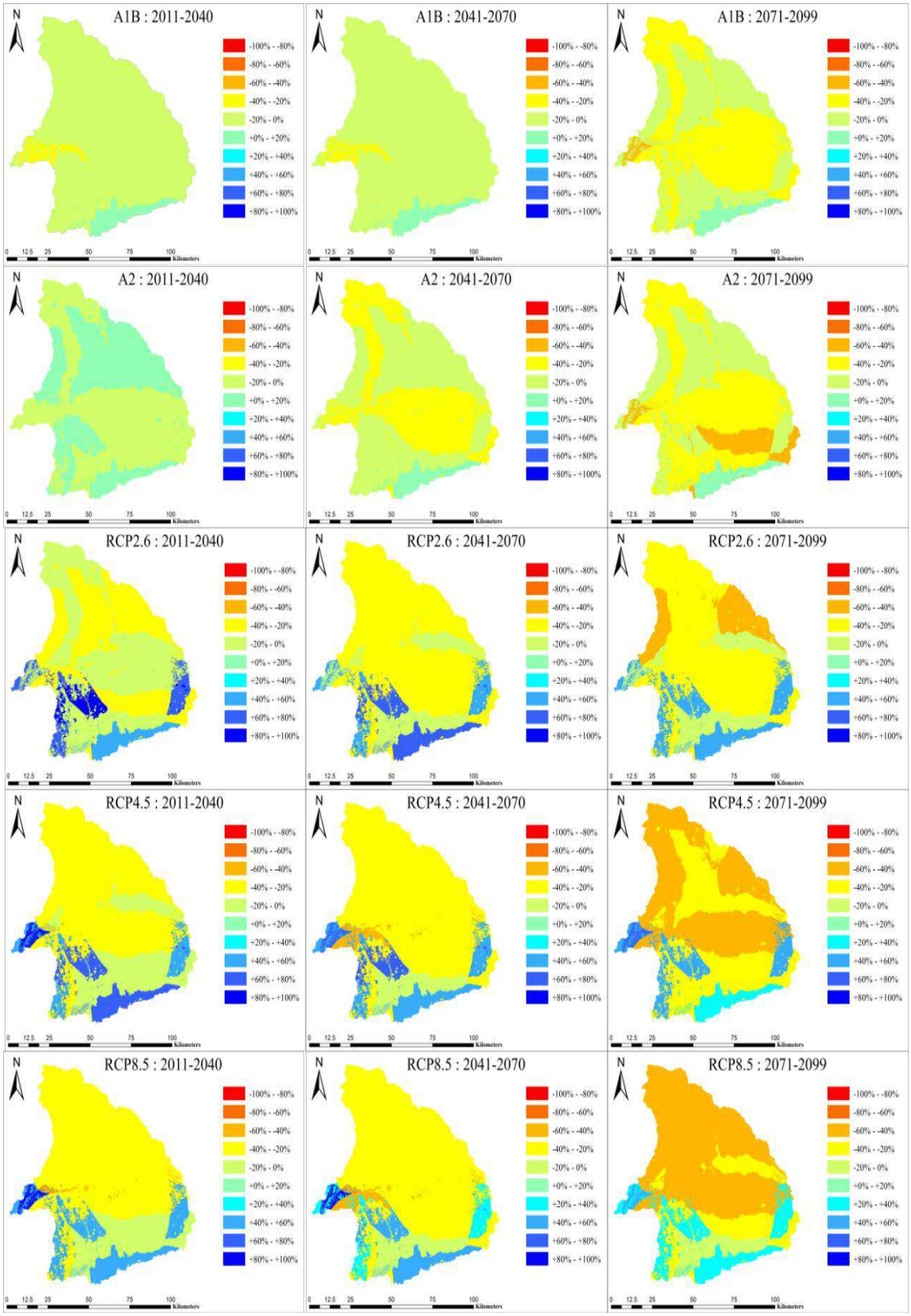

Figure 5.19: Spatial percentage change in annual average PRCP in comparison to the simulated baseline scenario (1986-1990)

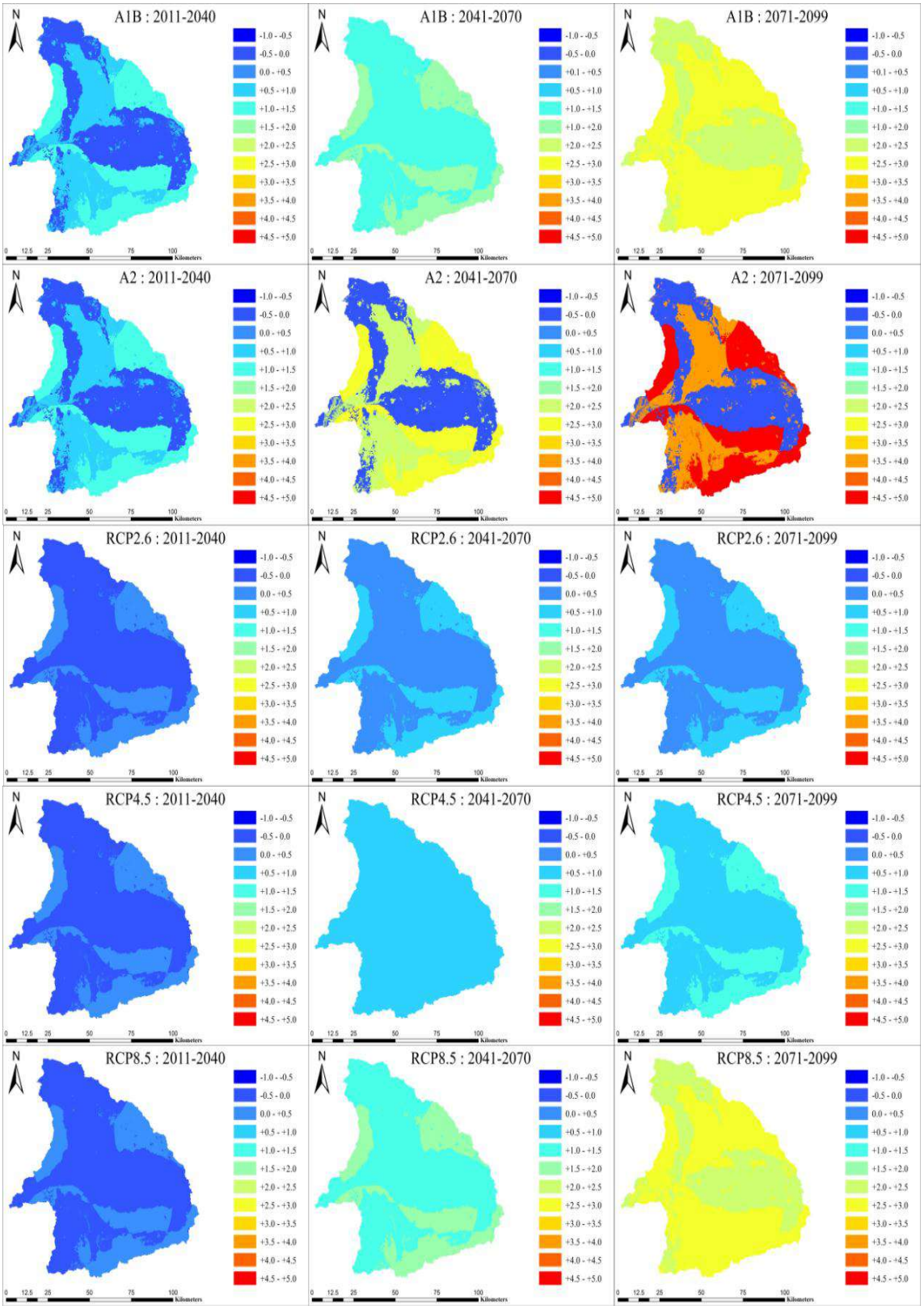

Figure 5.20: Spatial projected change of annual average surface Tmax (˚C) in comparison to the simulated baseline scenario (1986-1990)

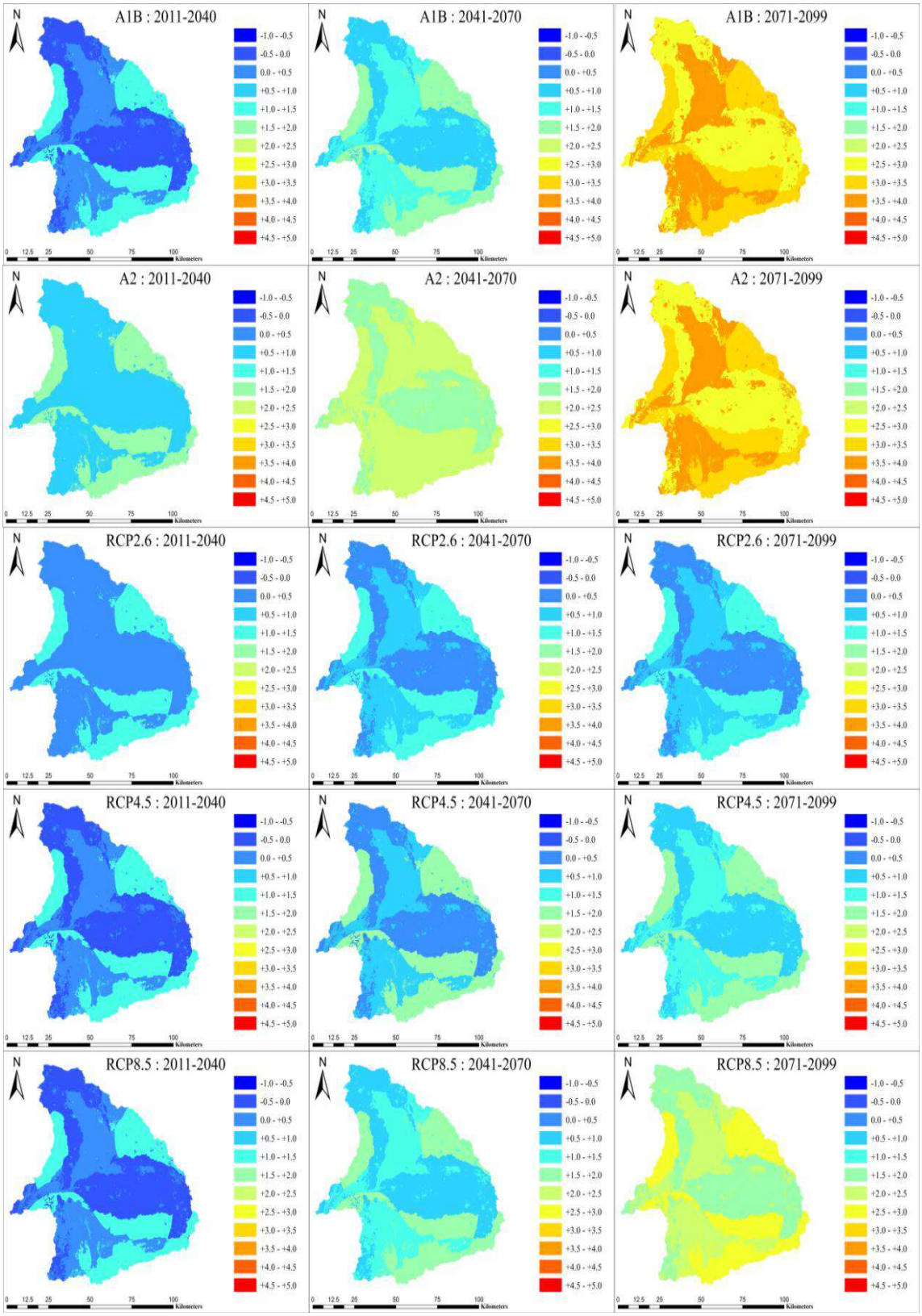

Figure 5.21: Spatial projected change of annual average surface Tmin (˚C) in comparison to the simulated baseline scenario (1986-1990)

Chapter Six: Hydrologic Response Evaluation

This chapter is devoted to present the results of predicting the spatial and temporal hydrologic response to the projected climate changes in the YRB using the Soil and Water Assessment Tool (SWAT) model for the pre-development and post-development conditions. In addition, the adaptation measures capable of minimizing the impacts of climate change will be elaborated on based on the literature review, governmental reports, and personal interviews.

6.1 Sensitivity Analysis, Calibration, and Validation

6.1.1 Pre-Development Conditions

It's important to determine the most significantly sensitive combination of parameters because parameters represent the processes. Therefore, the recognition of those parameters will illustrate what are the dominant processes in the hydrological cycle within the study area. In addition to that, it's well known that over-parameterization can affect a distributed hydrological model efficiency drastically making it necessary to reduce the parameters via an efficient sensitivity analysis (Whittaker 2010; Abbaspour 2007).

A preliminary sensitivity analysis had been executed to determine the most sensitive parameters based on experience, data availability, and relevant literature as well as the global sensitivity analysis of the candidate parameters. Previous studies of hydrology modeling using distributed models in adjacent basins to the YRB in Jordan included the ones by Al-Abed and Al-Sharif (2008), Abdulla et al. (2009), and the modeling of the Jordanian Yarmouk basin part by Hammouri et al. (2011).

The eight top significantly sensitive parameters that used to calibrate the model as well as the calibrated values and the realistic uncertainty ranges that had been used are shown in Table 6.1. The global sensitivity analysis results of the calibrated parameters are shown in Figure 6.1. These relative sensitivities estimate the average change in the objective function Nash-Sutcliffe efficiency when changing the targeted parameter while all other parameters are changing which gives partial information about the parameters sensitivity. The larger t-test-value and the smaller p-value are the more sensitive significantly (Abbaspour, 2007).

Table 6.1: The calibrated parameters and its ranges under the pre-development conditions

Sensitive parameter	Definition	Estimated value	Calibrated value	Units	Realistic uncertainty range		Hydrologic process
					Min	Max	
CN2	Curve number	76.7	65.88	None	60	90	Runoff
SOIL_AWC2	Available water capacity of the soil layer 2	0.098	0.11	mmH_2O/ mm soil	0.07	0.18	Soil
SOL_Z2	Depth of soil surface to the bottom	1000	1100	mm	900	1300	Soil
ESCO	Soil evaporation compensation factor	0.7	0.4	None	0.2	1	Evaporation
SOL_K1	Saturated hydraulic conductivity	1.49	5.01	mm/hr.	1	10	Soil
GW_DELAY	Groundwater delay	365	400	Days	300	500	Groundwater
GW_REVAP	Groundwater revap coefficient	0.12	0.02	None	0.02	0.2	Groundwater
CH-K	Effective hydraulic conductivity in main channel alluvium	0	0.5	mm/hr.	0	2	Channel

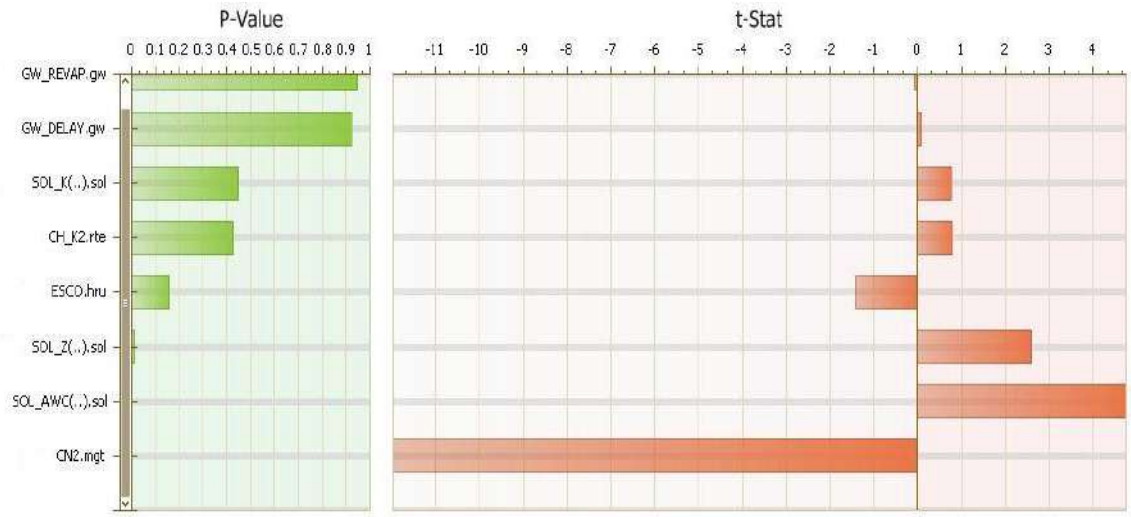

Figure 6.1: The calibrated parameters global sensitivity results within its realistic uncertainty ranges against the objective function Nash-Sutcliffe Efficiency (NSE)

For the model calibration, only monthly values of streamflow were used. It is very clear that the curve number (CN) which controls the flow partitioning into runoff and baseflow is the most sensitive parameter. This is actually a generality about CN for being the most important parameter when modeling the hydrologic response using SWAT (Van Griensven, 2006). The CN was reduced to 65 from its estimated value of 76 to assure enough recharge to the shallow aquifer so more match the estimated 55% baseflow/flow fraction. The second and third most sensitive parameters are the available water capacity (SOL_AWC) that measure of the ability of the soil to hold water and soil layer depth from its surface (SOL_Z). In addition to those parameters, there is the lower sensitivity saturated hydraulic conductivity (SOL_K) parameter that governs how much-infiltrated water would percolate to the shallow aquifer. Capturing this percolation process is very important in the YRB that's about 55% of its flow is due to a large number of springs discharge in the river that regarded as return flow. It's supposed that a balance exists between the springs discharge and percolated water but this is not the case where evaporation can remove the percolated water wherever the water-table rises enough to allow capillary action to bring the water into the zone of evaporation (Burdon, 1954). Because of that, those two parameters let to be adjusted seeking baseflow/flow ratio greater than 55% by increasing the SOL_AWC and SOL_Z within the allowed range. The fourth sensitive parameter is the evaporation compensation factor (ESCO) that govern soil evaporation calculations. The ESCO and the least sensitive groundwater re-evaporation (GR_REVAP) parameter were reduced to 0.4 and 0.02, respectively to extract more from the evaporative demand (Neitsch, 2011). This made the model able to simulate the dominant process of evaporation

were on average 0.81 of precipitation evaporates in the YRB as was estimated previously (Burdon, 1954).

The rest four sensitive parameters had been tuned the stream flow regime to match as possible the observed regime. The most influential parameter in tuning was the ground water delay time (GW_DELAY) that measures how long it takes for water to leave the root zone bottom to the shallow aquifer so can become return groundwater flow (Neitsch, 2011; Spruill, 2000). Large enough GW_DELAY days do smooth the release of groundwater over the entire year so the model becomes able to catch the stream baseflow response during no-rainfall months from June to September. The effective hydraulic conductivity (CH_K) that control the transmission losses to infiltration in the subbasin channels was increased to 0.5 mm/hr from its default 0 mm/hr that reflect the consolidated high silt-clay nature of the bed of the channel. This adjustment of CH_K allowed the simulated discharge peaks to be lowered and smoothed while keeping the water balance cycle intact. The water balance cycle components after the calibration have been done are believed to be in the appropriate range assuming that the model did simulate the processes within a realistic sense.

Table 6.2 summarizes the calculated objective function for both streamflow datasets for validation (1986-1995) and calibration (1996–2000). The time series plots of the observed and modeled streamflow at monthly and annual scales are depicted in Figure 6.2 and Figure 6.3 respectively. During the calibration evaluation measure are NSE = 0.66, RSR=0.58, PBIAS = -41.4 and small R-factor of 0.27 but still small P-factor 0.33. The modeling is further better on an annual basis as can be seen in Figure 6.3 providing R^2 of 0.92 and 0.87 for calibration and validation periods, respectively. It can be seen also that the winter-month flows were consistently overestimated by the model and peak flows were also overestimated for the high annual rainfall years.

However, the model performance during the calibration is not as good as the validation period based on the objective functions values in Table 6.2 and the monthly time discharge plot (Figure 6.2) at the best simulation match. That can be attributed to the SWAT modeling sensitivity to varied climatic measured datasets if representing drought, wet or average conditions as demonstrated by Wu and Johnston (2007). It was found that drought-calibrated version can perform much better than average conditions in the validation period. Additionally, the modeling using SWAT has a high sensitivity toward long return period storms. This applies to the current study where calibration period included the very long return period 1992 snow and rain storm.

Given the challenges in modeling the whole YRB due to Syrian part poor quality of data, soil map low scale and discharge extrapolation to resemble the historical flow regime during the calibration period, it is surprising that the model can still simulate the discharge with such satisfactory accuracy.

Table 6.2: Summary of the objective functions during the calibration and validation periods under the pre-development conditions

Objective function	Calibration (1986-1995)	Validation (1996-2000)
R^2	0.87	0.81
NS	0.66	0.80
RSR	0.58	0.45
PBIAS	-41.4	9.5
Mean_sim(Mean_obs) (m^3/s)	16.37(12.07)	8.65(9.56)
StdDev_sim(StdDev_obs) (m^3/s)	21.90(18.69)	13.03(10.83)

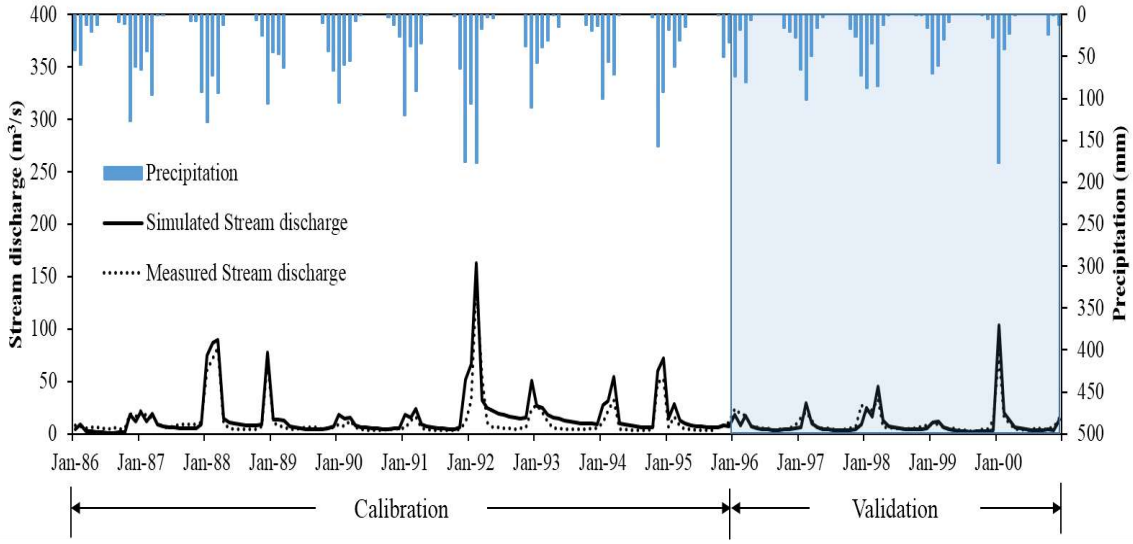

Figure 6.2: Measured and simulated monthly streamflow for the YR at Addasiya station as well as the monthly observed precipitation under pre-development conditions

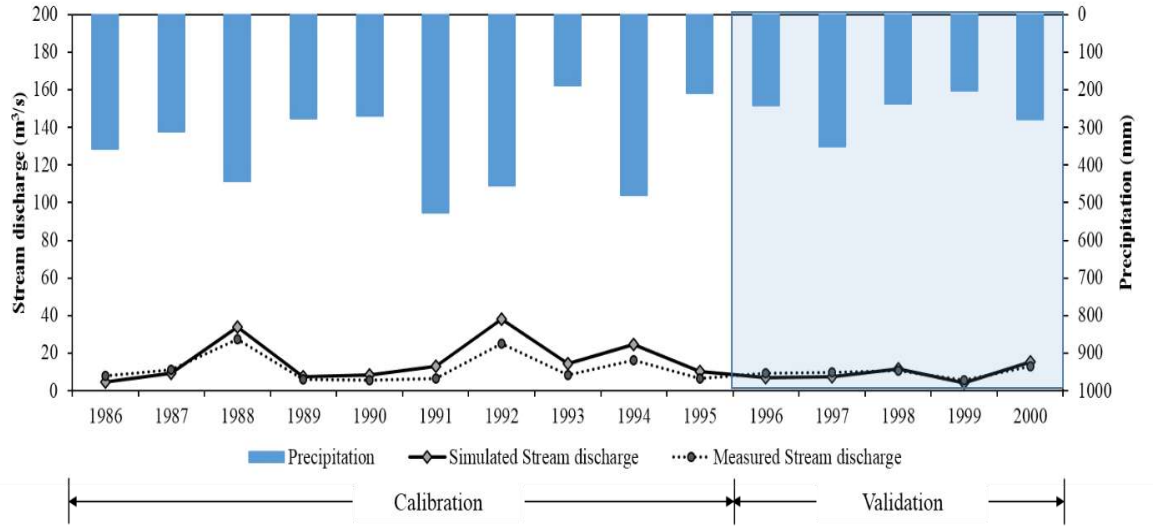

Figure 6.3: Measured and simulated annual streamflow for the YR at Addasiya station as well as the annually observed precipitation under pre-development conditions

The annual hydrologic water cycle components after the calibration have been finished are believed to be in the appropriate range. This is, in turn, let the authors assume that the model did simulate the processes within a realistic sense. The simulated hydrologic water cycle ratios during the calibration and validation that are shown in Figure 6.4 are comparable to the estimated average ratios relative to the annual precipitation by Burdon (1954) of 0.81 evapotranspiration, 0.16 streamflow (0.55 baseflow and 0.45 surface runoff) and 0.01 deep aquifer recharge. It's clear again that evapotranspiration is the dominant hydrologic process in the basin. Evapotranspiration is larger whenever dry conditions prevailed where it was 0.76 under average-wet calibration period and 0.83 under the validation dry conditions. This evapotranspiration variability affects the basin very much causing substantial variability in the basin annual water yield.

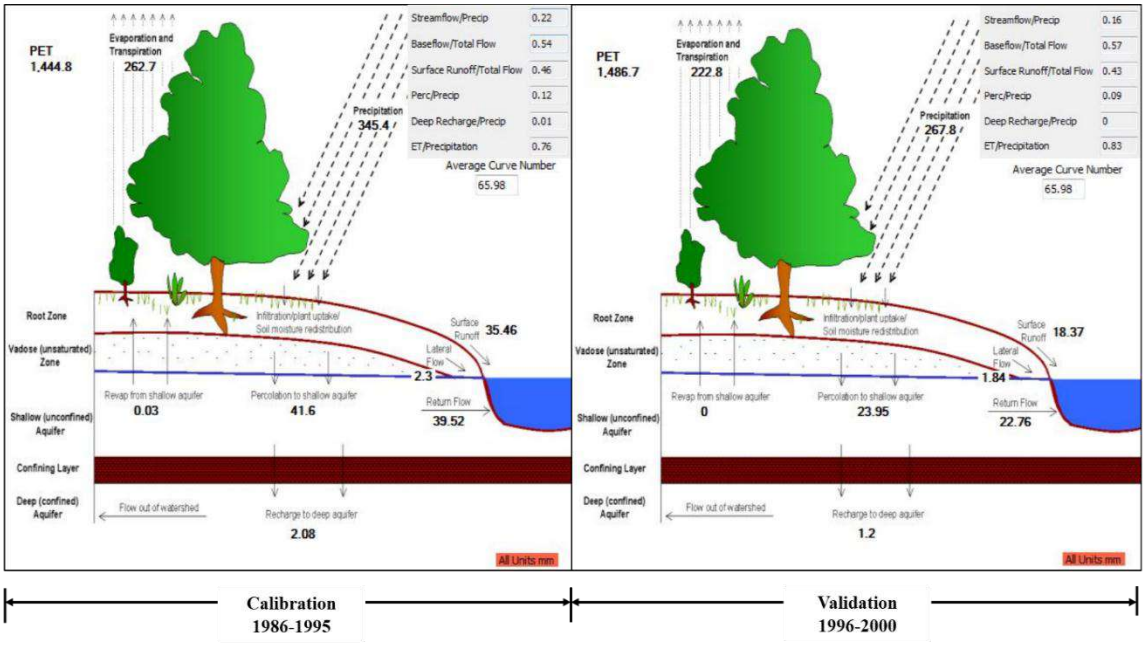

Figure 6.4: The simulated hydrologic water cycle components during the calibration and validation

6.1.2 Post-Development Conditions

The basin hydrological processes general circulation had been calibrated using a similar approach to the one used under the pre-development conditions plus management incorporation in the model. The most sensitive parameters and its calibrated values are shown in Table 6.3. The sensitivity analysis results are shown in Figure 6.5 that indicate that CH-K and CN are the most sensitive parameters. The automated calibration provided R-factor of 0.58 and P-factor of 0.52. The obtained objective functions values are shown in Table 6.4 for the calibration and validation periodsThe objective function values confirm a very good accuracy in compare to those under the pre-development conditions. In addition, a very clear and well-match is there between the observed and simulated of the monthly and annually flow regimes that are shown in Figure 6.6 and Figure 6.7 respectively. The results illustrate a satisfactory and better modeling for the stream flow under the post-development conditions.

This better performance is attributable to the larger flexibility to calibrate the model through the basin water management parameters. Such calibration enhancement was reported by Ouessar et al. (2009) after modeling the runoff water-harvesting systems using SWAT in an arid watershed in southeast Tunisia, which receives about 200 mm annual rainfall.

Table 6.3: The calibrated parameters and its ranges under the post-development conditions

Sensitive parameter	Definition	Estimated value	Calibrated value	Units	Realistic uncertainty range		Hydrologic process
					Min	Max	
CN2	Curve number	83.4	76.8	None	60	90	Runoff
SOIL_AWC2	Available water capacity of the soil layer 2	0.098	0.12	mmH_2O/ mm soil	0.07	0.15	Soil
ESCO	Soil evaporation compensation factor	0.8	0.7	None	0.5	0.1	Evaporation
GW_DELAY	Groundwater delay	365	450	Days	300	500	Groundwater
GW_REVAP	Groundwater revap coefficient	0.12	0.02	None	0.02	0.2	Groundwater
CH-K	Effective hydraulic conductivity in the main channel alluvium	2	11	mm/hr.	2	15	Channel

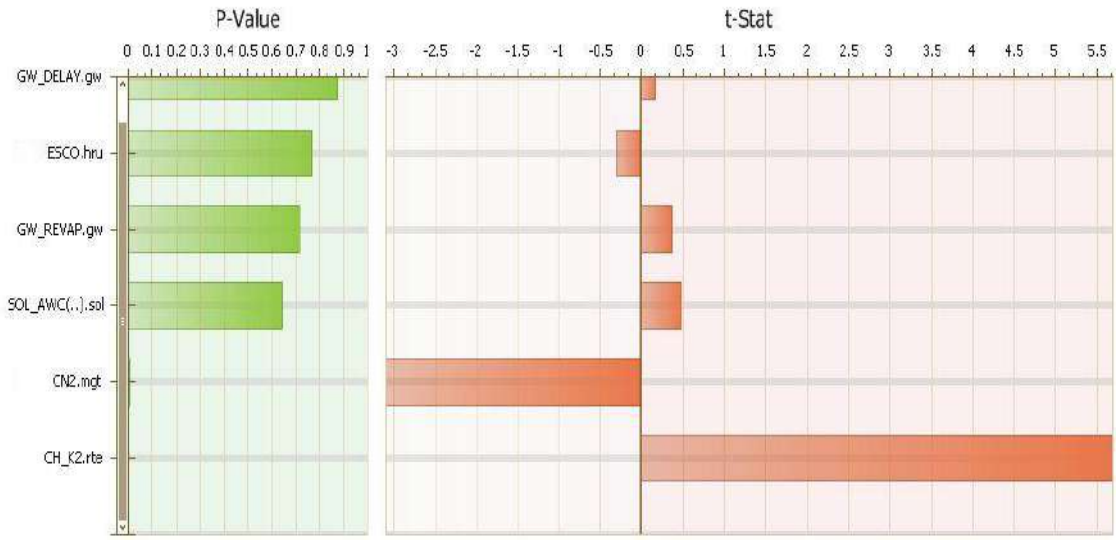

Figure 6.5: The selected parameters global sensitivity results within its realistic uncertainty ranges against the objective function Nash-Sutcliffe Efficiency (NSE) under the post-development conditions.

Table 6.4: Summary of the objective functions during the calibration and validation periods under the post-development conditions

Objective function	**Calibration (1986-1995)**	**Validation (1996-2000)**
R^2	0.89	0.81
NS	0.88	0.80
RSR	0.35	0.45
PBIAS	13.2	9.5
Mean_sim(Mean_obs) (m^3/s)	4.25(4.89)	2.78(2.56)
StdDev_sim(StdDev_obs) (m^3/s)	12.51(12.62)	6.35(5.04)

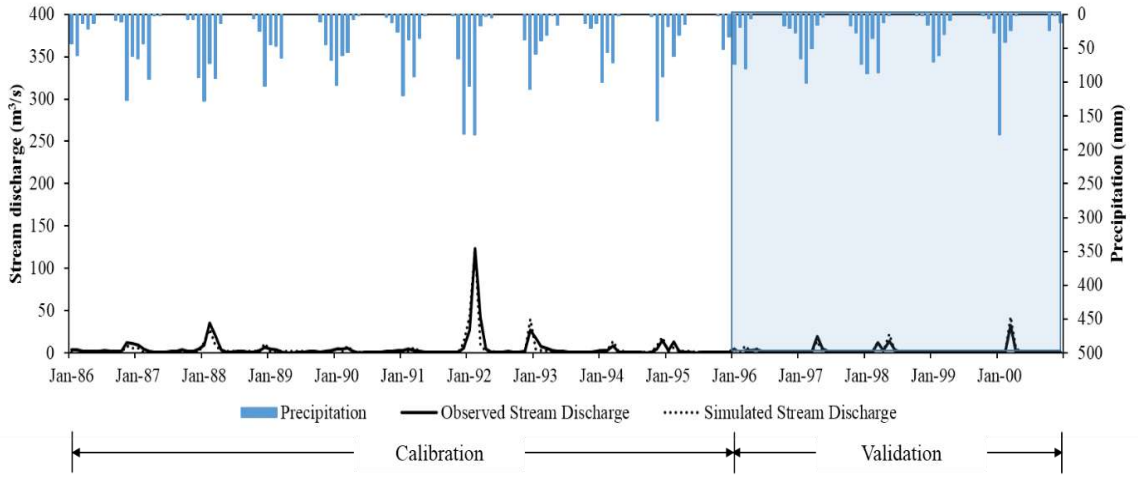

Figure 6.6: Measured and simulated monthly stream streamflow for the YR as well as the monthly observed precipitation under post-development conditions

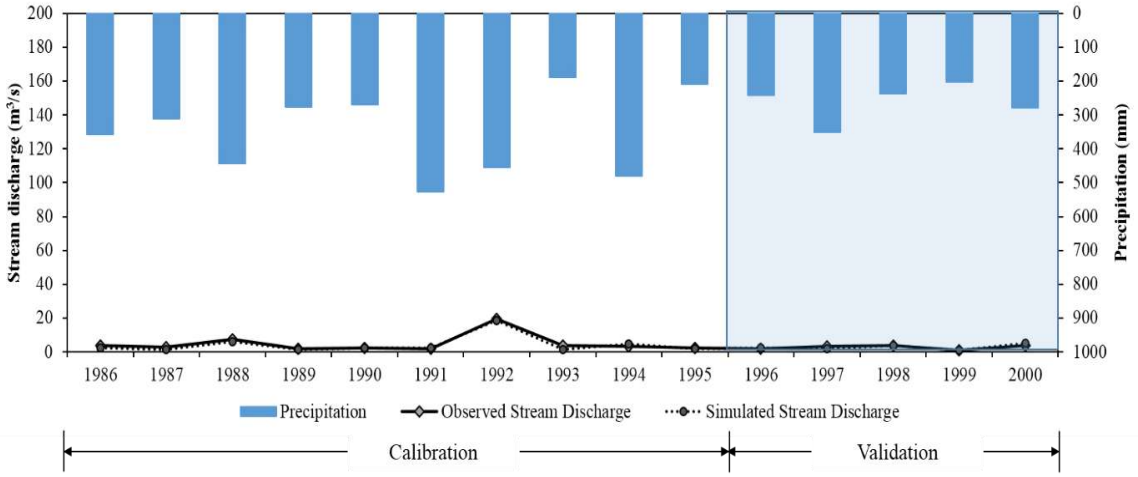

Figure 6.7: Measured and simulated annual streamflow for the YR at Addasiya station as well as the annually observed precipitation under post-development conditions

6.2 Climate Change Impacts

6.2.1 Pre-Development Conditions

The impact of climate change on YR flow regime and water cycle components under pre-development conditions was evaluated by driving a satisfactorily calibrated SWAT model under the projected 21st-century climate change scenarios. In this vein, the basin has been treated as a virgin basin without any manmade changes which are often useful to establish a first level adaptation strategy (Gosain, 2006). In addition, this is going to make it possible to evaluate how manmade changes affect the vulnerability of the basin to the climate change when comparing the impacts under the pre-development with the post-development conditions. The scenarios applied were the SRES A1B and A2 and CMIP5 RCP2.6, RCP4.5 and RCP8.5 scenarios (Table 5.5) that had been downscaled from the CGCM3 and CanESM2 climate variables output, respectively. The temporal climate change impacts were quantified at both monthly and annual scales.

The percentage changes during the 30 years' intervals 2011-2040, 2041-2070 and 2071-2099 average monthly simulated stream flow over the 21st century relative to the 15 years' simulated baseline weather scenario (1986–2000) are shown in Figure 6.8. SRES A1B and A2 tend to project minor impacts in basin streamflow ranging between -1.9% and 7.2% by the end of 2040. In the other hand, CMIP5 RCPs scenarios project much higher reduction ranging between 32.7% and 40 % by 2040. The annual average streamflow is projected to decline between 37.7%-58.0% and 38.4%-67.3% by the end of 2070 and 2099 respectively based on which path the CO_2 concentration will increase. Samadi et al. (2013) also suggest that there will be a significant reduction of streamflow, particularly in winter after studying how SDSM downscaled climate projections will affect future streamflow in a similar semi-arid catchment in Iran.

However, the obvious disproportionate change that has been reflected in a large reduction in average annual streamflow versus low relatively precipitation amount changes. In addition, the peak discharges may be underestimated where Chen et al. (2011) demonstrated that regression-based statistical methods such as used in SDSM usually produce considerable reductions in peak discharge. This is can be ascribed to the uncertain downscaled daily precipitation falling pattern. Where it is well known that precipitation characteristics are just as vital as the amount, in terms of the effects on the soil moisture and stream flow (Trenberth, 2011; Liu, 2011). Here, though the downscaled precipitation has kept significantly the observed precipitation characteristics, its falling pattern may

contain high uncertainties. The downscaled patterns in this study tended to some degree to have more prematurely precipitation and more often wet days with daily underestimated rainfall intensity. This is, in turn, let most precipitation falling to infiltrate to saturate the soils with no substantial amount available for surface runoff. In addition, the infiltrated water will become more exposed to evapotranspiration that will reduce and delay the contribution to the groundwater flow leading eventually to disproportionately low total flows. This is actually the case with most climate change models in the world in terms of producing too large water recycling and a too short lifetime of moisture in the atmosphere which influence surface runoff and soil moisture (Trenberth, 2011).

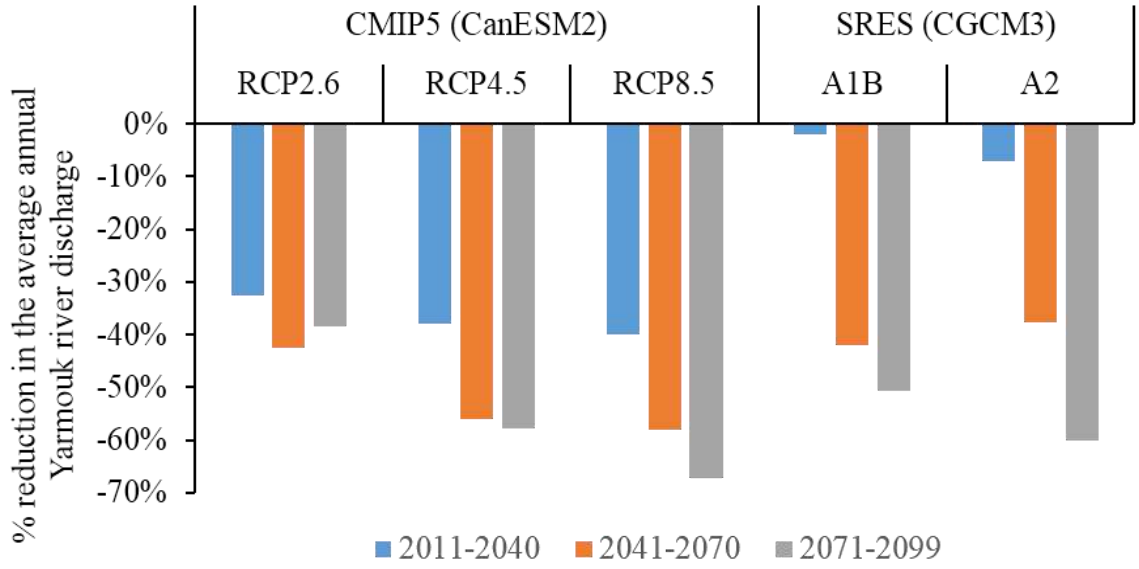

Figure 6.8: Average YR discharge change percentage under the climate applied change scenarios for the pre-development conditions

The YRB hydrologic water cycle components modeling during the 15 years' baseline period (1986-2000) demonstrated reasonable output and realistic interactions among them. The simulated amounts of the hydrologic cycle components evapotranspiration (ET) and water yield (WY) which represent the average amount of fresh water that runs off in an unregulated watershed are summarized in Table 6.5 and Table 6.6 for the RCPs and SRES scenarios respectively. The annual hydrologic cycle ratios of evapotranspiration and water yield relative to the annual precipitation under the climate change scenarios are exhibited in Figure 6.9.

Table 6.5: Simulated monthly hydrologic water cycle components under the RCPs climate change scenarios in mm where P, is the precipitation, ET is the evaporation and WY is the water yield

Period	Water budget component	Jan	Feb	Mar	Apr	May	Jun	Jul	Aug	Sep	Oct	Nov	Dec
Baseline 1986-2000	**P**	**76.44**	**50.62**	**59.11**	**15.89**	**5.34**	**0**	**0**	**0**	**0.13**	**13.6**	**40.28**	**38.86**
	ET	**33.49**	**42.92**	**57.49**	**49.86**	**17.3**	**1.75**	**0**	**0**	**0.02**	**8.66**	**21.25**	**21.35**
	WY	**7.83**	**7.35**	**7.67**	**2.69**	**2.45**	**2**	**1.9**	**1.75**	**1.57**	**1.66**	**3.05**	**5.46**
RCP2.6 2011-2040	P	59.1	53.31	60.64	18.51	3.15	0	0	0	0	12.35	36.38	55.24
	ET	34.29	45.32	60.44	49.98	21	2.02	0.01	0	0	7.43	19.16	27.74
	WY	4.16	4.52	4.67	2.47	2.05	1.76	1.67	1.54	1.38	1.74	1.77	3.08
RCP2.6 2041-2070	P	52.1	49.66	59.63	13.29	2.47	0	0	0	0	10.85	32.92	48.93
	ET	32.37	42.74	57.48	45.29	16.33	0.82	0.01	0	0	6.83	17.75	26.01
	WY	3.34	3.42	4.68	2.1	1.75	1.52	1.44	1.33	1.19	1.35	1.56	2.23
RCP2.6 2071-2099	P	52.73	43.49	60.37	14.72	3.83	0	0	0	0	12.88	34.04	50.19
	ET	32.19	40.82	56	46.27	17.15	0.88	0	0	0	8.31	17.41	25.1
	WY	3.68	3.34	4.45	2.26	1.93	1.67	1.58	1.46	1.31	1.54	1.7	2.83
RCP4.5 2011-2040	P	60.27	50.08	61.97	17.01	3.29	0	0	0	0	13.1	36.34	45.85
	ET	33	44.3	60.15	48.97	19.17	1.34	0	0	0	8.01	18.99	26.35
	WY	4.34	4.14	4.46	2.32	1.79	1.54	1.46	1.34	1.2	1.38	1.63	2.44
RCP4.5 2041-2070	P	45.94	45.65	57.4	15.45	3.58	0	0	0	0	11.88	36.55	44.96
	ET	31.12	40.83	55.94	45.1	16.16	0.66	0	0	0	7.23	18.55	25.69
	WY	2.5	2.65	4.02	1.47	1.28	1.04	0.98	0.9	0.8	1.06	1.23	1.85
RCP4.5 2071-2099	P	48.42	41.94	50.21	15.11	4.04	0	0	0	0	12.2	31.72	42.82
	ET	30.82	40.1	51.95	41.26	14.59	0.66	0	0	0	7.68	17.29	24.58
	WY	2.93	2.96	2.91	1.42	1.17	0.95	0.9	0.82	0.73	1.19	1.15	1.76
RCP8.5 2011-2040	P	60.23	50.35	58.23	16.49	2.89	0	0	0	0	12.15	33.46	45.38
	ET	33.2	45.03	58.2	47.41	19.63	1.25	0	0	0	7.43	17.81	25.95
	WY	4.06	4.08	4.7	2.15	1.67	1.45	1.37	1.26	1.13	1.29	1.58	2.38
RCP8.5 2041-2070	P	47.38	40.07	50.94	12.88	3.78	0	0	0	0	10.06	33.15	47.9
	ET	31.51	39.36	51.81	40.6	13.79	0	0	0	0	6.61	16.86	26.22
	WY	3.03	2.55	3.03	1.3	1.06	0.9	0.85	0.78	0.69	0.96	1.25	2.18
RCP8.5 2071-2099	P	47.26	37	49.16	12.36	2.59	0	0	0	0	11.36	24.97	41.35
	ET	30.15	37.91	50.13	37.9	9.06	0	0	0	0	8.15	14.41	23.47
	WY	2.53	1.97	2.61	1.05	0.88	0.75	0.7	0.64	0.57	0.69	0.83	1.43

Table 6.6: Simulated monthly hydrologic water cycle components under the SRES climate change scenarios in mm where P is the precipitation, EV is the evaporation and WY is the water yield.

Period	Water budget component	Jan	Feb	Mar	Apr	May	Jun	Jul	Aug	Sep	Oct	Nov	Dec
CGCM3	**P**	**75.55**	**51.61**	**58.82**	**17.23**	**4.01**	**0**	**0**	**0**	**0.13**	**13.72**	**41.54**	**63.8**
Baseline	**EV**	**36.17**	**44.08**	**60.12**	**52.33**	**18.59**	**1**	**0**	**0**	**0**	**8.93**	**20.29**	**28.48**
(1986-2000)	**WY**	**9.73**	**8.45**	**8.07**	**3.39**	**2.92**	**2.57**	**2.45**	**2.27**	**2.04**	**2.13**	**3.49**	**7.11**
A1B 2011-2040	P	71.05	61.25	66.2	20	3.18	0	0	0	0	10.81	45.22	69.22
	EV	37.95	48.81	67.83	56.79	20.2	2.61	0	0	0	7.76	22.31	31.85
	WY	7.67	8.96	8.56	3.84	3.17	2.81	2.69	2.49	2.23	2.28	2.84	5.19
A1B 2041-2070	P	60.26	43.64	62.96	16.35	3.06	0	0	0	0	10.09	35.8	56.79
	EV	34.08	42.22	59.78	51.21	15.75	0.83	0	0	0	7.74	18.99	27.73
	WY	5.32	4.03	5.34	2.11	1.71	1.49	1.41	1.3	1.17	1.23	1.73	3.71
A1B 2071-2099	P	52.93	39.17	51.28	14.4	2.67	0	0	0	0	10.65	35.3	48.6
	EV	31.86	38.91	52.52	42.76	11.13	0.37	0	0	0	7.58	18.77	25.44
	WY	4.61	3.53	4.53	1.77	1.4	1.22	1.16	1.07	0.96	1.04	1.68	3.23
A2 2011-2040	P	66.21	57.59	60.47	19.24	2.62	0	0	0	0	7.05	46.91	70.54
	EV	35.55	46.61	63.45	53.42	18.98	2.01	0	0	0	5.37	22.72	32.34
	P	9.25	7.54	7.93	3.43	2.73	2.41	2.3	2.13	1.91	1.92	2.6	5.59
A2 2041-2070	EV	59.91	43.27	56.82	15.85	3.81	0	0	0	0	11.74	39.3	51.33
	WY	32.69	39.89	58.1	46.91	14.56	1.05	0	0	0	8.44	20.75	27.71
	P	6.61	5.5	5.14	2.21	1.78	1.55	1.48	1.37	1.22	1.32	1.98	3.01
A2 2071-2099	EV	45.22	35.36	52.5	14.35	2.81	0	0	0	0	9.47	35.57	44.52
	WY	28.72	35.74	52.17	42.56	9.75	0.23	0	0	0	7.05	18.67	24.98
	P	3.28	3.6	3.59	1.32	1.1	0.96	0.91	0.83	0.75	0.87	1.78	2.29

Based on the results, average monthly water yield continues to decline for each month for all scenarios with the largest decreases being in Winter months Jan, Feb, and Dec. Average annual water yield results also exhibited similar continuous reduction as the average monthly water yields. The largest relative severe decline in average annual water yield was 60.1% against 31.4% precipitation decrease and 3.2^{o}C temperature increase under RCP8.5 (Figure 6.9). The evaporation/precipitation ratio is going to gradually increase under all scenarios with largest changes is expected under the scenario RCP8.5 of 10.6% increase by the end of 2099 relative to its baseline value of 85% (Figure 6.8). The partitioning into base flow and surface runoff is almost unaffected under the SRES A1B and A2 scenarios in comparison to its baseline scenario. On the other hand, the base flow contribution for the total steam flow will increase under all CMIP5 RCPs scenarios at the expense of the reduction of surface runoff contribution.

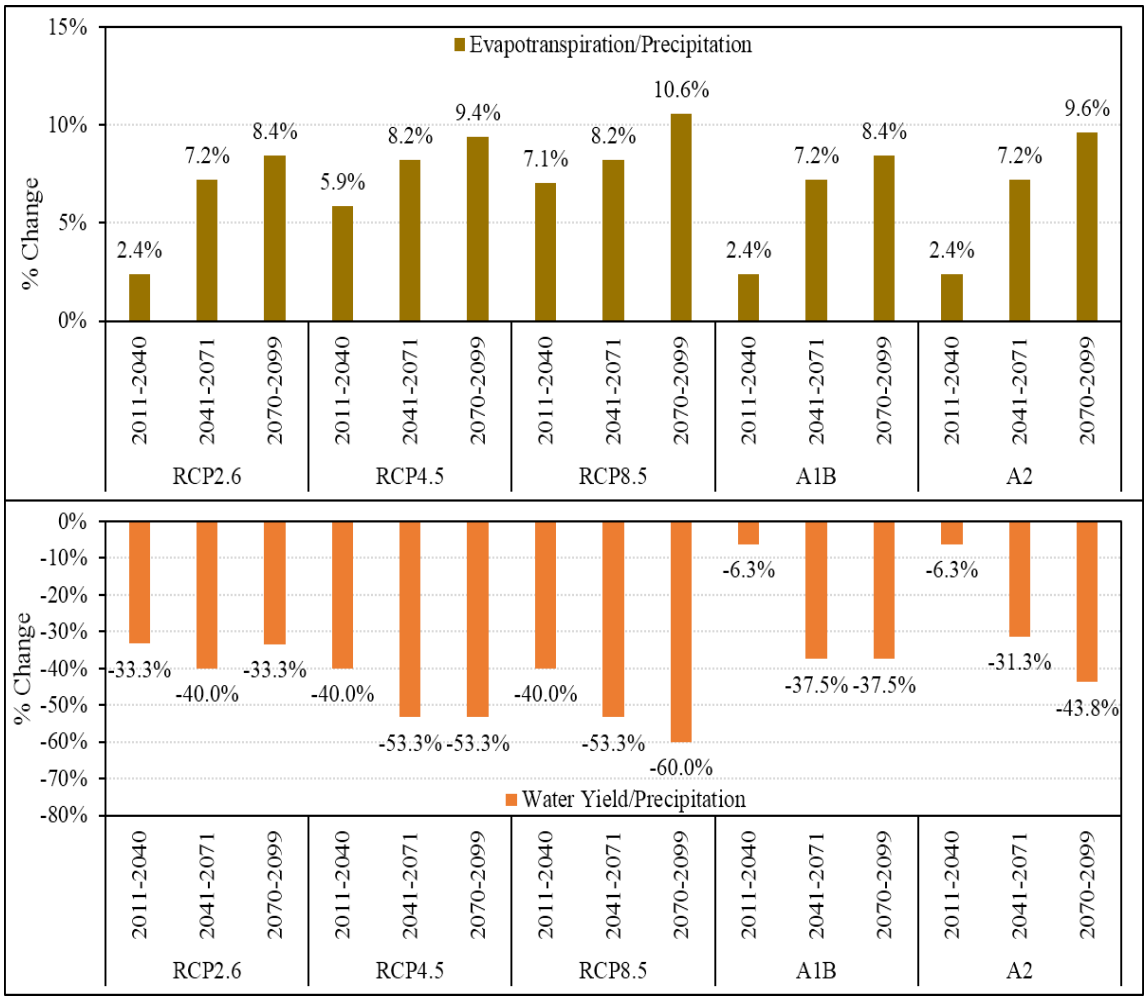

Figure 6.9: Simulated annual hydrologic water cycle ratios change under the climate change scenarios for the pre-development conditions

The spatial analysis of annual evapotranspiration (Figure 6.11) and water yield (Figure 6.12) changes across the YRB has been performed at subbasin level relative to its simulated baseline scenario. The baseline period reveals that the least evapotranspiration areas are in the basin middle east areas composing 28% of the total basin area where rainfall is the highest and average temperature is the least while the rest of basin is characterized with high evapotranspiration. This, in turn, is reflected in the fact that the most productive areas of water are the basin middle east areas as it contributes a percentage of 81% of the total basin water yield. These areas extend from Jabal Al-Arab to the east feeding Al-Batm, Negev, Al-Thalith, Abu Al-Dhahab, and Rimah Valleys that slowly flowing westward draining into the Harir and Zeizun streams and eventually pour into the YR as can be seen in Figure 6.10. The diverse scenarios applied predict that evapotranspiration increase and water yield decrease will be ubiquitous across the basin except for the basin southwest where the opposite is expected. The degree of vulnerability to climate change will vary across the basin where the wet areas will experience the largest amount of impact particularly the basin middle east. Overall, the spatial impacts are not coherent though it can be said that drought conditions will creep north to south and east to west. In terms of political boundaries, the Jordanian side is expected to be the least vulnerable to the drought climate changes and even, on the contrary, its territories are expected to increase in rainfall and thus water yield. That will be accompanied by no change in evapotranspiration rates, on average, and even may reduce in some scenarios.

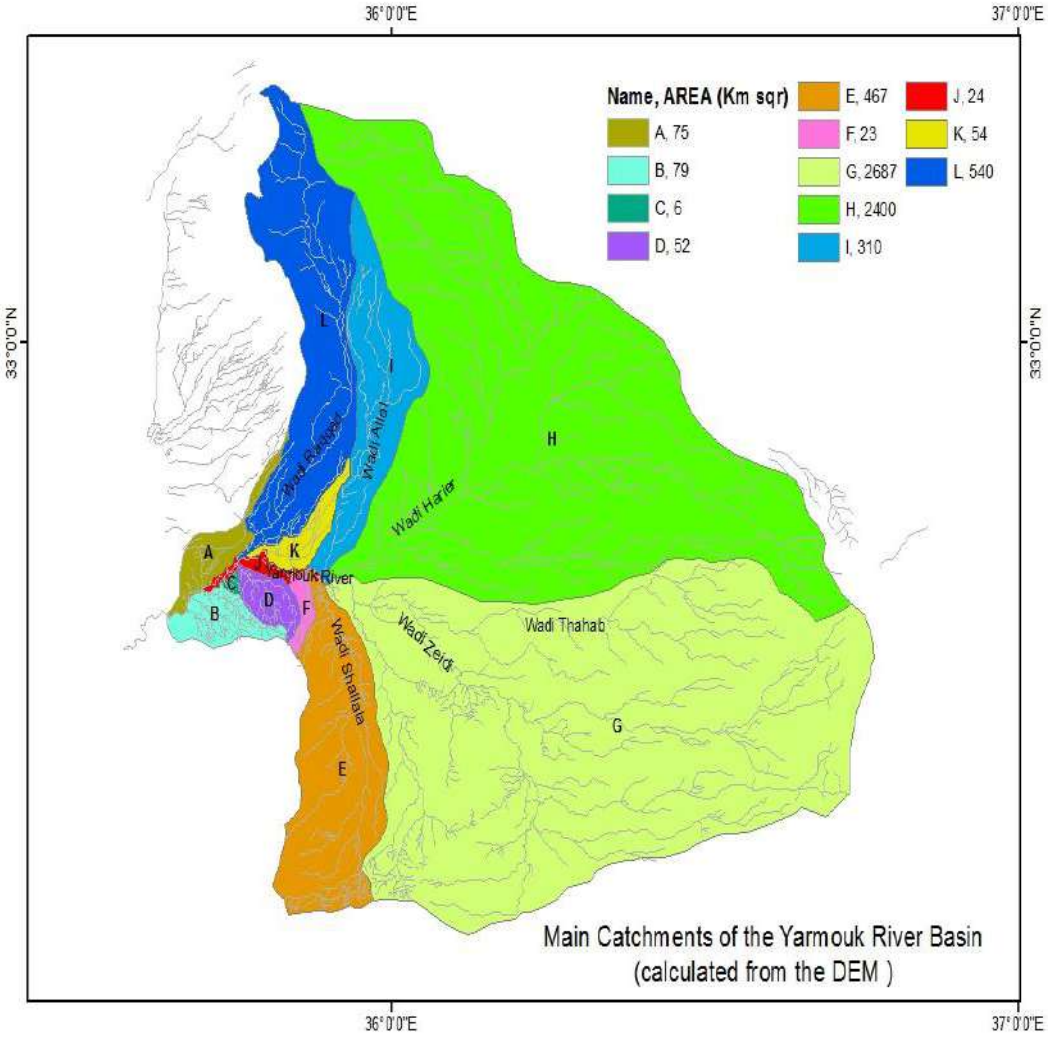

Figure 6.10: Yarmouk River Basin main valleys and its catchment areas

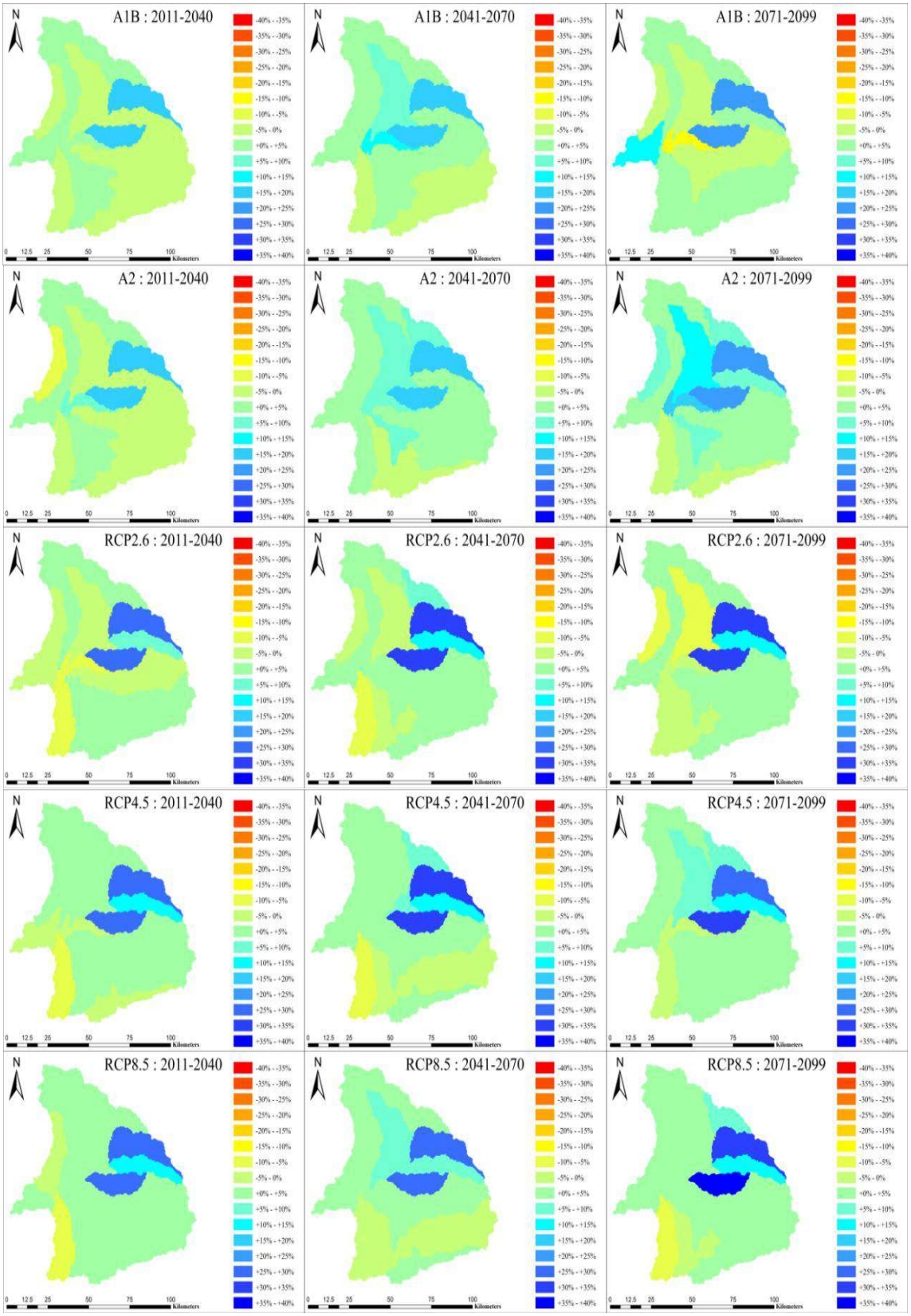

Figure 6.11: Spatial difference in annual average evapotranspiration/precipitation (ET/P) in comparison to the simulated baseline scenario (1986-1990) for pre-development conditions

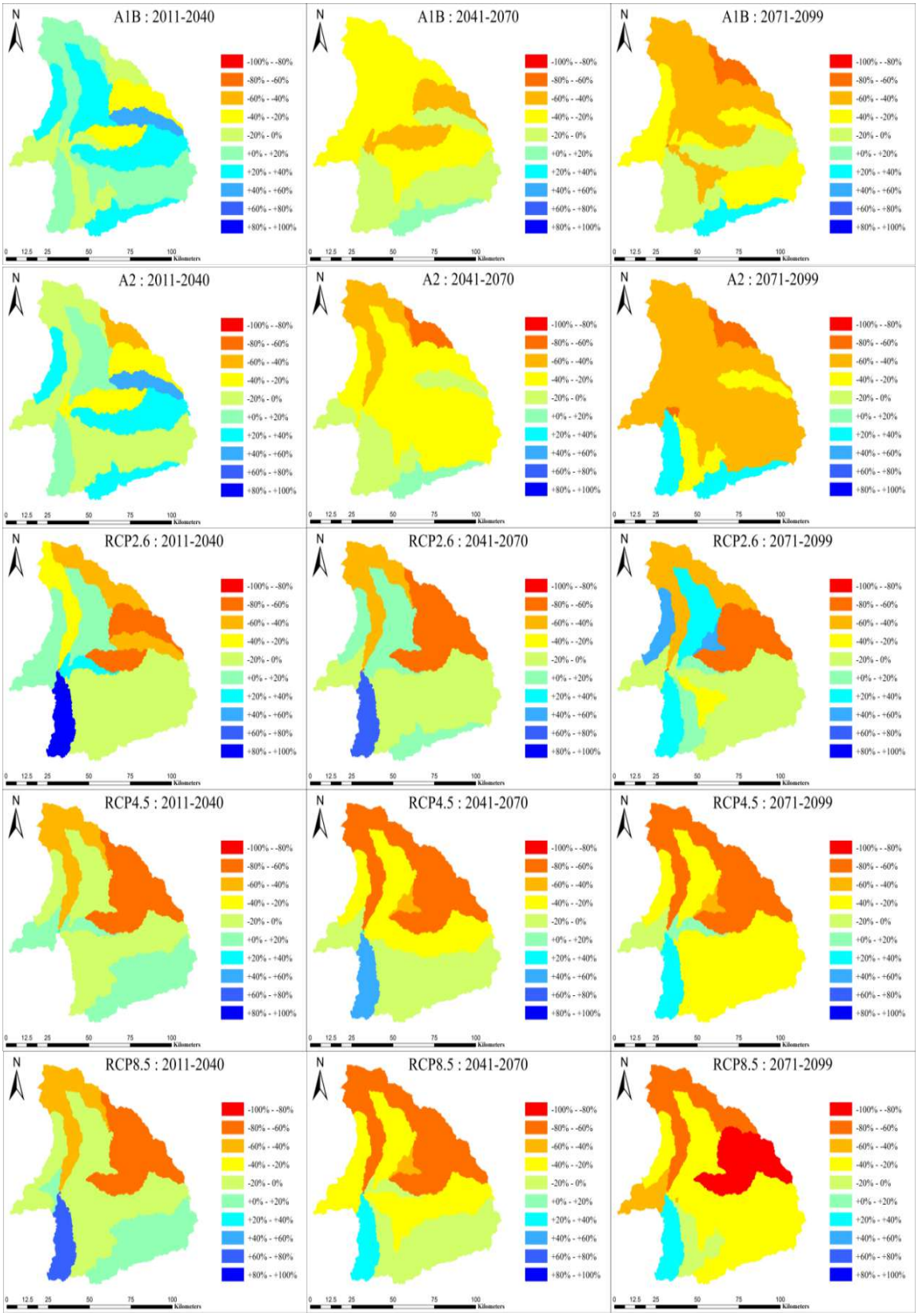

Figure 6.12: Spatial projected percentage change in annual average water yield in comparison to the simulated baseline scenario (1986-1990) for pre-development conditions

6.2.2 Post-Development Conditions

The implemented management practices within a watershed affect the hydrologic water cycle components and the flow regime highly. Therefore, including the water management as close as possible to the reality within the hydrological model will enhance the model substantially so becoming abler to retrieve more accurately the impacts (Arnold, 2005). Here, the impacts of climate change in the YRB after the post-development conditions that feature modeling the irrigation and the primary runoff water-harvesting system are going to be presented.

Temporally, the basin vulnerability toward any potential climate change has been found to be dependent on the basin water resources storing, diversion schemes and the consumptive water use. The projected reduction in the river discharge under various climate change scenarios is shown in Figure 6.13 relative to the baseline period 1986-2000 for the post-development conditions. The discharge reduction results illustrate that the change percentage will vary from -0% to -36.4% under post-development conditions comparing to -2.6%-60% under the pre-development conditions (see Figure 6.8). This makes the authors form a perception that the management of water resources will reduce the risks of climate change, by reducing evapotranspiration compared to what will be if the watershed kept at its virgin conditions. This can be explained that the water exposed to the evaporation will become less dramatically though the increase of evaporation rate display. These impacts are considered proportionate under the projected climate change scenarios. Similar proportionate results were reached by Samuels et al. (2010) and Kunstmann et al. (2007) after driving the distributed hydrological models with climate change scenarios within the Jordan River area.

Spatially, the evapotranspiration will increase with varying percentage and may decrease in few locations based on the nature of the location. The water yield will decrease with varying amount and may increase in few locations based on the nature of the location. The Northeastern locations are expected to witness the highest increase in evapotranspiration and the lowest decrease in water yield. These spatial variations of the climate change impacts are important for the adaptation measures plans such as water harvesting that prefers the locations of the lowest evapotranspiration and the highest water yield.

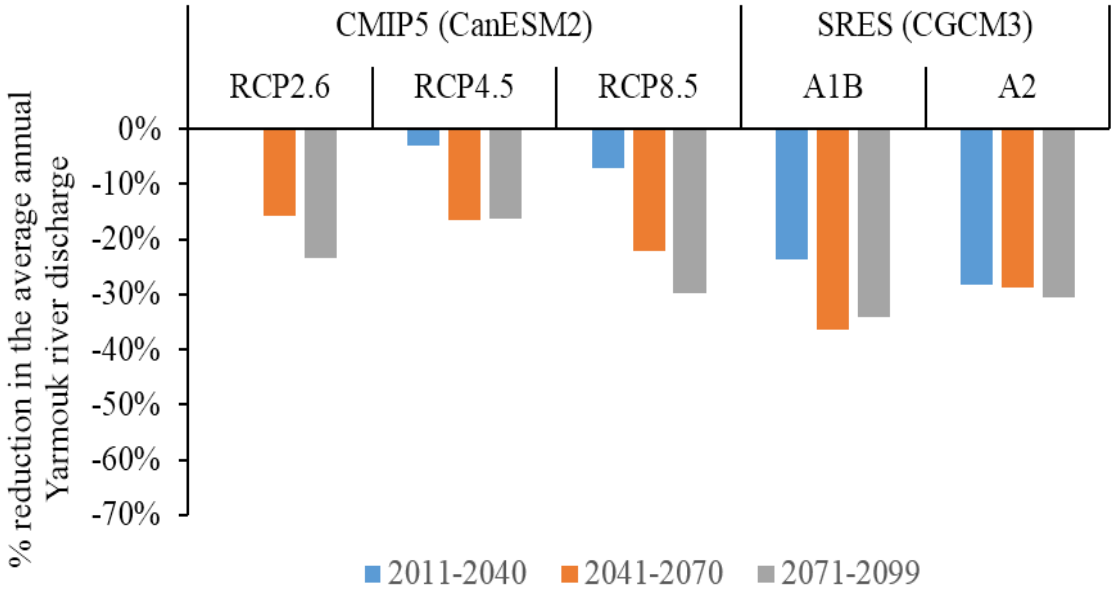

Figure 6.13: Average YR discharge change percentage under the applied climate change scenarios for the post-development conditions

Overall, these results are in agreement with IPCC 5AR results based on the observed 20th-century climate changes and climate modeling that regions which are dry currently are expected to become further drier while wet regions will become further wetter though some local conditions can flip the case (Stocker, 2013). In addition, the common potential runoff decrease in the Jordan basins is in agreement with the climate change impact study performed by Abdulla and Al-Omari (2008) when applying a precipitation decrease and temperature increase climate change scenarios on an adjacent basin. However, it should be kept in mind that an assessment of the basin vulnerability toward the projected climate change does not necessarily indicate that those impacts are likely especially in the light of the obvious intrinsic uncertainty of the GCM climate projections as well as other sources of uncertainty including the downscaling technique, the hydrological modeling, observed daily rainfall, observed runoff and the applied management practices. This impact assessment will only provide a worthy insight into the watershed hydrologic response sensitivity against the potential precipitation reduction and temperature increases based on its current conditions. This can boost the water resource strategic plans in the riparian countries of the YRB efficiently.

6.3 Adaptation Measures

Adaptation refers to dealing with the impacts of climate change that involves taking practical actions to manage risks from climate impacts, protect communities and strengthen the resilience of the economy (IPCC, 2014). The Jordan's National Communication reports on Climate Change in 2009 and 2014 have provided a comprehensive vulnerability assessment and addressed thoroughly potential adaptation measures to mitigate the impacts of climate change in Jordan (Framework Convention on Climate Change (UNFCCC) 2009; Framework Convention on Climate Change (UNFCCC) 2014). Based on the reports, the author's knowledge, personal interviews, and the climate change impact assessment that has been performed in the YRB, the most properly feasible and effective combination of adaptation measures is going to be presented.

The combination of desalination, water harvesting as well as wastewater reuse plans in Jordan is expected to make Jordan able to adapt to climate change. The currently under construction Red Sea Desalination Project (RDP) will provide about 550 MCM of desalinated water per year by the year 2022 (Jordan Valley Authority, 2016a). Al-Omari et al. (2014) have investigated the role of RDC project in adapting to climate change using the WEAP model for the climate scenarios; the business as usual (BAU) scenario and the climate change (CC). It was found that the implementation of the RDC project will satisfy the domestic demand from 2022 till 2050 and reduce the deficit (currently 250-300 MCM) in agricultural demand for the Jordan Valley (currently 250-300 MCM) by about 195 MCM and 85 MCM for BAU and CC scenarios respectively. These positive implications of the project are due to the increased treated wastewater flow to the valley from Azaq-Zarqa Basin (AZB) and the conservation of groundwater resources. Bonzi et al. (2016) stated that the positive effects of desalination and the increased use of treated wastewater in the project area can be strongly limited by insufficient water transport infrastructure and/or a lack of cooperation. This statement was derived after integrating the socio-economic scenarios and water management strategies resulting from a stakeholder process using WEAP model under four regional scenarios up to the year 2050 within the Global Change and the Hydrological Cycle (GLOWA)-Jordan River project.

Jordan has come a long way in the field of macro water harvesting. A FAO evaluation report of the water-harvesting sector in Jordan proved that water harvesting assists the Government of Jordan to meet its stated objectives for agricultural water management (Food and Agriculture Organization (FAO) 2016). In addition, the national

communication reports on climate change have given water harvesting the highest propriety as adaptation measure because it is feasible, efficient, and easily to be implemented with reasonable costs. Currently, more than 300 water-harvesting sites spread in the highlands, Jordan Badia, the pastoral areas of desert, and areas in which groundwater resides on the far depths with low quality with a storage capacity of 108 MCM. No exact amount available about the water-harvesting contribution in the national water budget due to the lake of the monitoring system in the water harvesting sites. Based on the current plans, the creation of water harvesting sites will continue until the year 2019, where the size of the harvesting will grow at the rate of 1.5-2 MCM per year. However, water harvesting sector still needs to handle the issue of assuring a site economic viability or sustainability. Many water-harvesting sites are either of small size or uncertain to be filled each year or far from the main roads particularly those in the Jordan Badia letting farmers non-encouraged to start projects around (Jordan Valley Authority, 2016b). No widespread practice of micro-scale water harvesting is available yet in Jordan. A study performed in Jordan by Abdulla and Al-Shareef (2009) recommended the spread of micro water harvesting after showing that a rooftop of $100m^2$ can easily harvest around $32m^3$ per year, where the average design-rainfall is about 400 mm per year and the losses are about 20%. On-farm rainwater micro-harvesting can be applied easily to increase the water available for supplementary irrigation, i.e. small farm ponds for micro irrigation using drip or sprinkler irrigation systems (Framework Convention on Climate Change (UNFCCC) 2014).

Wastewater treatment and reuse in the agricultural sector is a feasible option and already in use in Jordan. Actually, Jordan is one of few countries in the world of the highest centralized WWTP coverage and almost 91% of treated wastewater is reused for agriculture to reallocate fresh water for domestic purposes. The current and planned central WWTP are expected to treat 240 MCM per year by 2025. However, the centralized wastewater requires technical expertise, massive operation and maintenance costs which may present issues that reduce it's the WWTPs capacity. This leads to a call to expand the decentralized wastewater treatment also especially for farmers. Actually, few households currently own and operate decentralized wastewater treatment units due to either the knowledge and/or the financial lack. Boosting decentralized wastewater treatment can be achieved by establishing a good strategy to aware and prompt farmers to install decentralized units. It is expected that; the capacity of the suggested decentralized units can reach $200m^3$/day (Ministry of Water and Irrigation, 2016).

Chapter Seven: Summary, Conclusions, and Recommendations

7.1 Summary

The present study has been implemented for the sake of making available some comprehensive simulations of precipitation and temperatures changes and its related impact on the hydrology of the trans-boundary Yarmouk River Basin (YRB) that is shared between Jordan and Syria. The climate changes were forecasted using statistical downscaling approach using the SDSM tool of two global climate models (GCMs) under various GHS emission scenarios for three future intervals: 2011–2040, 2041–2070, and 2071–2099. A total of 13 mean and extreme indices, frequency analysis and Mann-Whitney statistical test were evaluated to explore SDSM skill. In addition, this study has underlined the challenge of downscaling semi-arid mean and extreme climate using the SDSM. After that, the downscaled climate changes have been used to drive a well-known and reliable distributed physically-based hydrological model which is the Soil and Water Assessment Tool (SWAT) to evaluate the climate change impact on the YRB hydrology. At final, an efficient combination of adaptation measures has been outlined presented based the author's overviews.

7.2 Conclusions

- The precipitation decrease, temperature increase, drought/dry days' increase and evaporation increase are the main determinants of climate change risks in the YRB.
- The YRB vulnerability to the downscaled climate change is relatively high and the basin can undergo severe impact under the worst scenarios by the end of the 21st century unless something to be done to stop, mitigate or adapt to the continued climate changes.
- Water storage and harvesting of rainwater modeling in the YRB has significantly reduced evaporation because the available quantities for evaporation become less, which is the basic process in which a basin water yield that located in the dry or semi-dry region gets lost. Hence, the basin becomes abler to adapt to the climatic changes expected. Additionally, this will add to the flood prevention measures that such basin is highly exposed to.

7.3 Recommendations

The main recommendations arising from this study for future researchers are:

- During the modeling process, a specific database for the Yarmouk River Basin has been prepared which is equivalent to the USA basins database system. Those researchers can use these data easily for other management objectives such as sediment yield modeling, water quality modeling and non-point sources loads of pollution estimation.
- The statistical downscaling at monthly scale using the software SDSM cannot be executed by popping out an overflow error as long as there are whole months without rain, which is the case in most areas that have dry or semi-dry climate such as the Yarmouk River Basin. Hence, it is required the user to provide fictitious rainfall amounts and then modify the parameters in the calibration files to zero for the dry months which raise doubts and difficulty for the user to use the model. Therefore, it is advised to the SDSM developers or who are interested in developing in the model to study this problem and its impact on the statistical downscaling as well as trying to solve it by modifying the SDSM code so the model SDSM can execute normally even for the dry months.
- The statistical downscaling method is able to project a dry or semi-dry climate satisfactorily with accepted uncertainty such as the projections have been obtained in this study. However, there still remains the need to develop a dynamical regional model (RCM) on the level of the country or the region to forecast more accurately how climate would change in the coming decades and compare it with the statistical downscaling projecting.

References:

Abbasnia, M. and Toros, H. (2016). Future changes in maximum temperature using the statistical downscaling model (SDSM) at selected stations of Iran. *Modeling Earth Systems and Environment*, 2(2), 1–7.

Abbaspour, K.C. (2007). User manual for SWAT-CUP, SWAT calibration and uncertainty analysis programs. *Swiss Federal Institute of Aquatic Science and Technology, Eawag, Duebendorf, Switzerland*.

Abbaspour, K.C., Rouholahnejad, E., Vaghefi, S., Srinivasan, R., Yang, H. and Kløve, B. (2015). A continental-scale hydrology and water quality model for Europe: Calibration and uncertainty of a high-resolution large-scale SWAT model. *Journal of Hydrology*, 524, 733–752.

Abbaspour, K.C., Vejdani, M. and Haghighat, S. (2007). SWAT-CUP calibration and uncertainty programs for SWAT. *InMODSIM 2007 International Congress on Modelling and Simulation, Modelling and Simulation Society of Australia and New Zealand*.

Abdulla, F.A. and Al-Shareef, A.W. (2009). Roof rainwater harvesting systems for household water supply in Jordan. *Desalination*, 243(1), 195–207.

Abdulla, F. and Al-Omari, A. (2008). Impact of climate change on the monthly runoff of a semi-arid catchment: Case study Zarqa River Basin (Jordan). *Journal of Applied Biological Sciences*, 2(1), 43–50.

Abdulla, F., Eshtawi, T. and Assaf, H. (2009). Assessment of the impact of potential climate change on the water balance of a semi-arid watershed. *Water resources management*, 23(10), 2051–2068.

Abu-Jaber, N. and Ismail, M. (2003). Hydrogeochemical modeling of the shallow groundwater in the northern Jordan Valley. *Environmental Geology*, 44(4), 391–399.

Al-Abed, N. and Al-Sharif, M. (2008). Hydrological modeling of Zarqa River basin–Jordan using the hydrological simulation program–FORTRAN (HSPF) model. *Water resources management*, 22(9), 1203–1220.

Al-malabeh, A.A., Sada, A.A., Abu-allaban, M. and Al-malabeh, A. (2016). Temporal and spatial analysis of climate change at northern Jordanian Badia. *Jordan Journal of Earth and Environmental Sciences*, 2, 87–93.

Al-Momani, M.A.O. (1993). *The Yarmouk River and Arab Water Security study in the geo-political* 2nd ed., Amman.

Al-Omari, A., Salman, A. and Karablieh, E. (2014). The Red Dead Canal project: an adaptation option to climate change in Jordan. *Desalination and Water Treatment*, 52(13–15), 2833–2840.

Anandhi, A., Srinivas, V. V, Nanjundiah, R.S. and Nagesh Kumar, D. (2008). Downscaling precipitation to river basin in India for IPCC SRES scenarios using support vector machine. *International Journal of Climatology*, 28(3), 401–420.

Arnold, J.G. and Allen, P.M. (1996(. Estimating hydrologic budgets for three Illinois watersheds. *Journal of hydrology*, 176(1), 57–77.

Arnold, J.G., Allen, P.M. and Bernhardt, G. (1993). A comprehensive surface-groundwater flow model. *Journal of hydrology*, 142(1), 47–69.

Arnold, J.G. and Fohrer, N. (2005). SWAT2000: current capabilities and research opportunities in applied watershed modelling. *Hydrological processes*, 19(3), 563–572.

Arnold, J.G., Moriasi, D.N., Gassman, P.W., Abbaspour, K.C., White, M.J., Srinivasan, R., Santhi, C., Harmel, R.D., Van Griensven, A. and Van Liew, M.W. (2012). SWAT: Model use, calibration, and validation. *Transactions of the ASABE*, 55(4), 1491–1508.

Arnold, J.G., Srinivasan, R., Muttiah, R.S. and Williams, J.R. (1998). Large area hydrologic modeling and assessment part I: Model development1.

Betsill, M.M. (2001). Mitigating climate change in US cities: opportunities and obstacles. *Local environment*, 6(4), 393–406.

Bonzi, C., Onigkeit, J., Hoff, H., Joyce, B. and Tielbörger, K. (2016). Analysing stakeholder driven scenarios with a transboundary water planning tool for IWRM in the Jordan River Basin. In *Integrated Water Resources Management: Concept, Research and Implementation*. Springer, 413–433.

Broxton, P.D., Zeng, X., Sulla-Menashe, D. and Troch, P.A. (2014). A global land cover climatology using MODIS data. *Journal of Applied Meteorology and Climatology*, 53(6), 1593–1605.

Burdon, D.J. (1954). Infiltration rates in the Yarmouk basin of Syria-Jordan. *International Association Science Hydrology*, 37, 343–355.

Canadell, J.G. and Raupach, M.R. (2008). Managing forests for climate change mitigation. *science*, 320(5882), 1456–1457.

Cavazos, T. and Hewitson, B.C. (2005). Performance of NCEP–NCAR reanalysis variables in statistical downscaling of daily precipitation. *Climate Research*, 28(2), 95–107.

Chen, J., Brissette, F.P. and Leconte, R. (2011). Uncertainty of downscaling method in quantifying the impact of climate change on hydrology. *Journal of Hydrology*, 401(3), 190–202.

Chenoweth, J., Hadjinicolaou, P., Bruggeman, A., Lelieveld, J., Levin, Z., Lange, M.A., Xoplaki, E. and Hadjikakou, M. (2011). Impact of climate change on the water resources of the eastern Mediterranean and Middle East region: Modeled 21st century changes and implications. *Water Resources Research*, 47(6).

Chu, J.T., Xia, J., Xu, C.-Y. and Singh, V.P. (2010). Statistical downscaling of daily mean temperature, pan evaporation and precipitation for climate change scenarios in Haihe River, China. *Theoretical and Applied Climatology*, 99(1–2), 149–161.

Dahamsheh, A. and Aksoy, H. (2007). Structural characteristics of annual precipitation data in Jordan. *Theoretical and Applied Climatology*, 88(3–4), 201–212.

Dibike, Y.B., Gachon, P., St-Hilaire, A., Ouarda, T. and Nguyen, V.T.-V. (2008). Uncertainty analysis of statistically downscaled temperature and precipitation regimes in Northern Canada. *Theoretical and Applied Climatology*, 91(1–4), 149–170.

Dore, M.H.I. (2005). Climate change and changes in global precipitation patterns: what do we know? *Environment international*, 31(8), 1167–1181.

Easterling, D.R., Meehl, G.A., Parmesan, C., Changnon, S.A., Karl, T.R. and Mearns, L.O. (2000). Climate Extremes: Observations, Modeling, and Impacts. *Science*, 289(5487), 2068–2074. Available at:

http://www.sciencemag.org/cgi/doi/10.1126/science.289.5487.2068.

Evans, J.P. (2009). 21st century climate change in the Middle East. *Climatic Change*, 92(3–4), 417–432.

Ficklin, D.L., Luo, Y., Luedeling, E. and Zhang, M. (2009). Climate change sensitivity assessment of a highly agricultural watershed using SWAT. *Journal of Hydrology*, 374(1), 16–29.

Field, C.B. (2012). *Managing the risks of extreme events and disasters to advance climate change adaptation: special report of the intergovernmental panel on climate change*, Cambridge University Press.

Flato, G., Marotzke, J., Abiodun, B., Braconnot, P., Chou, S.C., Collins, W.J., Cox, P., Driouech, F., Emori, S. and Eyring, V. (2013). Evaluation of Climate Models. In: Climate Change 2013: The Physical Science Basis. Contribution of Working Group I to the Fifth Assessment Report of the Intergovernmental Panel on Climate Change. *Climate Change 2013*, 5, 741–866.

Food and Agriculture Organization (FAO). (2016). *Assessment of the water harvesting sector in Jordan Final report*, Rome.

Food and Agriculture Organization (FAO). (2009). *FAO Syrian water report.*

Fowler, H.J., Blenkinsop, S. and Tebaldi, C. (2007). Linking climate change modelling to impacts studies: recent advances in downscaling techniques for hydrological modelling. *International journal of climatology*, 27(12), 1547–1578.

Framework Convention on Climate Change (UNFCCC). (2009). *Jordan's Second National Communication to the United Nations*, Amman.

Framework Convention on Climate Change (UNFCCC). (2014). *Jordan ' s Third National Communication on Climate Change*, Amman.

Gachon, P., St-Hilaire, A., Ouarda, T., Nguyen, V.T. V, Lin, C., Milton, J., Chaumont, D., Goldstein, J., Hessami, M. and Nguyen, T.D. (2005). A first evaluation of the strength and weaknesses of statistical downscaling methods for simulating extremes over various regions of eastern Canada. *Final report, Sub-component, Climate Change Action Fund (CCAF), Environment Canada, Montréal, Québec, Canada*, 15.

Gagnon, S., Singh, B., Rousselle, J. and Roy, L. (2005). An application of the statistical downscaling model (SDSM) to simulate climatic data for streamflow modelling in Québec. *Canadian Water Resources Journal*, 30(4), 297–314.

Giorgi, F. and Lionello, P. (2008). Climate change projections for the Mediterranean region. *Global and planetary change*, 63(2), 90–104.

Githui, F., Gitau, W., Mutua, F. and Bauwens, W. (2009). Climate change impact on SWAT simulated streamflow in western Kenya. *International Journal of Climatology*, 29(12), 1823–1834.

Gocic, M. and Trajkovic, S. (2013). Analysis of changes in meteorological variables using Mann-Kendall and Sen's slope estimator statistical tests in Serbia. *Global and Planetary Change*, 100, 172–182.

Goodland, R. and Anhang, J. (2009). Livestock and climate change: What if the key actors in climate change are... cows, pigs, and chickens? *Livestock and climate change: what if the key actors in climate change are.... cows, pigs, and chickens?*

Gosain, A.K., Rao, S. and Basuray, D. (2006). Climate change impact assessment on hydrology of Indian river basins. *Current science*, 90(3), 346–353.

Van Griensven, A., Meixner, T., Grunwald, S., Bishop, T., Diluzio, M. and Srinivasan, R. (2006). A global sensitivity analysis tool for the parameters of multi-variable catchment models. *Journal of hydrology*, 324(1), 10–23.

Gu, H., Wang, G., Yu, Z. and Mei, R. (2012). Assessing future climate changes and extreme indicators in east and south Asia using the RegCM4 regional climate model. *Climatic Change*, 114(2), 301–317.

Hadadin, N., Qaqish, M., Akawwi, E. and Bdour, A. (2010). Water shortage in Jordan—Sustainable solutions. *Desalination*, 250(1), 197–202.

Hamdi, M.R., Abu-Allaban, M., Elshaieb, A., Jaber, M. and Momani, N.M. (2009). Climate change in Jordan: a comprehensive examination approach. *American Journal of Environmental Sciences*, 5(1), 740–750.

Hamed, K.H. and Ramachandra Rao, A. (1998). A modified Mann-Kendall trend test for autocorrelated data. *Journal of Hydrology*, 204(1–4), 182–196. Available at: http://www.sciencedirect.com/science/article/pii/S002216949700125X [Accessed March 3, 2016].

Hammouri, N., Adamowski, J., Freiwan, M. and Prasher, S. (2011). Using SWAT to Assess the Impacts of Climate Change on the Water Resources of North Jordan. *Inter-Islamic Network on Space Sciences and Technology (ISNET) Royal Jordanian Geographic Centre (RJGC)*, p.65.

Hashmi, M.Z., Shamseldin, A.Y. and Melville, B.W. (2011). Comparison of SDSM and LARS-WG for simulation and downscaling of extreme precipitation events in a watershed. *Stochastic Environmental Research and Risk Assessment*, 25(4), 475–484.

Hegerl, G., Meehl, G., Covey, C., Latif, M., McAveney, B. and Stouffer, R. (2003). 20C3M: CMIP collecting data from 20th century coupled model simulations. *CLIVAR exchanges*, 26(8 (1)), p.Suppl.

Huang, J., Zhang, J., Zhang, Z., Xu, C., Wang, B. and Yao, J. (2011). Estimation of future precipitation change in the Yangtze River basin by using statistical downscaling method. *Stochastic Environmental Research and Risk Assessment*, 25(6), 781–792.

IPCC. (2007). *Climate Change 2007: Mitigation of Climate Change*, Cambridge University Press: Cambridge, UK New York, NY, USA.

IPCC. (2014). *Climate Change 2014–Impacts, Adaptation and Vulnerability: Regional Aspects*, Cambridge University Press.

IPCC. (2015). *Climate change 2014: mitigation of climate change*, Cambridge University Press.

IPCC. (2011). IPCC special report on renewable energy sources and climate change mitigation.

Jacobsson, S., Bergek, A., Finon, D., Lauber, V., Mitchell, C., Toke, D. and Verbruggen, A. (2009). EU renewable energy support policy: Faith or facts? *Energy policy*, 37(6), 2143–2146.

Jha, M., Pan, Z., Takle, E.S. and Gu, R. (2004). Impacts of climate change on streamflow in the Upper Mississippi River Basin: A regional climate model perspective. *Journal of Geophysical Research: Atmospheres*, 109(D9).

Jordan Atomic Energy Commission (JAEC). (2011). *White Paper on Nuclear Energy in Jordan "Final Report,"* Amman.

Jordan Valley Authority. (2016a). Red Sea Dead Sea Project. Available at: http://www.jva.gov.jo/sites/en-us/RSDS/SiteAssets/summary4.aspx.

Jordan Valley Authority. (2016b). *Water Harvesting Directorate, Achievements Report*, Amman.

Karmeshu, N. (2012). Trend detection in annual temperature and precipitation using the Mann Kendall test–A case study to assess climate change on select states in the northeastern United States.

Katz, R.W. and Brown, B.G. (1992). Extreme events in a changing climate: variability is more important than averages. *Climatic change*, 21(3), 289–302.

Khan, M., Aftab, M., Chauhan, V. and Kaushal, J. (2015). Antimicrobial Efficacy of Green Silver Nanoparticles and Potential Implications for Human Health and the Environment. *Journal of Chemistry, Environmental Sciences and its Applications*, 1(2), 81–90. Available at: http://dspace.chitkara.edu.in/jspui/bitstream/1/553/1/12008_JCE_Kaushal.pdf.

Khan, M.S., Coulibaly, P. and Dibike, Y. (2006). Uncertainty analysis of statistical downscaling methods. *Journal of Hydrology*, 319(1), 357–382.

Khordagui, H. (2014). Regional Assessment of Past Drought and Flood Episodes and Their Management in Selected SWIM-SM PCs (Tunisia, Jordan and Palestine).

Kottek, M., Grieser, J., Beck, C., Rudolf, B. and Rubel, F. (2006). World map of the Köppen-Geiger climate classification updated. *Meteorologische Zeitschrift*, 15(3), 259–263.

Kunstmann, H., Suppan, P., Heckl, A. and Rimmer, A. (2007). Regional climate change in the Middle East and impact on hydrology in the Upper Jordan catchment. *IAHS publication*, 313, 141.

Lelieveld, J., Hadjinicolaou, P., Kostopoulou, E., Chenoweth, J., El Maayar, M., Giannakopoulos, C., Hannides, C., Lange, M.A., Tanarhte, M. and Tyrlis, E. (2012). Climate change and impacts in the Eastern Mediterranean and the Middle East. *Climatic Change*, 114(3–4), 667–687.

Liu, X., Cheng, Z., Yan, L. and Yin, Z.-Y. (2009). Elevation dependency of recent and future minimum surface air temperature trends in the Tibetan Plateau and its surroundings. *Global and Planetary Change*, 68(3), 164–174.

Liu, Z., Xu, Z., Charles, S.P., Fu, G. and Liu, L. (2011). Evaluation of two statistical downscaling models for daily precipitation over an arid basin in China. *International Journal of Climatology*, 31(13), 2006–2020.

Mahmood, R. and Babel, M.S. (2013). Evaluation of SDSM developed by annual and monthly sub-models for downscaling temperature and precipitation in the Jhelum basin, Pakistan and India. *Theoretical and applied climatology*, 113(1–2), 27–44.

Maidment, D.R. (1996). GIS and hydrologic modeling-an assessment of progress. In *Third International Conference on GIS and Environmental Modeling, Santa Fe, New Mexico*.

Maidment, D.R. (1992). *Handbook of hydrology.*, McGraw-Hill Inc.

Mann, H.B. (1945). Nonparametric tests against trend. *Econometrica: Journal of the Econometric Society*, 245–259.

Mann, H.B. and Whitney, D.R. (1947). On a test of whether one of two random variables is stochastically larger than the other. *The annals of mathematical statistics*, 50–60.

Maraun, D., Wetterhall, F., Ireson, A.M., Chandler, R.E., Kendon, E.J., Widmann, M., Brienen, S., Rust, H.W., Sauter, T. and Themeßl, M. (2010). Precipitation downscaling under climate change: Recent developments to bridge the gap between dynamical models and the end user. *Reviews of Geophysics*, 48(3).

McCright, A.M., Dunlap, R.E. and Xiao, C. (2013). Perceived scientific agreement and support for government action on climate change in the USA. *Climatic Change*, 119(2), 511–518.

Meehl, G.A., Stocker, T.F., Collins, W.D., Friedlingstein, P., Gaye, A.T., Gregory, J.M., Kitoh, A., Knutti, R., Murphy, J.M. and Noda, A. (2007). Global climate projections. *Climate change*, 3495, 747–845.

Merriam, C.F. (1937). A comprehensive study of the rainfall on the Susquehanna Valley. *Eos, Transactions American Geophysical Union*, 18(2), 471–476.

Ministry of Water and Irrigation. (2016). *National water strategy 2016-2025*, Amman.

Moriasi, D.N., Arnold, J.G., Van Liew, M.W., Bingner, R.L., Harmel, R.D. and Veith, T.L. (2007). Model evaluation guidelines for systematic quantification of accuracy in watershed simulations. *Transactions of the ASABE*, 50(3), 885–900.

Neitsch, S.L., Williams, J.R., Arnold, J.G. and Kiniry, J.R. (2011). *Soil and water assessment tool theoretical documentation version 2009*, Texas Water Resources Institute.

Network, C.C.S. (2007). Canadian Climate Change Scenarios Network (CCCSN).

Oni, S.K., Futter, M.N., Molot, L.A., Dillon, P.J. and Crossman, J. (2014). Uncertainty assessments and hydrological implications of climate change in two adjacent agricultural catchments of a rapidly urbanizing watershed. *Science of the Total Environment*, 473, 326–337.

Pallant, J. (2007). SPSS survival manual: A step-by-step guide to data analysis using SPSS version 15. *Nova Iorque: McGraw Hill*.

Peidong, Z., Yanli, Y., Yonghong, Z., Lisheng, W. and Xinrong, L. (2009). Opportunities and challenges for renewable energy policy in China. *Renewable and Sustainable Energy Reviews*, 13(2), 439–449.

Peterson, T.C. and Manton, M.J. (2008). Monitoring changes in climate extremes: a tale of international collaboration. *Bulletin of the American Meteorological Society*, 89(9), 1266–1271.

Prudhomme, C. and Davies, H. (2009). Assessing uncertainties in climate change impact analyses on the river flow regimes in the UK. Part 1: Baseline climate. *Climatic Change*, 93(1–2), 177–195.

Raggad, M., Salameh, E., Magri, F., Siebert, C., Roediger, T. and Moller, P. (2016). Groundwater recharge in a semi-arid environment under high climatic variability and over-pumping: Ajlun Highlands example, Jordan. In *EGU General Assembly Conference Abstracts*. p. 10292.

Samadi, S., Carbone, G.J., Mahdavi, M., Sharifi, F. and Bihamta, M.R. (2013). Statistical downscaling of river runoff in a semi arid catchment. *Water resources management*, 27(1), 117–136.

Samuels, R., Rimmer, A., Hartmann, A., Krichak, S. and Alpert, P. (2010). Climate change impacts on Jordan River flow: downscaling application from a regional climate model. *Journal of Hydrometeorology*, 11(4), 860–879.

Samuels, R., Smiatek, G., Krichak, S., Kunstmann, H. and Alpert, P. (2011). Extreme value indicators in highly resolved climate change simulations for the Jordan River area. *Journal of Geophysical Research: Atmospheres*, 116(D24).

Searcy, J.K. and Hardison, C.H. (1960). Double-mass curves.

Semenov, M.A. and Stratonovitch, P. (2010). Use of multi-model ensembles from global climate models for assessment of climate change impacts. *Climate research*, 41(1), 1–14.

Sen, P.K. (1968). Estimates of the regression coefficient based on Kendall's tau. *Journal of the American Statistical Association*, 63(324), 1379–1389.

Shatanawi, K., Rahbeh, M. and Shatanawi, M. (2013). Characterizing, monitoring and forecasting of drought in Jordan River basin. *Journal of Water Resource and Protection*, 2013.

Sillmann, J., Kharin, V. V, Zwiers, F.W., Zhang, X. and Bronaugh, D. (2013). Climate extremes indices in the CMIP5 multimodel ensemble: Part 2. Future climate projections. *Journal of Geophysical Research: Atmospheres*, 118(6), 2473–2493.

Singh, V.P. (1989). *Hydrologic systems: watershed modeling*, Prentice Hall.

Smadi, M.M. (2006). Observed abrupt changes in minimum and maximum temperatures in Jordan in the 20th century. *Am. J. Environ. Sci*, 2(3), 114–120.

Smiatek, G. and Kunstmann, H. (2015). Expected future runoff of the Upper Jordan River simulated with CORDEX climate change data. In *EGU General Assembly Conference Abstracts*. p. 4624.

Smiatek, G., Kunstmann, H. and Heckl, A. (2011). High-resolution climate change simulations for the Jordan River area. *Journal of Geophysical Research: Atmospheres*, 116(D16).

De Smith, M.J. (2015). STATSREF: Statistical Analysis Handbook-a web-based statistics.".

Souvignet, M., Gaese, H., Ribbe, L., Kretschmer, N. and Oyarzún, R. (2010). Statistical downscaling of precipitation and temperature in north-central Chile: an assessment of possible climate change impacts in an arid Andean watershed. *Hydrological Sciences Journal–Journal des Sciences Hydrologiques*, 55(1), 41–57.

Souvignet, M. and Heinrich, J. (2011). Statistical downscaling in the arid central Andes: uncertainty analysis of multi-model simulated temperature and precipitation. *Theoretical and applied climatology*, 106(1–2), 229–244.

Spruill, C.A., Workman, S.R. and Taraba, J.L. (2000). Simulation of daily and monthly stream discharge from small watersheds using the SWAT model. *Transactions of the ASAE*, 43(6), p.1431.

Stocker, T.F., Qin, D., Plattner, G.K., Tignor, M., Allen, S.K., Boschung, J., Nauels, A., Xia, Y., Bex, B. and Midgley, B.M. (2013). IPCC, 2013: climate change 2013: the physical science basis. Contribution of working group I to the fifth assessment report of the intergovernmental panel on climate change.

Stuart, A. and Kendall, M.G. (1968). *The advanced theory of statistics*, Charles Griffin.

The Goverment of Sweden. (2016). Fossil Free Sweden. Available at: http://www.government.se/government-policy/fossil-free-sweden/ [Accessed July 11, 2016].

The Offical Website of the Denmark. (2016). Independent from fossil fuels by 2050. Available at: http://denmark.dk/en/green-living/strategies-and-policies/independent-from-fossil-fuels-by-2050/ [Accessed July 11, 2016].

Thiessen, A.H. (1911). Precipitation averages for large areas. *Monthly weather review*, 39(7), 1082–1089.

Toews, M.W. and Allen, D.M. (2009). Evaluating different GCMs for predicting spatial recharge in an irrigated arid region. *Journal of Hydrology*, 374(3), 265–281.

Trenberth, K.E. (2011). Changes in precipitation with climate change. *Climate Research*, 47(1–2), 123–138.

Tryhorn, L. and DeGaetano, A. (2011). A comparison of techniques for downscaling extreme precipitation over the Northeastern United States. *International Journal of Climatology*, 31(13), 1975–1989.

UN-ESCWA, B.G.R. (2013). Inventory of shared water resources in Western Asia: Chapter 6 Jordan River Basin. United Nations Economic and Social Commission for Western Asia. *Federal Institute for Geosciences and Natural Resources, Beirut*.

Uniated Nations Framework convention on Climate Change (unfccc). (2015). The Paris Agreement. Available at: http://unfccc.int/paris_agreement/items/9485.php [Accessed November 8, 2016].

USDA Agricultural Research Service. (2016). Fact Sheet-Soil and Water Assessment Tool (SWAT). Available at: http://swat.tamu.edu/fact-sheet/ [Accessed November 9, 2016].

Wade, A.J., Black, E., Brayshaw, D.J., El-Bastawesy, M., Holmes, P.A.C., Butterfield, D., Nuimat, S. and Jamjoum, K. (2010). A model-based assessment of the effects of projected climate change on the water resources of Jordan. *Philosophical Transactions of the Royal Society of London A: Mathematical, Physical and Engineering Sciences*, 368(1931), 5151–5172.

Whittaker, G., Confesor, R., Di Luzio, M. and Arnold, J.G. (2010). Detection of overparameterization and overfitting in an automatic calibration of SWAT. *Transactions of the ASABE*, 53(5), 1487–1499.

Wilby, R.L. and Dawson, C.W. (2007). Using SDSM Version 4.1 SDSM 4.2. 2—a decision support tool for the assessment of regional climate change impacts. *User Manual, Leicestershire, UK*.

Wilby, R.L., Dawson, C.W. and Barrow, E.M. (2002). SDSM—a decision support tool for the assessment of regional climate change impacts. *Environmental Modelling and Software*, 17(2), 145–157.

Wilby, R.L., Hay, L.E. and Leavesley, G.H. (1999). A comparison of downscaled and raw GCM output: implications for climate change scenarios in the San Juan River basin, Colorado. *Journal of Hydrology*, 225(1), 67–91.

Wilby, R.L., Tomlinson, O.J. and Dawson, C.W. (2003). Multi-site simulation of precipitation by conditional resampling. *Climate Research*, 23(3), 183–194.

Wilby, R.L. and Wigley, T.M.L. (1997). Downscaling general circulation model output: a review of methods and limitations. *Progress in Physical Geography*, 21(4), 530–548.

Wu, K. and Johnston, C.A. (2007). Hydrologic response to climatic variability in a Great Lakes Watershed: A case study with the SWAT model. *Journal of Hydrology*, 337(1), 187–199.

Xu, C. (1999). Climate change and hydrologic models: A review of existing gaps and recent research developments. *Water Resources Management*, 13(5), 369–382.

Yue, S., Pilon, P. and Cavadias, G. (2002). Power of the Mann–Kendall and Spearman's rho tests for detecting monotonic trends in hydrological series. *Journal of hydrology*, 259(1), 254–271.

Zhang, X., Aguilar, E., Sensoy, S., Melkonyan, H., Tagiyeva, U., Ahmed, N., Kutaladze, N., Rahimzadeh, F., Taghipour, A. and Hantosh, T.H. (2005). Trends in Middle East climate extreme indices from 1950 to 2003. *Journal of Geophysical Research: Atmospheres*, 110(D22).

محاكاة الميزانية الهيدرولوجية لمياه حوض اليرموك مكانيا وزمانيا تحت تأثير كل من المناخ الحالي والتغيرات المناخية المتوقعة مستقبليا

إعداد: الهام وليد سعود الشرفات

الملخص

في هذه الدراسة، قمنا في البداية بتوقع التغيرات المناخية المستقبلية من خلال محاكاه المناخ الحالي بدقه قدر المستطاع بواسطه نموذج SDSM لتصغير نماذج الدوران المناخية العالمية (GCMs) من نطاقها الكبير الى نطاق أصغر يمثل الحوض الهيدرولوجي لتوقع تغير الهطول ودرجات الحرارة الكبرى والصغرى عبر القرن الواحد والعشرين في حوض اليرموك المشترك بين الأردن وسوريا، حوض اليرموك هو من أهم مصادر المياه في الأردن وذو مساحة كبيرة نسبياً حيث تبلغ مساحته حوالي 7004 كم^2 ويمتلك مناخ البحر الأبيض المتوسط الشبه جاف مما يتطلب الري المستمر لديمومة الزراعة، تم توقع التغيرات المناخية تحت عدة سيناريوهات لانبعاث الغازات الدفيئة وشمل ذلك المسارات الممثلة لتركيز غاز ثاني أكسيد الكربون RCPs بواسطة CanESM3 GCM وسيناريوهات انبعاث غاز ثاني أكسيد الكربون SRES بواسطة CGCM3 GCM، اتفقت التوقعات وفق جميع السيناريوهات على أن معدل هطول الأمطار السنوي سوف يستمر في الانخفاض وقد يصل إلى -30% في حين ستستمر درجة الحرارة في الازدياد تدريجيا وقد تصل إلى 3.5°س فرق وفقا لأسوأ سيناريو ما لم يتم بذل جهود عالمية لوقف ظاهرة الاحتباس الحراري أو التخفيف منها، كان هناك ثقة إحصائية جيدة في هذه التوقعات بناء على نتائج تحليل عدم الدقة على المستوى الشهري والسنوي، وأوضحت النتائج التي توصلنا إليها إلى أن نموذج SDSM لديه قدرة جيدة على محاكاة كلاً من خصائص الهطول ودرجات الحرارة المتوسطة والمتطرفة ولكن أقل قدرة على محاكاه نمط هطول الأمطار اليومي، ومع ذلك، فإنه يمكن اعتماد بيانات هذه التوقعات بثقة مرضية لأي دراسة تُعنى بدارسة تأثير التغيرات المناخية على حوض نهر اليرموك.

بعد ذلك، تم توقع تأثيرات التغير المناخي على تدفق نهر اليرموك ومكونات الموازنة المائية في حوض اليرموك تحت كل من ظروف الحوض قبل التنمية (قبل 1950) وبعد التنمية زمانياً ومكانياً، لتحقيق هذا الهدف، تم نمذجة هيدرولوجيا الحوض باستخدام أداة تقييم التربة والمياه (SWAT) وقد أشارت معايير التقييم أن النمذجة كانت مرضية على المستوى الشهري، أشارت النتائج أن تغير المناخ سيؤدي إلى ارتفاع متوسط التبخر الذي سيترافق مع انخفاض الإنتاج المائي وتدفق المجاري المائية على نطاق واسع مكانيا، وأظهرت الدراسة أيضاً ان مخاطر التغير المناخي أقل بكثير بعد نمذجة ظروف أدارة الحوض من تخزين مياه المجاري والأنهار وتحويل بعض المجاري حيث يقلل ذلك كثيراً من كميات المياه المعرضة للتبخر، من ناحية الحدود السياسية يتوقع ان تأثيرات التغير المناخي سوف تكون الأقل في الأراضي الأردنية مقارنة بالأراضي السورية وان هناك العديد من الطرق الفعالة للتكيف مع آثار التغير المناخي مثل حصاد المياه، واستيراد المياه الافتراضية، وإعادة استخدام مياه الصرف الصحي، وتعزيز تكنولوجيات الري وتحلية مياه البحر.